UNIVERSITEIT VAN PRETORIA
UNIVERSITY OF PRETORIA
YUNIBESITHI YA PRETORIA

In vitro cytotoxic effects and ultrastructural changes in myocardial (H9c2) and neuroblastoma (Neuro-2a) cell lines following exposure to three different cardiac glycosides

By

Danielle Henn

Submitted in partial fulfilment of the requirements for the degree

Master of Science in Veterinary Science

in the

Department of Paraclinical Sciences

Faculty of Veterinary Science

UNIVERSITY OF PRETORIA

October 2018

FACULTY OF VETERINARY SCIENCE

DECLARATION OF ORIGINALITY

**This document must be signed and submitted with every
essay, report, project, assignment, mini-dissertation, dissertation and/or thesis**
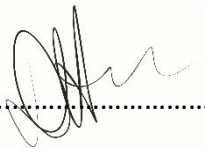
Full names of student: Danielle Henn

Student number: 13009410

Declaration:

1. I understand what plagiarism is and am aware of the University's policy in this regard.

2. I declare that this dissertation is my own original work. Where other people's work has been used (either from a printed source, Internet or any other source), this has been properly acknowledged and referenced in accordance with departmental requirements.

3. I have not used work previously produced by another student or any other person to hand in as my own.

4. I have not allowed, and will not allow, anyone to copy my work with the intention of passing it off as his or her own work.

Signature of student: ……………………………………….

Signature of supervisor: …………………...……………

ACKNOWLEDGMENTS

SUMMARY

In vitro cytotoxic effects and ultrastructural changes in myocardial (H9c2) and neuroblastoma (neuro-2a) cell lines following exposure to three different cardiac glycosides

By

Danielle Henn

Supervisor: Prof. C.J. Botha

Department: Paraclinical Sciences

University: University of Pretoria

Degree: Master of Science in Veterinary Science

Cardiac glycosides are often found within plants and can be classified as either cardenolides or bufadienolides depending on their structure. Cardenolide-containing plants are seldom eaten by livestock and of little veterinary importance. Comparatively, bufadienolide-containing plants are eaten much more often and cause a significant number of livestock mortalities. The compounds classified as bufadienolides can further be divided into two groups i.e. non-cumulative bufadienolides, which cause acute bufadienolide poisoning, and cumulative bufadienolides, that beside acute poisoning, also cause chronic intoxication. The chronic form of bufadienolide induced poisoning is a paretic condition known as krimpsiekte that mainly affect small stock. Our study objectives of this project were to confirm the neurotoxicity of the cumulative bufadienolides *in vitro* and compare the effects of different types of cardiac glycosides on myocardial and neuroblastoma cell lines. The *in vitro* cytotoxicity of the cardenolide digoxin, the non-cumulative bufadienolide 1α,2α-epoxyscillirosidine and the cumulative bufadienolide lanceotoxin B on H9c2 and Neuro-2a cells were determined using the MTT assay. The cytotoxicity of 1α,2α-epoxyscillirosidine on H9c2 cells was the greatest of the three cardiac glycosides tested. In contrast, Neuro-2a cells suffered the highest degree of cytotoxicity when exposed to lanceotoxin B. Ultrastructural changes induced by the different cardiac glycosides were examined using electron microscopy. The morphological changes induced by the cardiac glycosides was used to indicate the possible mechanism of cell death. The majority of H9c2 cells exposed to digoxin and 1α,2α-epoxyscillirosidine died via necrosis, while H9c2 cells exposed to lanceotoxin B died via apoptosis. The Neuro-2a cells exposed to digoxin showed signs of dying via apoptosis. 1α,2α-Epoxyscillirosidine caused necrosis in Neuro-2a cells, with some cells dying via the apoptotic pathway. Finally, lanceotoxin B caused many cells to exhibit the hallmark features of apoptosis, but the large autophagic vesicles present within the cytoplasm could be indicative of the involvement of autophagy in cell death.

List of Abbreviations

ANOVA	Analysis of Variance
ATCC	American Type Culture Collection
ATP	Adenosine Triphosphate
CI	Confidence Interval
DISC	Death Inducing Signalling Complex
DMEM	Dulbecco Modified Eagle Medium
DMSO	Dimethyl Sulfoxide
DNA	Deoxyribonucleic Acid
EC_{50}	Half Maximal Effective Concentration
EGFR	Epidermal Growth Factor Receptor
ER	Endoplasmic Reticulum
FBS	Foetal Bovine Serum
HDMS	Hexamethyldisilazane
LD_{50}	Half Maximal Lethal Dose
MAPK	Mitogen Activated Protein Kinase
MPT	Mitochondrial Permeability Transition
MTT	3-(4,5-dimethylthiazol-2-yl)-2,5-diphenyl tetrazolium bromide
MW	Molecular Weight
Na^+/Ca^{2+}-exchanger	Sodium/Calcium-Exchanger
Na^+/K^+-ATPase	Sodium/Potassium-Adenosine Triphosphatase
NCCD	Nomenclature Committee on Cell Death
PBS	Phosphate-Buffered Saline
PI3K	Phosphoinositide 3-Kinase
PKC	Protein Kinase C
PLC	Phospholipase C
RER	Rough Endoplasmic Reticulum
R_f	Retention Factor
ROS	Reactive Oxygen Species
SEM	Scanning Electron Microscopy
Spp.	Species
TEM	Transmission Electron Microscopy
TLC	Thin Layer Chromatography
TNF	Tumour Necrosis Factor
UV	Ultraviolet

Contents

List of Figures

List of Tables

Chapter 1 Introduction

1.1 Brief introduction to poisonous plants and cardiac glycoside poisoning

Consumption of cardiac glycoside-containing plants has a large impact on livestock production in South Africa (Kellerman et al., 1996). Cardiac glycosides can be classified as either cardenolides or bufadienolides, based on their chemical structure. The bufadienolides can then further be divided into non-cumulative and cumulative bufadienolides. Both cardenolides and non-cumulative bufadienolides can cause acute poisoning in livestock, affecting the cardiovascular, gastrointestinal, nervous and respiratory systems of the animals. Cumulative bufadienolides, in addition to acute poisoning, can also cause a chronic, paretic condition known as krimpsiekte that mainly affect the nervous system. Krimpsiekte is usually a disease of small stock, but larger stock such as cattle is also susceptible. Poisoning of livestock by bufadienolide-containing plants occur more often compared to cardenolide-containing plants and is thus of more importance from a veterinary perspective. Cardenolides are found in plants such as *Digitalis purpurea* (foxglove), *Nerium oleander* (selonsroos) and *Ghomhocarpus* spp. (milkweed) among other. Non-cumulative bufadienolides can be found in plants *Moraea* spp. (tulp) and *Drimia* spp. (slangkop). "Tulp" induced poisoning is the most important plant-associated poisoning of cattle in South Africa (Kellerman et al., 1996). Members of the genera *Crassulaceae* (*Cotyledon*, *Tylecodon* and *Kalanchoe*), also known colloquially as "plakkies" contain the neurotoxic, cumulative bufadienolides.

Cardiac glycosides act by inhibiting the sodium/potassium adenosine triphosphatase (Na^+/K^+-ATPase), disrupting the cellular Na^+ and K^+ homeostasis and trans-activating various signalling cascades (Riganti et al., 2011). This eventually triggers downstream processes and leads to effects such as an increase in the intracellular calcium concentration and the production of reactive oxygen species (ROS). These events influence the ultrastructure of the cells and eventually lead to cell death. Cell death can occur through more than one pathway including apoptosis, necrosis and autophagy.

The difference between the neurotoxic effects of the cumulative bufadienolides and the acute cardiac glycoside poisoning observed with cardenolides and non-cumulative bufadienolides are of scientific importance. In this study we compared the effects of three different types of cardiac glycosides on both myocardial and neuroblastoma cells with the hope of identifying the similarities and differences.

1.2 Problem statement

Poisoning of livestock by cardiac glycoside-containing plants has one of the largest impacts on the South African economy of all plant poisonings. Both acute and chronic poisoning are responsible for a large number of livestock mortalities annually (Kellerman et al., 1996). One of the largest limiting factors for small stock production in the Little Karoo and southern edges of the Great Karoo is krimpsiekte. The toxicosis of krimpsiekte is caused by cumulative bufadienolides, which has neurotoxic properties unique to the compounds in the *Crassulaceae* family. We aim to demonstrate the neurotoxic properties of cumulative bufadienolides *in vitro*. The differences between the effects of cardenolides, non-cumulative bufadienolides and cumulative bufadienolides on myocardial and nerve cell ultrastructure have also not been investigated.

1.3 Aims and objectives

The study objectives of this project were to confirm the neurotoxicity of the cumulative bufadienolides *in vitro* and compare the effects of digoxin (cardenolide), 1α,2α-epoxyscillirosidine (non-cumulative bufadienolide) and lanceotoxin B (cumulative bufadienolide) on myocardial and neuroblastoma cell lines.

- ❖ The cytotoxic effect of three different cardiac glycosides on rat myocardial (H9c2) and mouse neuroblastoma (Neuro-2a) cells were examined using the 3-(4,5-dimethylthiazol-2-yl)-2,5-diphenyl tetrazolium bromide (MTT) assay.
- ❖ Subcellular changes induced by the different cardiac glycosides were examined using transmission electron microscopy (TEM).
- ❖ Changes on the surface of the cells due to cardiac glycoside exposure were examined using scanning electron microscopy (SEM).

Chapter 2 Literature Review

2.1 Cardiac glycoside poisoning

2.1.1 General

South Africa is home to a rich variety of flora, including a wide range of poisonous plants, many unique to this region. Poisonous plants can often be found in cultivated lands, pastures and grassland or even as hay contaminants, where grazing stock are at risk of consuming them, leading to both direct and indirect loss. Direct losses include mortalities, reproduction failure and weight loss; while fencing, treatment costs, supplemental feeding and other management costs associated with minimising the risk of intoxication are counted as indirect losses (James et al., 1992). Although cardiac glycoside-containing plants are distributed across the world, cases of significant livestock poisoning have only been reported in South Africa and to a lesser extent in Australia (Kellerman et al., 1996; Seawright et al., 1989). Of the many plant-induced poisonings, cardiac glycoside poisoning is one of the six most important poisonings of cattle and small stock in South Africa (Kellerman et al., 1996). Interestingly, cardiac glycosides have also been found in various toad (genus *Bufo*) species, snake (genus *Rhabdophis*) species and insects such as certain firefly (genus *Photinus*) species, the monarch butterfly and locust (Azuma et al., 1986; Radford et al., 1986; Steyn and van Heerden, 1998).

Depending on the type of cardiac glycoside (cardenolide or bufadienolide) within the plant, symptoms of intoxication may vary, and poisoning can be described as either acute or chronic (Kellerman et al., 2005). Both cardenolide-containing and bufadienolide-containing plants can cause acute intoxication of livestock. From a veterinary perspective bufadienolide-containing plants are of greater importance, as they are more often responsible for livestock intoxication, while livestock seldom consume cardenolide-containing plants (Kellerman et al., 2005). Plants from the families Iridaceae, Hyacinthaceae and Santalaceae contain non-cumulative bufadienolides and are most often implicated in acute intoxication of livestock, with symptoms affecting the respiratory, cardiovascular, gastrointestinal and nervous systems. Plants from the family Crassulaceae contain cumulative bufadienolides that can cause both acute and chronic intoxication. When tiny amounts of these cumulative bufadienolide-containing plants are consumed over a period of time, it causes a paretic condition known as cotyledonosis or colloquially as "krimpsiekte". Krimpsiekte mainly

affect small stock and is considered a limiting factor of small stock production in the Little Karoo and southern edges of the Great Karoo of South Africa (Kellerman et al., 1996). Cumulative bufadienolides primarily affect the nervous system, whereas the effects on the respiratory, cardiovascular, gastrointestinal systems are decreased or entirely absent (Kellerman et al., 2005).

2.1.2 Poisonous principles

Cardiac glycosides are organic molecules that are comprised of three parts: a sugar (glycoside) moiety, an aglycone (steroid) moiety and an R-group at carbon 17 (Kellerman et al., 2005). The molecule can further be classified as either a cardenolide or a bufadienolide depending on the R-group at the C-17 position (**Figure 1**). Cardenolides contain a single unsaturated, 5-membered lactone ring attached to C-17, where bufadienolides contain a double unsaturated, 6-membered lactone ring attached to C-17. The pharmacological action of the cardiac glycosides is mainly due to the aglycone portion. The sugar portion has no cardiac activity by itself, however, when attached to the 3-hydroxyl group of the aglycone moiety, it modifies the activity of the molecule (Kren and Martínková, 2001). The sugar portion also plays a key role in the pharmacokinetics of the cardiac glycoside, since the presence of a sugar moiety lowers the dissociation constant of the molecule to the receptor (Wallick et al., 1980; Yoda, 1974; Yoda and Hokin, 1970).
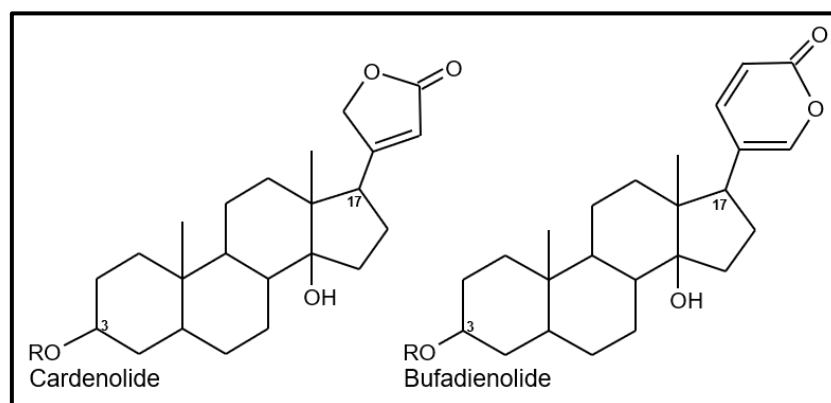
Figure 1 The structure of the aglycone portion of cardenolides and bufadienolides.

2.1.2.1 Cardenolides

The "card" in the name cardenolide refers to the cardiac effect of the molecule. Cardenolides have been used for treating congestive heart failure and cardiac arrhythmias for centuries. Some studies have shown the potential of cardenolides in treating various diseases such as cancer (Calderón-Montaño et al., 2014; Platz et al.,

2011; Tailler et al., 2012; Zhang et al., 2008). One of the best known cardenolides is digoxin (Molecular weight (MW): 780.949 g/mol) (**Figure 2**), a cardiac glycoside isolated by Smith et al. in 1930 from *Digitalis lanata* (foxglove) (Smith, 1930). It has been approved by the Medicine Control Council in South Africa for control of irregular heartbeats such as atrial fibrillation and in the management of congestive heart failure and is listed on the World Health Organization's list of essential medicines (Department of health, 2015; World Health Organization, 2017).

2.1.2.2 Bufadienolides

The term bufadienolide can be divided into three parts; the 'bufo' being from the toad genus *Bufo* that secrets bufadienolides; the -*adien*- and -*olide* referring to the two double bonds in the lactone ring and the lactone structure respectively (Kamboj et al., 2013). Related structures with only one double bond are called bufenolides and related saturated structures are called bufanolides. These compounds are mainly known for their toxicity to livestock, but studies have shown that they might play a role in cancer treatment (Masuda et al., 1995; Nogawa et al., 2001; Yeh et al., 2003). Bufadienolides can further be divided into non-cumulative and cumulative bufadienolides.

Non-cumulative Bufadienolides

Non-cumulative bufadienolides cause acute cardiac glycoside poisoning. The main toxic compound of *M. pallida* responsible for causing acute cardiac glycoside poisoning in livestock was isolated by Naudé and Potgieter (1966) and identified as 1α,2α-epoxyscillirosidine (MW: 472.53 g/mol) (**Figure 2**) (Enslin et al., 1966). The concentration of 1α,2α-epoxyscillirosidine in *M. pallida* differs between geographical regions and individual plants explaining why the toxicity of *M. pallida* varies between locality, geographical condition and growth stage (Botha et al., 2013; Kellerman et al., 2005). A subcutaneous half maximal lethal dose (LD_{50}) for 1α,2α-epoxyscillirosidine of 0.194 mg/kg for guinea-pigs and 3.6 mg/kg for mice was determined (Naude and Potgieter, 1990).

Cumulative Bufadienolides

Cumulative bufadienolides can cause acute cardiac glycoside poisoning but are also considered neurotoxic, causing krimpsiekte when ingested in small doses over a period of time. The cumulative nature of these bufadienolides might be contributed to their stereochemistry. The cumulative bufadienolides isolated from Crassulaceae had

sugar moieties strongly bonded to their aglycone moieties, laevorotatory sugars attached to the C3 position and most had an unusual epoxy-group at position C7,8 (Botha, 2016). Three compounds were isolated from *K. lanceolata* including the cumulative bufadienolides lanceotoxin A (K28A) and lanceotoxin B (K28B) (Anderson et al., 1983b). Lanceotoxin B (MW: 604.693 g/mol) (**Figure 2**) represents the first characterisation of a *5*-O-acetylhellebrigenin (Anderson et al., 1984). Anderson et al. (1983) managed to induce krimpsiekte in sheep by administering small doses of lanceotoxin A and lanceotoxin B intravenously (Anderson et al., 1983b). The acute subcutaneous LD_{50} of lanceotoxin B was 0.10 mg/kg in guinea-pigs (Anderson et al., 1983b).
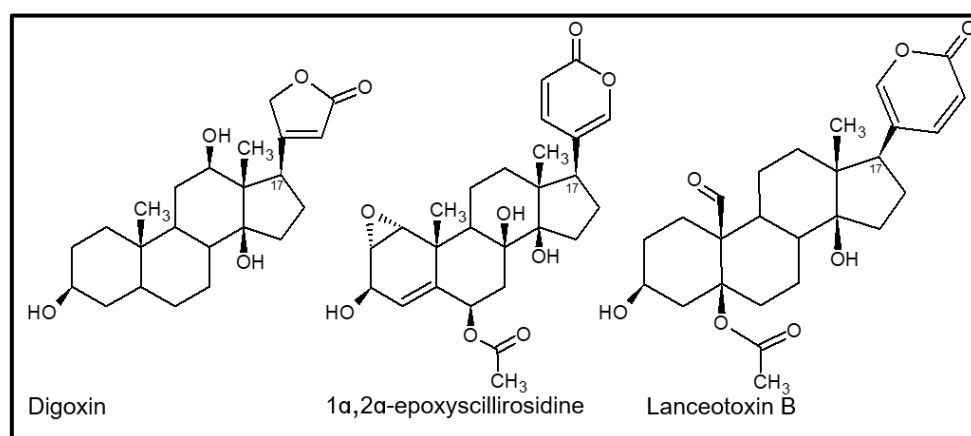
Figure 2 The aglycone structure of the cardiac glycosides i.e. the cardenolide (digoxin), the non-cumulative bufadienolide (1α,2α-epoxyscillirosidine) and the cumulative bufadienolide (lanceotoxin B).

2.1.3 Toxicokinetics

Depending on the specific type of cardiac glycoside ingested, the absorption, metabolism and excretion may vary. The absorption of the different cardiac glycosides from the gastrointestinal tract range from zero to nearly 100% (Katzung et al., 2004). Microorganisms living in the rumen of livestock can break down cardiac glycosides. When given a high enough dose, cardiac glycosides are absorbed at a rate exceeding that at which the microorganisms can inactivate the molecules, leading to cardiac glycoside intoxication. Once the cardiac glycoside is in the blood, it is distributed to all tissues even crossing the blood-brain barrier entering the central nervous system (Kellerman et al., 2005). The rates at which the cardiac glycosides are metabolised and excreted depend on the cardiac glycoside itself. Some cardiac glycosides, such as digoxin, are not extensively metabolised and excreted unchanged by the kidneys (Katzung et al., 2004).

2.1.4 Mechanism of action

The Na^+/K^+-ATPase [EC 3.6.3.9] is the only known receptor of cardiac glycosides. A cell usually maintains an electrochemical gradient across its plasma membrane, using the Na^+/K^+-ATPase to keep the intracellular potassium concentration high and the intracellular sodium concentration low. In contrast to the ion concentration inside the cell, the extracellular concentration of potassium is kept low, while the sodium concentration is kept high. The Na^+/K^+-ATPase uses the energy released by the hydrolysis of an adenosine triphosphate (ATP) molecule to transport three Na^+ ions out and two K^+ ions into the cell (Lodish, 2012). Many cellular functions such as cell volume, pH and free calcium is directly and indirectly regulated by the Na^+/K^+-ATPase and the Na^+ gradient is used as a source of energy for transporting various ions and solutes. The action potential of nerve and muscle cells also depend on the Na^+/K^+-ATPase.

Cardiac glycosides inhibit the Na^+/K^+-ATPase, preventing the transport of Na^+ and K^+ ions (**Figure 3**). When the ionic gradient is not actively maintained, the Na^+ and K^+ ions steadily diffuse across the plasma membrane, increasing the intracellular concentration of Na^+ and extracellular concentration of K^+. As a result of the increase in intracellular Na^+, the sodium/calcium-exchanger (Na^+/Ca^{2+}-exchanger), responsible for extruding calcium ions, is inhibited. The Na^+/Ca^{2+}-exchanger transports one Ca^{2+} to the outside of a cell in exchange for transporting three Na^+ into the cell, however its inhibition causes the build-up of intracellular calcium. Increased intracellular calcium causes stronger myocardial contractions and various other secondary effects.
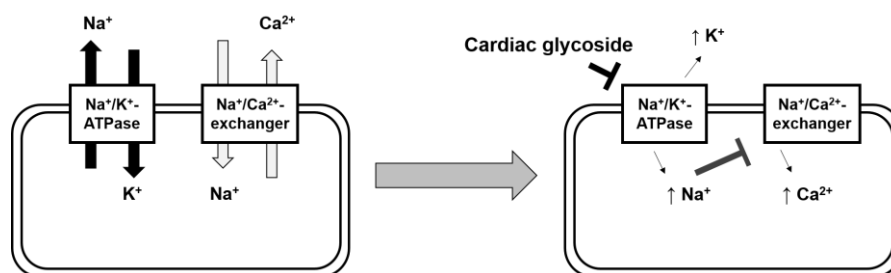
Figure 3 Cardiac glycoside mechanism of action. Cardiac glycosides inhibit the Na^+/K^+-ATPase causing an increase in intracellular sodium and extracellular potassium concentrations. The increased intracellular sodium in turn inhibit the Na^+/Ca^{2+}-exchanger and causes a rise in intracellular calcium.

The mechanism behind the development of krimpsiekte is not yet fully understood. Botha et al. (2002) demonstrated that the cumulative bufadienolides, cotyledoside and

tyledoside F, have a cholinergic effect and could possibly be agonists of post-synaptic nicotinic receptors (Botha et al., 2002).

The Na$^+$/K$^+$-ATPase also acts as a signal transducer for different cellular pathways (Aperia et al., 2016). Cardiac glycoside exposure thus additionally results in non-ionic effects independent of Na$^+$/K$^+$-ATPase inhibition by triggering downstream pathways. These pathways include the Src/Epidermal Growth Factor Receptor (EGFR)/Ras/Mitogen Activated Protein Kinase (MAPK), Phospholipase C (PLC)/ Phosphokinase C (PKC) and Phosphoinositide 3-kinase (PI3K)/Akt signal transduction pathways among others (Riganti et al., 2011). These pathways affect different cellular processes i.e. cell proliferation (Aydemir-Koksoy et al., 2001; Li et al., 2006), cell migration and attachment (Contreras et al., 2004; Contreras et al., 1999), cell metabolism, transcriptional control and cell death (Riganti et al., 2011).

2.1.5 Plants, distribution

2.1.5.1 Plants containing non-cumulative bufadienolides

Moraea ("tulp"), *Drimia* ("slangkop") and *Thesium* ("witstorm") species contain non-cumulative bufadienolides as their active principle and cause acute cardiac glycoside poisoning when ingested by livestock.

Moraea spp. (Iridaceae)

The *Moraea* spp. is the only genus of the plant family Iridaceae that cause cardiac glycoside poisoning in livestock. The species are colloquially referred to as "tulp" but should not be confused with Dutch tulips (*Tulipa gesneriana*) (Vahrmeijer, 1981).

Moraea pallida (yellow "tulp") (**Figure 4a**) is distributed throughout South Africa, excluding the Western Cape, and can also be found in Namibia and Botswana. The plant grows in different soil types, topographical situations and various climatic conditions, but is most often found in the drier western parts of the country (Vahrmeijer, 1981). *M. pallida* sprouts annually from a white, perennial corm buried deep in the ground and can grow up to 40 cm high. The mature plant usually only has one, long, leathery leaf that sheaths the base of the flowering stalk. The flowering period lasts from September to October and during this time a single, branched inflorescence bears six to ten flowers (Vahrmeijer, 1981). The flowers are yellow, star-shaped with six petals. *M. pallida* is very invasive and often incriminated in livestock poisoning (Kellerman et al., 1996).

Moraea miniata (red "tulp") (**Figure 4b**) occurs in the Western and Northern Cape provinces of South Africa and grow in various soil types. It is found in both very dry areas as well as areas with heavy rainfall (Vahrmeijer, 1981). *M. miniata* sprouts from a perennial corm that is covered in dark filaments. The plant has one to four, ribbon-like leaves that sheaths the base of the flowering stalk. The flowering period lasts from August to October (Vahrmeijer, 1981). The flowers are pink with a distinct yellow-shaped mark at the centre and borne on top of a much-branched inflorescence.

Moraea polystachya (blue "tulp") (**Figure 4c**) is widely distributed in South Africa, Botswana and Namibia, growing in open veld, marshy areas and brackish soil (Vahrmeijer, 1981). The plant is highly invasive, found in over-grazed or trampled areas and difficult to eradicate once established. Like the other *Moraea* species, the aerial parts of the plant sprout annually from a perennial corm buried deep in the ground. *M. polystachya* produce one to five (usually four) leaves that sheathes the flowering stalk. The flowering period occurs during autumn and winter, lasting from April to June. The flowers are iris-like and mauve or violet-blue with a yellow mark at the base of the outer petals (Vahrmeijer, 1981).

There are various other *Moraea* species distributed across southern Africa that should be regarded as potentially toxic until proven otherwise (Vahrmeijer, 1981).
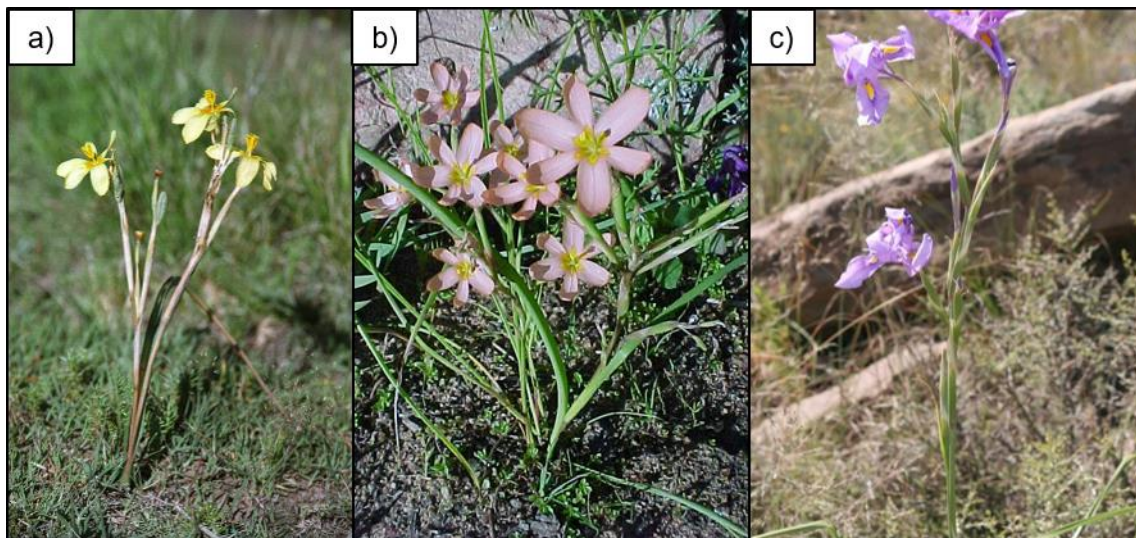
Figure 4 a) *Moraea pallida* (Yellow tulp), b) *Moraea miniata* (Red tulp) and c) *Moraea polystachya* (Bue tulp).

Drimia spp. (Hyacinthaceae)

"Slangkop" is the vernacular name used to describe some of the *Drimia* species and other members of the family Hyacinthaceae, due to the snake-like appearance of the newly emerged flower heads.

Drimia sanguinea ("Transvaal slangkop") (**Figure 5a, b**) is widely distributed throughout southern Africa, growing in a variety of soil types including sandy soil, clay soil and limestone soil (Vahrmeijer, 1981). The plant has a reddish-brown, pear-shaped perennial bulb, enclosed in dark papery scales that is buried just below the surface of the soil. A single flowering stalk emerges annually from the bulb with numerous small white or cream coloured flowers. The flowers are white with a green or brown stripe down the middle of the flower petals. The leaves of *D. sanguinea* appear after the inflorescence and are grey-green in colour. The species is very invasive and is the most important and best known of all the "slangkop" species (Kellerman et al., 2005).

Drimia macrocentra ("Natal slangkop") is distributed along the coast of KwaZulu-Natal and inland up to an altitude of *c.*1000 m (Kellerman et al., 2005). The plant grows on the periphery of marshes and on damp ground in localised patches. *Drimia macrocentra* has a small bulb that is covered in white, fleshy scales. The inflorescence appears in spring and carries star-shaped, lilac-coloured flowers. A single, long, cylindrical leaf is produced after the flowers (Henning, 1932).

Drimia altissima ("Maerman") (**Figure 5c**) is found in the Eastern Cape, KwaZulu-Natal, Mpumalanga and Limpopo provinces, extending upward into Zimbabwe, Kenya and Uganda (Botha and Naudé, 2002). It can be found in a variety of soil types, from peat and loam to sandy soils and stony hills (Vahrmeijer, 1981). The perennial bulbs are white, with a brown outer layer consisting of dead scales. *Drimia altissima* is the tallest of the *Drimia* species. The bulb gives rise to a single inflorescence that can reach up to 2.5 m in length. The flowering period last from October to February and the flowers are white, with a green streak down the middle of each petal (Vahrmeijer, 1981). As with *D. sanguinea and D. macrocentra*, the leaves appear after the flowers and is arranged in a circle at the base of the stem.

Other plants from the family Hyacinthaceae implicated in cardiac glycoside poisoning include *D. depressa* ("Berg slangkop"), *D. physodes*, *Pseudogaltonia clavata* ("groenlelie") and *Merwilla plumbea* ("blouslangkop") (Kellerman et al., 2005).

   Thesium spp. (Santalaceae)
Thesium spp. are root parasites, with *Felicia muricate*, *F. filifolia*, *Chrysocoma ciliata*, *Pteronia sordida* and *Melianthus comosus* serving as hosts to the plant (Vahrmeijer, 1981).

Thesium namaquense (poison bush, "gifbossie") is found in the southern half of Africa, in dry streambeds, open fields and brackish soil (Cheeke, 1989; Vahrmeijer, 1981). The perennial shrub grows up to 1 m high and has many thin, greenish branches. The leaves are reduced, triangular scales. Yellowish-white flowers are borne near the tip of the branches in the leaf-axis and small spherical fruits form after the flowers have been fertilized. The plant has been implicated in small stock losses in the Great Karoo (Cheeke, 1989).

Thesium lineatum ("vaalstorm", "witsorm") (**Figure 5d**) has also been implicated in cardiac glycoside poisoning of livestock (Kellerman et al., 2005).
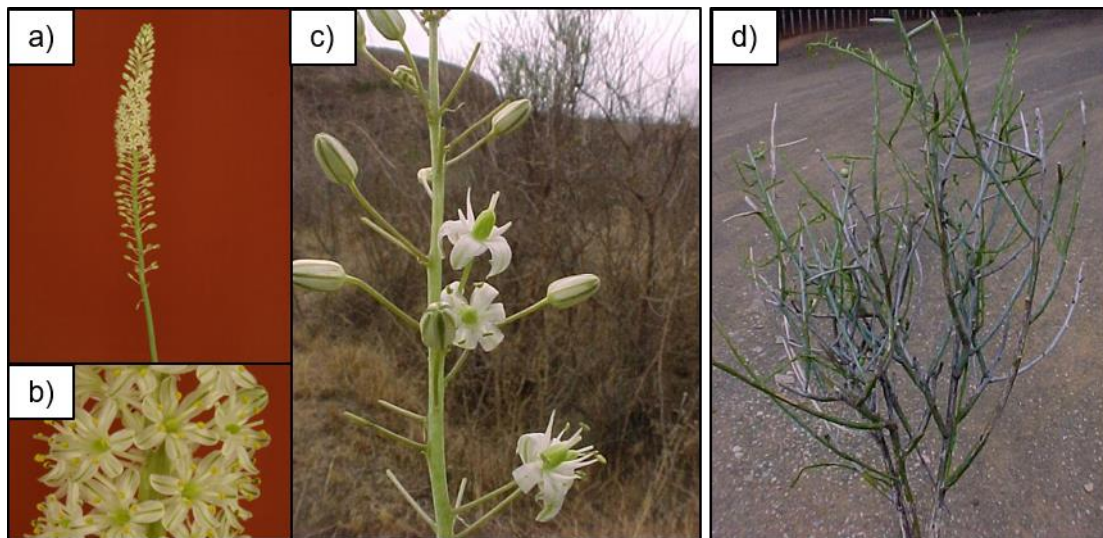
Figure 5 a, b) *Drimia sanguinea* (Transvaal slangkop), c) *Drimia altissima* (Maerman) and d) *Thesium lineatum* (Witstorm).

2.1.5.2 Plants containing cumulative bufadienolides
   Cotyledon, Tylecodon and Kalanchoe spp. (Crassulaceae)
Krimpsiekte is caused by the cumulative, neurotoxic bufadienolides found in some *Cotyledon*, *Tylecodon* and *Kalanchoe* spp., collectively known as "plakkies", from the family Crassulaceae.

Cotyledon orbiculata (pig ears or "hondeoor-plakkie") (**Figure 6a**) is widely distributed in South Africa. The plant prefers sandy soils and rocky slopes. There are different varieties of *C. orbiculata*, such as *C. orbiculata* var. *dactylopsis* and *C. orbiculata* var. *oblonga* (Vahrmeijer, 1981). The plant is a succulent sub-shrub, with a thick stem and grows to about 40 cm high. The leaves are fleshy, round and grey-green surrounded with a red margin. The flowers are pendulous and bell-shaped, varying in colour from light orange-red to dark purple-red.

Tylecodon wallichii (nenta or "kandelaarsbos") (**Figure 6b**) grows in the Western and Northern Cape Provinces and is classified as a xerophyte, growing in well-drained stony and sandy soils (Kellerman et al., 2005; Vahrmeijer, 1981). The plant is a succulent shrubbery that can grow up to half a meter in height with long finger-like leaves. The leaves are grey-green, fleshy and grow at the end of the branches. The flowering period lasts from November to February, with erect, terminal inflorescence bearing the small flowers (Vahrmeijer, 1981). Yellow-green, bell-shaped flowers appear after the leaves have fallen off.

Tylecodon ventricosus ("klipnenta") is wide spread in the Northern, Western and Eastern Cape provinces of South Africa and grows in isolated patches (Botha et al., 1998). The perennial plant has a tuberous base, from which one or more fleshy stems emerge, and has linear or oblanceolate leaves, arranged spirally around the base (Botha et al., 1998; Kellerman et al., 2005). The flowering period last from September to March. A terminally branched peduncle, give rise to flowers born upright in a contracted panicle (Botha et al., 1998; Kellerman et al., 2005). The flowers are yellowish-green, with purple veins.

Tylecodon grandiflorus ("rooisuikerboom") has a fairly restricted distribution, growing mostly in the winter rainfall region of the Cape, on the western slopes of the Cape Peninsula and the mountains northwards along the coast to Clanwilliam (Anderson et al., 1983a). The plant favours sandy soil, rocky hillsides and crevices in granite boulders. *T. grandiflorus* is a semi-succulent, perennial bush, with decumbent stems covered in leaf scars (Anderson et al., 1983a; Kellerman et al., 2005). The leaves are deciduous and spirally arranged at the end of the branches. The flowering period lasts from January to March, after the leaves have fallen off, and an erect, unbranched

inflorescence bears tubular flowers (Kellerman et al., 2005). The colour of the flowers range from orange to red or yellow with red streaks.

Kalanchoe lanceolata (**Figure 6c**) is found in the northern provinces of South Africa, as well as the tropical regions of Africa (Kellerman et al., 2005). It grows in the shade, often in dense communities. The plant is an annual, occasional perennial, succulent that is unbranched and erect, growing up to 1 m in height. The leaves are cupped or boat-shaped, lacking stalks and arranged in alternative pairs (Vahrmeijer, 1981). The inflorescence bears star-shaped, four-merous flowers that are apricot or yellow in colour.
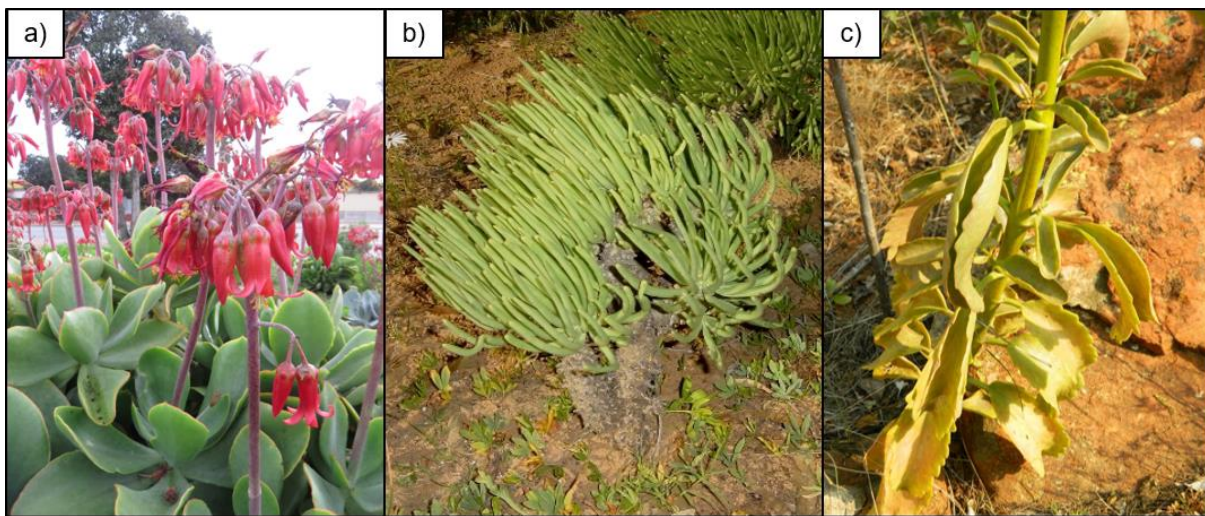
Figure 6 a) *Cotyledon orbiculata*, b) *Tylecodon wallichii* and c) *Kalanchoe lanceolata* collectively known as "plakkies".

2.1.5.3 Plants containing cardenolides

Cardenolide containing plants are of lesser veterinary importance as they are only occasionally involved in poisoning of livestock. Compared to other plant families, the plant family Apocynaceae has the greatest number of cardenolide containing plants. The family contains more than half of the 55 cardenolide containing genera, including the *Gomphocarpus* and *Strophanthus* genera which has the most cardenolide bearing species (Krishna et al., 2015).

Nerium spp. (Apocynaceae)

Nerium oleander (oleander/ "selonsroos") (**Figure 7a**) is indigenous to eastern Europe and Asia and is often grown as ornamental plants in South Africa. The plant is a much-branched shrub that can grow up to 5 m high (Vahrmeijer, 1981). The leaves are narrow, leathery and stiff, with parallel venation and arranged in whorls of three (Kellerman et al., 2005). Flowers are produced at the tip of the branches and come in

various colour varieties (dark red, pink or white). All parts of the plant are poisonous and produce a watery latex. *Thevetia peruviana* (yellow oleander) is from the same family as *N. oleander* and cause poisoning under similar circumstances (Kellerman et al., 2005).

Gomphocarpus spp. (Apocynaceae)
Gomphocarpus fruticosus (milkweed/"melkbos") (**Figure 7b**) is indigenous to South Africa and occurs throughout the country, especially on disturbed soil and alongside roads or waterways (Vahrmeijer, 1981). The shrub grows up to 1.5 m high, with cylindrical, grey green stems that are covered in fine hair and narrow, oblong leaves that are alternatively arranged. The flowering period lasts from October to April and flowers are born at the tip of the branches, in dense clusters. The flowers are white to yellowish-green and hang face down. The distinct fruits are inflated and balloon-like, with hair-like processes. When damaged the plant secretes white latex (Kellerman et al., 2005; Vahrmeijer, 1981).

Acokanthera spp. (Apocynaceae)
Acokanthera oblongifolia is found near the coast of the Eastern Cape Province to Mozambique and is often planted in gardens (Henning, 1932). The evergreen shrub or tree can grow up to 6 m high and has thick, leathery, dark-green leaves that can be described as broadly elliptic (Vahrmeijer, 1981). The flowering period lasts from July to November and the flowers appear in dense clusters, among the leaves near the tip of the branches (Vahrmeijer, 1981). *A. oppositfolia* is similar to *A. oblongifolia* but smaller and with shorter flowers, found in the dry bushveld of the former Transvaal and along the east coast.

There are various other cardenolide containing plants such as *Strophanthus* spp. (poison rope, "giftou"), *Cryptostegia grandiflora* (rubber vine) and *Adenium multiflorum* (Impala lily) (Kellerman et al., 2005).

Figure 7 a) *Nerium oleander* (Selonsroos) and b) *Gomphocarpus fruticosus* (Milkweed).

2.1.6 Species affected

Cardiac glycoside poisoning often occurs in newly introduced, young and naïve animals (Kellerman et al., 1996). Hungry stock is at risk of being poisoned, especially in winter before the rains, when there is little greenery available. Cardiac glycosides-containing plants are generally unpalatable to stock and can induce a strong aversion, so animals that grow up with exposure to these plants usually learn to avoid them (Kellerman et al., 1996). Stock can be poisoned when consuming contaminated hay or fodder as cardiac glycosides-containing plants retain their toxicity after desiccation. Horses are not poisoned as often as other stock, due to them being fastidious grazers and avoiding the plant.

Not many cases of cardenolide poisoning have been reported in South Africa, since cardenolide-containing plants are seldom eaten by stock, leading to a lack in available literature on the subject. Cases of accidental and experimental oleander poisoning have been reported in cattle (Aslani and Rezakhani, 2000; Mahin et al., 1984; Rezakhani and Maham, 1992; Wilson, 1909), horses (Hughes et al., 2002; Renier et al., 2013; Wilson, 1909), goats (Aslani et al., 2007), sheep (Aslani et al., 2004; Wilson, 1909), donkeys (Renier et al., 2013; Smith et al., 2003; Wilson, 1909), cats and dogs (Milewski and Khan, 2006). *C. grandiflora* is poisonous to sheep, goats, cattle and especially horses (Cook et al., 1990; McGavin, 1969; WT. Parsons, 2001). Elephants have also reportedly been poisoned by *C. grandiflora* (Brain, 1994). *Acokanthera* species have been implicated in poisoning of sheep, goats, donkeys, ostriches and cattle, with cattle being the most commonly affected (Henning, 1932).

Different from cardenolide-containing plants, bufadienolide-containing plants are frequently responsible for poisoning in livestock. All animals are susceptible to "tulp" poisoning, but under natural conditions sheep, goats and cattle are more likely to be

poisoned, with cattle being most often affected (Henning, 1932; Kellerman et al., 1996; Steyn, 1928). *D. sanguinea* generally affect sheep and goats, while *D. macrocentra* generally affect cattle (Henning, 1932). As with "tulp" poisoning, all animals are susceptible to "slangkop" poisoning, but most remain unaffected due to avoiding the plant (Henning, 1932). *Thesium namaquense* mostly cause poisoning in sheep, but can also cause stock losses in goats and cattle (Cheeke, 1989; Vahrmeijer, 1981).

Krimpsiekte is primarily a disease of small stock, although all animals are susceptible (Henning, 1932; Kellerman et al., 1996). The highest incidence of the disease occurs in goats, with Angora goats reportedly more inclined to the disease compared to Boer goats. Krimpsiekte does not often occur in cattle and horses under natural conditions. Secondary intoxication can occur, especially in dogs, when fed the carcass or entrails of an animal that has died of krimpsiekte (Henning, 1932; Kellerman et al., 2005).

2.1.7 Clinical signs, acute and chronic

Clinical signs of acute cardiac glycoside poisoning (**Figure 8a**) vary depending on the type and quantity of the plant ingested, but signs are generally exclusive to the cardiovascular, gastrointestinal, respiratory and nervous systems.

At therapeutic doses cardiac glycosides have a positive inotropic and negative chronotropic effect, causing stronger myocardial contraction and bradycardia respectively (Kellerman et al., 2005). At higher doses the toxin has a negative dromotropic effect, eventually causing atrioventricular dissociation leading to first, second and third-degree heart-block (Kellerman et al., 2005). The heart rate of intoxicated animals increases after the initial bradycardia, proceeding to sinus tachycardia with periods of ventricular tachycardia (Button et al., 1983; Gunn, 1924). Severe arrhythmia occurs, leading to complete atrioventricular dissociation and fibrillation (Button et al., 1983; Gunn, 1924). Due to the increased extracellular potassium concentration, hyperkalaemia arises, which also contributes to bradycardia (Joubert, 1982a). Affected animals should not be stressed, as even the slightest exertion can cause cardiac arrest and sudden death. A loss of appetite, ruminal stasis and colic are commonly seen in intoxicated animals (Joubert, 1982a, b; Nel et al., 1987). Diarrhoea, with liquid faeces, is almost always observed (Joubert, 1982a, b; Nel et al., 1987). There is often blood and shreds of the mucosal lining within the faeces (Mitchell et al., 1934). Instead of diarrhoea, constipation is observed in animals poisoned by *M. miniata* (Button et al., 1983; Vahrmeijer, 1981). Animals might show

signs of tympany and gassy-bloat, which can be alleviated by trocar (Henning, 1932; Kellerman et al., 2005). The animal might be dehydrated, but drinking water aggravates the symptoms. Animals are weak, depressed and apathetic, standing with their heads down (Joubert, 1982b). Other signs include posterior paresis; the animal walks with a swaying gait and is uncoordinated, easily loosing balance (Henning, 1932; Kellerman et al., 2005; Vahrmeijer, 1981). Hypersensitivity, muscle spasms and torticollis are also observed in poisoned animals (Naude and Potgieter, 1990). The respiratory distress experienced by intoxicated animals is believed to be neuromuscular in origin. It is noted that breathing may appear laborious, rapid and irregular with bouts of apnoea (Button et al., 1983; Naudé, 1990). After a lethal dose is administered, death might occur within a few hours or might be delayed to a couple of days before the animal collapses and dies (Button et al., 1983; Henning, 1932; Joubert, 1982a, b).

During chronic intoxication the cardiovascular, gastrointestinal and respiratory signs are diminished, and nervous system signs dominate. The name krimpsiekte is derived from the pose taken by affected animals, with their head down, back arched and feet together (**Figure 8b**). When the animal is subjected to lethal doses, death might occur before the onset of symptoms. The characteristic signs of chronic intoxication only appear gradually after the animal was exposed to sub-lethal doses or after surviving a relatively high dose (Botha et al., 1998; Henning, 1932). Exercise and direct sunlight cause the symptoms to escalate and hasten death (Henning, 1932; Kellerman et al., 2005). Intoxicated animals tire easily, lags behind the flock and is reluctant to stand (Anderson et al., 1983a). Frequent mouthing movements and excessive salivation can be seen, with the animal periodically protruding its tongue (Henning, 1932; Tustin, 1984). Chronic intoxication causes the muscles to twitch, later progressing to clonic spasms. The head, neck and back muscles are affected causing torticollis, which can last for months or years (Vahrmeijer, 1981). The animal's appetite remains good, but due to the losing control of the muscles of mastication, eating becomes difficult and the food collects at the back of the mouth (Henning, 1932). As the disease develops, breathing becomes laborious and irregular and the animal has a fast pulse (Anderson et al., 1983a; Botha et al., 1998). The animal retains consciousness until the end.
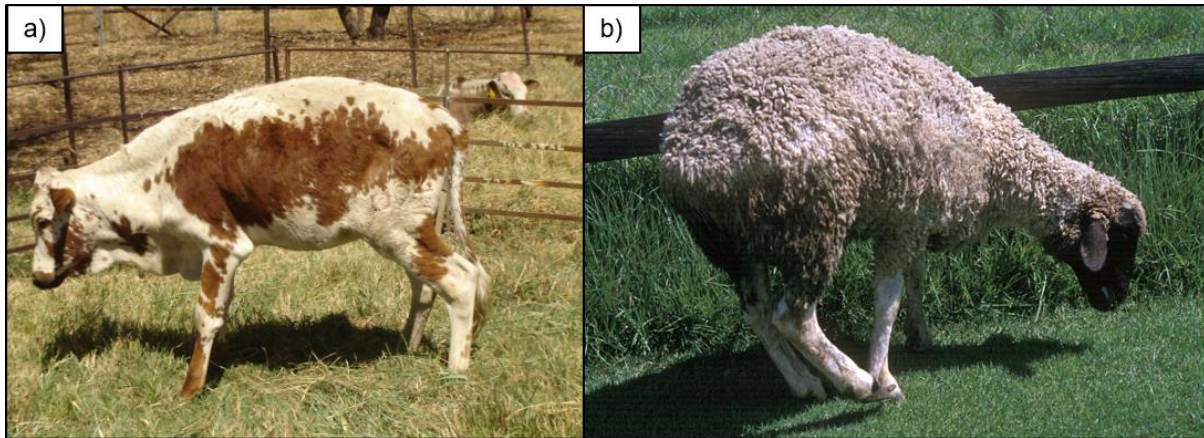
Figure 8 a) A heifer affected by acute cardiac glycoside poisoning and b) a sheep affected by krimpsiekte.

2.2 Cytotoxicity studies

In vitro studies are an important part of research, helping us to understand, amongst other things, the underlying mechanisms behind cell death. The term '*in vitro'* means 'within the glass' and refers to experiments carried out in a controlled environment. Unfortunately, due to being controlled the environment differs to that of normal biological systems and thus the results obtained from *in vitro* studies are not always an accurate representation of what really occur. It is difficult to mimic *in vivo* pharmacokinetics of absorption, distribution, binding, metabolism and excretion of compounds in cell culture studies (Freshney, 2001). Within an animal or human, several types of cells interact with each other and the extracellular matrix, forming tissues, organs and complete organisms. The complex interplay is lacking in most *in vitro* studies, where cell cultures consist of only one type of cell. Another limitation of cultured cells, especially cells in continuous culture, is their genetic instability, since selection pressure can cause cells to diverge completely from the original cell type (Freshney, 2001). Nevertheless, the simplification of the system in question allows for more focused, convenient and detailed analysis that would not be possible with studies focusing on the whole organism. In *in vitro* cytotoxicity studies, the concentration and exposure time of a compound can be controlled more precisely compared to *in vivo* studies, increasing the consistency and reproducibility of data obtained (Freshney, 2001). *In vitro* assays also have the advantage of being cost-effective, while the set-up and analysis are relatively simple and straightforward.

In vitro cytotoxicity assays determine the toxic potential of a compound or plant extract and are the first step in confirming the toxin's mechanism of action. A compound can be considered cytotoxic if it alters cellular morphology, negatively affects cell-surface attachment, growth and proliferation or causes cell death and disintegration (Horvath, 1980). According to the Nomenclature Committee on Cell Death (NCCD) a cell is dead only when the integrity of the cell plasma membrane has been lost; the cell has completely fragmented into apoptotic bodies; or the cell has been phagocytosed by adjacent cells (Kroemer et al., 2009). Historically, cell death has been classified into three forms based on morphological criteria, namely apoptosis (type I cell death), autophagy (type II cell death) and necrosis (type III cell death). Despite the various limitations, morphological classification is still of use today and, combined with molecular classification, allows us to describe the various pathways by which a cell meets its end.

2.2.1 Apoptosis (type I cell death)

Apoptosis is a highly regulated, energy-dependent process involving a complex cascade of events that plays a critical role in embryogenesis, regulation of cell populations and removal of damaged cells (Elmore, 2007; Renehan et al., 2001). Abnormal levels of apoptosis lead to pathological conditions such as autoimmune disease, neurological degeneration, developmental defects and cancer (Elmore, 2007).

Apoptotic cells can be identified by light and electron microscopy based on their distinct morphology. The cytoplasm and the nucleus of apoptotic cells condense, followed by nuclear fragmentation (karyorrhexis) and blebbing of the plasma membrane, finally forming apoptotic bodies (Kerr et al., 1972). Cell shrinkage causes the cell to appear round or oval, with densely packed cytoplasmic organelles. Nuclear condensation or pyknosis is a characteristic feature of apoptosis and nuclear material can be seen condensed peripherally under the nuclear membrane or as uniformly dense nuclei (Elmore, 2007). Apoptotic bodies, consisting of closely packed organelles, with or without nuclear fragments and surrounded by an intact plasma membrane, is released from the cell and engulfed by neighbouring phagocytic cells (Kerr et al., 1972).

Apoptosis is induced by either the extrinsic (death receptor) or the intrinsic (mitochondrial) pathway, both of which converge at the executioner pathway (**Figure 9**).

The extrinsic pathway is initiated through transmembrane receptor mediated interaction. A group of receptors from the tumour necrosis factor (TNF) receptor gene superfamily contains a cytoplasmic 'death domain' responsible for transmitting a death signal from the surface of the cell (Ashkenazi and Dixit, 1998; Smith et al., 1994). Upon ligand binding, the death receptor recruits and binds an adapter protein with a corresponding death domain. The adapter protein associates with procaspase-8 via dimerization of the death effector domain. A death inducing signalling complex (DISC) is formed, resulting in the activation of procaspase-8 by autocatalysis (Kischkel et al., 1995). The activation of caspase-8 leads to the activation of the executioner pathway.

The intrinsic pathway involves a diverse range of non-receptor mediated stimuli which act in either a positive or negative manner to generate intracellular signals (Elmore, 2007). The absence of certain growth factors, hormones or cytokines may cause failure to regulate death programmes, negatively regulating apoptosis. Stimuli such as radiation, toxins, hypoxia, etc. act in a positive manner, causing apoptosis. The signals generated by the various stimuli act on the inner mitochondrial membrane, causing the opening of the mitochondrial permeability transition (MPT) pore. The subsequent loss of mitochondrial membrane potential leads to the release of pro-apoptotic proteins, including cytochrome c (Raff, 1998). Cytochrome c binds to Apaf1 and procaspase-9 forming a complex known as an 'apoptosome' (Saelens et al., 2004). The formation of the apoptosome in turn leads to the activation of caspase-9 and triggers the executioner pathway. Mitochondrial membrane permeability is regulated by members if the Bcl-2 protein family that can be either pro-apoptotic or anti-apoptotic (Saelens et al., 2004).

 An additional induction pathway known as the perforin/granzyme pathway involves T-cell mediated cytotoxicity and perforin-granzyme dependent killing of cells (Elmore, 2007).

The initiation pathways converge at the execution pathway, which involve the cleavage of execution caspases (e.g. caspase-3), resulting in deoxyribonucleic acid (DNA) cleavage, degradation of nuclear and cytoskeletal proteins, cross-linking of proteins,

formation of apoptotic bodies and externalisation of phosphatidyl serine (Elmore, 2007). The final stage of apoptosis is phagocytosis of the apoptotic cell. Apoptotic bodies are engulfed by neighbouring phagocytic cells such as macrophages *in vivo;* thereby the inflammatory response is reduced as the cells do not release their constituents into the surrounding environment. During *in vitro* studies apoptotic bodies are not phagocytosed and eventually cells enter secondary necrosis.

Cells dying via apoptosis can be determined through a variety of methods based on their morphological, biochemical and molecular characteristics. Electron microscopy is often used to inspect dying cells for the classical features of apoptosis. Additionally, techniques such as those measuring caspase activation, phosphatidyl serine externalisation, DNA fragmentation etc. can be used to identify apoptotic cells biochemically.
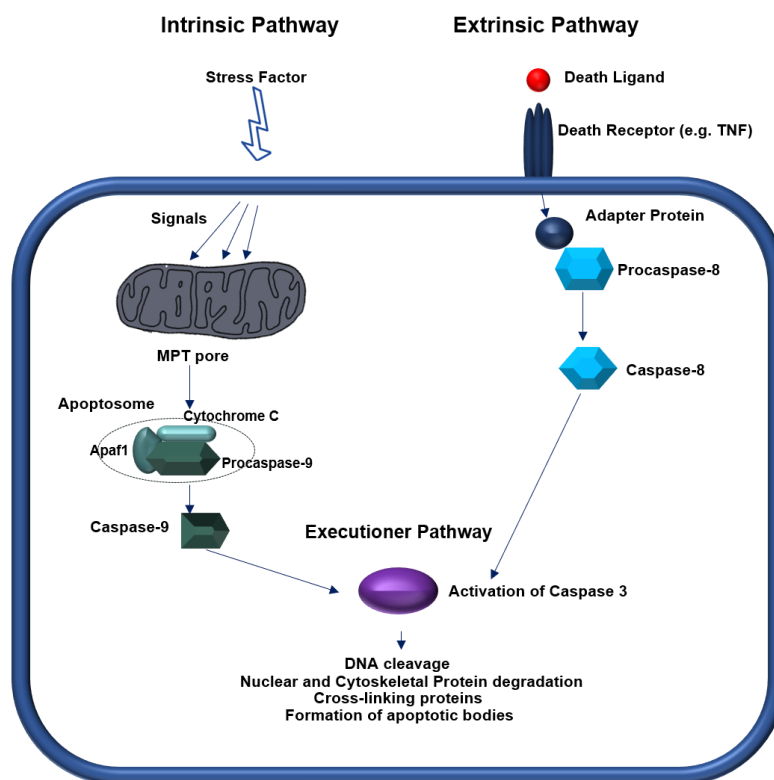
Figure 9 A schematic presentation illustrating the intrinsic and extrinsic apoptotic pathway. The intrinsic apoptotic pathway is triggered through various stimuli resulting in the occurrence of mitochondrial permeability transition that allows the release of pro-apoptotic proteins from the mitochondria. These proteins form a complex known as the apoptosome that activates caspase-9, which in turn, leads to the executioner pathway. The extrinsic pathway is triggered by the binding of a death ligand to a death receptor, causing the recruitment of an adapter protein and the activation of caspase-8. This then leads to the executioner pathway and the various signs of apoptosis.

2.2.2 Autophagy (type II cell death)

Autophagic cell death is morphologically defined as a type of cell death accompanied by extensive autophagic vacuolisation of the cytoplasm, while chromatin condensation is absent (Kroemer et al., 2009). However, the term 'autophagic cell death' is a misnomer since it is most often used to describe cell death with autophagy as oppose to cell death by autophagy (Kroemer and Levine, 2008). In macroautophagy (referred to as "autophagy" from now on), cellular material is sequestered in a double membraned structure called the autophagosome (Yonekawa and Thorburn, 2013). The autophagosome fuse with lysosomes forming the autolysosome, a single membrane structure containing degenerating organelles. Autophagy is a physiological process that assists with cell survival during starvation, growth factor depravation and other stress conditions by recycling nutrients, maintaining energy homeostasis and degrading toxic cellular contents (Kroemer and Levine, 2008). The high levels of autophagy in apoptotic and necrotic cells can be considered a 'self-clearance' mechanism and is essential for the removal of dead cells (Levine and Yuan, 2005; Qu et al., 2007).

Liu et al. (2015) described an autophagic cell death termed autosis, with distinct morphological featured and which is mediated by the Na^+/K^+-ATPase (Liu and Levine, 2015). Autosis is characterised by enhanced cell-substrate adherence; swelling, fragmentation and disappearance of the endoplasmic reticulum (ER); twisting of the nuclear membrane and focal swelling of the perinuclear space.

Autophagy can be clearly identified using transmission electron microscopy, however molecular techniques are required to determine whether cells die via the autophagic death pathway. A cell can be defined as dying via autophagy if genetic manipulation of at least two distinct autophagic regulators/genes such as AMBRA1, ATG5, ATG12 or beclin 1 inhibits cell death (Galluzzi et al., 2012).

2.2.3 Necrosis (type III cell death)

Historically necrosis was believed to be an accidental, uncontrolled form of cell death; however, more recent evidence suggest that the process of necrosis is in fact regulated by various signal transduction pathways and catabolic mechanisms (Festjens et al., 2006; Golstein and Kroemer, 2007). Cells undergoing necrosis are characterised by an increase in cell volume (oncosis); swelling of organelles such as the ER, Golgi apparatus and mitochondria; permeabilization of the plasma membrane;

and finally, loss of cellular content (Kroemer et al., 2009). Necrosis is often associated with inflammation *in vivo*, since upon lysis the constituent of the cell is released into the surrounding tissues. Several other processes have also been linked to necrosis including production of reactive oxygen species by mitochondria, ATP depletion, Ca^{2+} overload, perinuclear clustering of organelles, activation of non-apoptotic proteases and lysosomal rupture (Golstein and Kroemer, 2007). Biochemically necrosis is defined as cell death lacking apoptotic or autophagic markers.

As with apoptosis, necrosis can be determined through studying the morphology of the cells using electron microscopy. Additionally, assays such as the LDH assay and propidium iodide staining can be used to identify necrotic cells.

Chapter 3 Materials and Methods

3.1 Cell culture maintenance

The cell lines used in this study i.e. H9c2(2-1) (ATCC® CRL-1446™) (**Figure 10a**) and Neuro-2a (ATCC® CCL-131™) (**Figure 10b**) were obtained from the American Type Culture Collection (ATCC). All cultures were grown in HyClone Dulbecco's Modified Eagle Medium (DMEM)-High Glucose media, supplemented with 10% Gibco foetal bovine serum (FBS); 100 U/ml penicillin and 100 U/ml streptomycin (complete medium) from Lonza. The adherent cells were cultured in T_{75} flasks and harvested using a trypsin (170 U/L)-EDTA (200 mg/L) solution (Lonza). All cultures were maintained in an incubator at 37 ºC with a humidified atmosphere of 5% CO_2. The passage number for both cell lines were kept below 25 and used between passage 18 and 25 for the H9c2 cell line and between passage 10 and 25 for the Neuro-2a cell line, for all experiments.
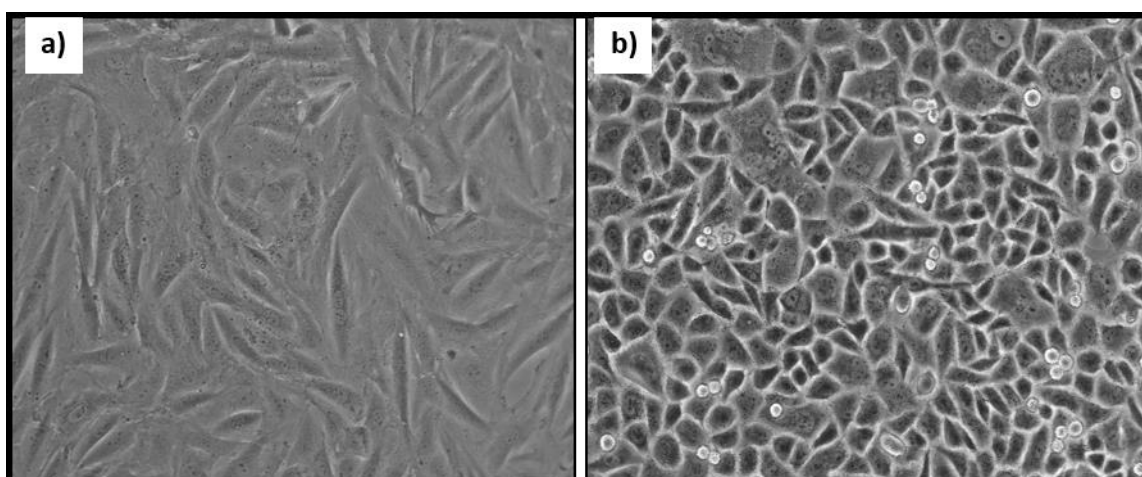
Figure 10 Confluent cultures of H9c2 (a) and Neuro-2a (b) cells at a 100X magnification.

3.2 Cardiac glycosides

The cardiac glycosides, 1α,2α-epoxyscillirosidine and lanceotoxin B, were previously isolated by Dr Anderson from plant material of *M. pallida* and *K. lanceolata* respectively. The toxins are part of the natural toxin collection of the Department of Paraclinical Sciences, Faculty of Veterinary Science, Onderstepoort and have been kept in a dried form, in the dark, in a locked safe. Two batches of 1α,2α-epoxyscillirosidine, with different grades of purity, were used during the course of this project due to the stock of the first batch being depleted. The first batch of 1α,2α-epoxyscillirosidine with a higher purity grade was used for the MTT assays and TEM

analysis. The second batch with the lower purity grade compared to the first batch was used for the SEM analysis. Digoxin was obtained from Sigma-Aldrich. The stock solutions of 1α,2α-epoxyscillirosidine were prepared by solubilizing the compound in a 1:1 acetone complete HyClone DMEM media mixture. The stock solutions of digoxin and lanceotoxin B were prepared in dimethyl sulfoxide (DMSO) by sonication for 1 min.

3.3 Thin layer chromatography

Thin layer chromatography (TLC) was used to evaluate the purity of the cardiac glycosides isolated by Dr Anderson. The compounds were dissolved in acetone and spotted on a TLC plate (TLC Silica gel 60 F_{254} from Merck), before being developed in the mobile phase in a glass chamber. The mobile phase consisted of 90% ethyl acetate (from Merck) and 10% ethanol. The retention factor (R_f) was calculated by dividing the distance travelled by the compound with the distance travelled by the solvent front. The plate was first visualised using ultraviolet (UV) light (350 µm) and then dipped in a potassium permanganate solution. In addition, the second batch of 1α,2α-epoxyscillirosidine was also developed using 98% ethyl acetate and 2% methanol as a mobile phase and the plates were visualised by spraying either vanillin or an ethanol/sulphuric acid solution.

The solutions were made up as follows:

Potassium permanganate solution: Dissolve 1.5 g $KMnO_4$, 10 g K_2CO_3 and 1.25 ml 10% NaOH in 200 ml water.

Vanillin solution: Dissolve 0.1 g vanillin in 28 ml methanol and 1 ml sulphuric acid.

Ethanol/sulphuric acid solution: 95% ethanol and 5% sulphuric acid.

3.4 MTT assay

The MTT assay was first described by Mosmann et al.1983 (Mosmann, 1983). The assay is based on the ability of viable cells to reduce the yellow water-soluble tetrazolium salt, MTT to a purple, insoluble formazan. The half maximal effective concentrations (EC_{50}) of digoxin, 1α,2α-epoxyscillirosidine and lanceotoxin B on H9c2 and Neuro-2a cells, respectively, were determined for exposure times of 24, 48 and 72 h. Twenty four hours prior to the commencement of the exposure study, the cells were seeded into a 96-well cell culture treated plate at a concentration of 1×10^4 H9c2 cells/well and 5×10^3 Neuro-2a cells/well respectively, allowing sufficient time for the

cells to adhere to the surface of the plate and recover. After the initial incubation, the cells were exposed to a 2x serial dilution of the different cardiac glycoside solutions after which the plates were incubated for 24, 48 or 72 h. The cytotoxicity of digoxin and lanceotoxin B on both cell lines were tested over a range of 0.4 to 100 µM and 0.8 to 200 µM, respectively. The 1α,2α-epoxyscillirosidine concentrations tested ranged between 1.6 to 400 µM for H9c2 cells and 7.8 to 2000 µM for Neuro-2a cells. The percentage solvent was kept constant for each dilution at 0.5% solvent/well. The controls used for each assay included two solvent controls of 0.5% acetone and DMSO respectively, a positive control of 20 µM doxorubicin (doxorubicin hydrochloride from Pfizer), a negative control consisting of cells and media and a blank with only media.

At the end of the exposure time, each well was washed with 200 µl phosphate buffered saline (PBS), before adding 200 µl complete DMEM and 20 µl of 0.005 g/ml Thiazolyl Blue Tetrazolium Bromide (dissolved in PBS) from Sigma. The plates were incubated in the dark at 37 ºC for a further 2 h, after which 100 µl DMSO was added to each well and the plates shaken gently for 10 min on a microplate shaker to solubilize the formazan. The absorbance of the reduced MTT product (formazan) was measured at 570 nm and the background at 630 nm using a Synergy HT BioTek microplate reader. The results were analysed on Office Excel (365) and GraphPad Prism (version 6.0). The cell viability was calculated as percentage absorbance measured, relative to the absorbance of the solvent control with the background and medium absorbance subtracted (see below). All assays were carried out in triplicate for at least three biological repeats.

$$\% \, Cell \, survival = \frac{Viable \, cells^{(Ab \, 570 \, nm - Ab \, 630 \, nm)} - Media^{(Ab \, 570 \, nm - Ab \, 630 \, nm)}}{Solvent \, control^{(Ab \, 570 \, nm - Ab \, 630 \, nm)} - Media^{(Ab \, 570 \, nm - Ab \, 630 \, nm)}} \times 100$$

3.5 Statistical analysis

The data obtained was analysed using GraphPad Prism (version 6.0) and Microsoft Office Excel 365. The replicates of all biological repeats were grouped together, and the outliers were removed. The following equation was used to remove the outliers: Lower bound = [Quartile 1 - (Inter Quartile range x 1.5)]; Upper bound = [Quartile 3 + (Inter Quartile range x 1.5)]. All values that did not fall within this range was excluded as outliers. After the outliers were removed, the D'Agostino & Pearson omnibus

normality test as well as the Shapiro-Wilk normality test was used to confirm whether data was normally distributed. The Brown-Forsythe test and Bartlett's test was used to determine whether the variation between data sets differed. After confirming that the data was both normally distributed and had homogeneous variance, a factorial analysis of variance (ANOVA) test was used to analyse the data. The ANOVA test was used to see whether the EC_{50}s of digoxin, 1α,2α-epoxyscillirosidine and lanceotoxin B differed at the 5% level of significance after 24, 48 and 72 h incubation. In the event that the ANOVA picked up a significant difference between the means of the data sets, an unpaired, two tailed t-test was used. Since the Neuro-2a and H9c2 cell lines originate from different species, the values from the different cell lines were not compared.

The 95% confidence interval (CI) was calculated using the following equation:

$$95\% \; CI \; = Average \; cell \; survival \; at \; highest \; tested \; conc. \pm (1.96 \; \times SEM)$$

3.6 Transmission electron microscopy

The effect of the different cardiac glycosides on H9c2 and Neuro-2a cell ultrastructure were investigated using transmission electron microscopy. The cells were seeded into a 6-well plate at a concentration of 1 x 10^5 cells/well for both H9c2 and Neuro-2a cell lines. After 24 h, the cells were exposed to 5, 25 and 100 µM of digoxin, 1α,2α-epoxyscillirosidine and lanceotoxin B and incubated for 24, 48 and 72 h.

After termination of the exposure, the medium was carefully removed from the wells and replaced with 2.5% glutaraldehyde in 0.075 M sodium phosphate buffer ($NaPO_4$, pH 7.4) for 1 h. The cells were scraped from the well surface and added to a 2 ml microtube, before being spun down at 950 x g. After rinsing the cell pellets three times for 10 min at a time in 0.075 M phosphate buffer, they were post-fixed for 1 h with 1% osmium tetroxide (OsO_4) and rinsed again with 0.075 M phosphate buffer for 10 min. The samples were then dehydrated with increasing concentrations i.e. 30%, 50%, 70%, 90% and 100% ethanol. Dehydration in 100% ethanol was done three times. Samples were imbedded in TAAB 812 epoxy resin (Luft, 1961) and sectioned using an ultra-microtome Leica EM UC7. Each section was contrasted with a 2% aqueous uranyl acetate for 10 min and lead citrate for 2 min (Reynolds, 1963). The sections were examined using a Philips CM10 Transmission Electron Microscope.

3.7 Scanning electron microscopy

A 24 well-plate containing coverslips, were seeded with H9c2 and Neuro-2a cells at a concentration of 6x10^4 cells/well for both cell lines. The cells were allowed 24 h to attach to the coverslips, then exposed to a 100 µM of digoxin, 1α,2α-epoxyscillirosidine and lanceotoxin B for 24 and 48 h. After termination of the exposure, the cells were fixed with glutaraldehyde. The coverslips were then removed from the wells and prepared following the same method as the TEM preparation, up to the dehydration step with 100% ethanol. The coverslips were then treated with hexamethyldisilazane (HDMS) (Araujo et al., 2003) and air dried, before being mounted on aluminium studs and made conductive by exposing them to ruthenium tetroxide (RuO$_4$) vapour for 30 min in a sealed environment. The coverslips were examined using a Zeiss Ultra FEG scanning electron microscope.

Chapter 4 Results

4.1 Thin layer chromatography of the cardiac glycosides

The purity of the cardiac glycosides isolated by Dr Anderson was evaluated using TLC. The compounds were spotted on an aluminium silica plate (stationary phase) and run using 90% ethyl acetate and 10% ethanol solution (mobile phase). The plate was visualised first by UV, followed by developing the plate in a potassium permanganate solution.

Two batches of 1α,2α-epoxyscillirosidine, with different purity grades, were tested. When run on the TLC plate, the first batch 1α,2α-epoxyscillirosidine (**Figure 11 no.1**) had a clear spot with a R_f value of 0.84 (black). This spot could be seen under UV light and when visualised with the potassium permanganate solution and assumed to represent 1α,2α-epoxyscillirosidine. The second batch of 1α,2α-epoxyscillirosidine had a lower purity grade; with the initial spotted toxin separating into five distinct spots when separated using TLC (**Figure 11 no.2**). The first spot (pink) was at the origin, not having travelled with the mobile phase (R_f =0). The second (yellow), fourth (blue) and fifth (red) spots had a R_f value of 0.6, 0.9 and 0.95 respectively. These spots were very light, only slightly visible when placed under UV and immediately after the plate was developed in potassium permanganate. The third spot (black) was the largest and, similarly to the first batch of 1α,2α-epoxyscillirosidine tested, had a R_f value of 0.84. To confirm that the second batch of 1α,2α-epoxyscillirosidine had five spots, the TLC plate was repeated, but using 98% ethyl acetate and 2% methanol as the mobile phase. The plate was then visualised using UV light, vanillin and an ethanol/sulphuric acid solution. Both plates showed five spots, with the first being at the origin (R_f =0). The second spot had a R_f of 0.27 and 0.28 on the plates visualised with vanillin and the ethanol/sulphuric acid solution respectively. The third spot, representing 1α,2α-epoxyscillirosidine had a R_f of 0.61 on both plates. Finally, the fourth and fifth spots had R_f values of 0.71 and 0.78, respectively on the plate visualised using vanillin and

R$_f$ values of 0.72 and 0.8, respectively on the plate visualised using the ethanol/sulphuric acid solution.

In addition to testing 1α,2α-epoxyscillirosidine, lanceotoxin B was also run on the TLC plate (**Figure 11 no.3**). Lanceotoxin B showed only one spot (white) under both UV and when developed in potassium permanganate, with a R$_f$ value of 0.42.
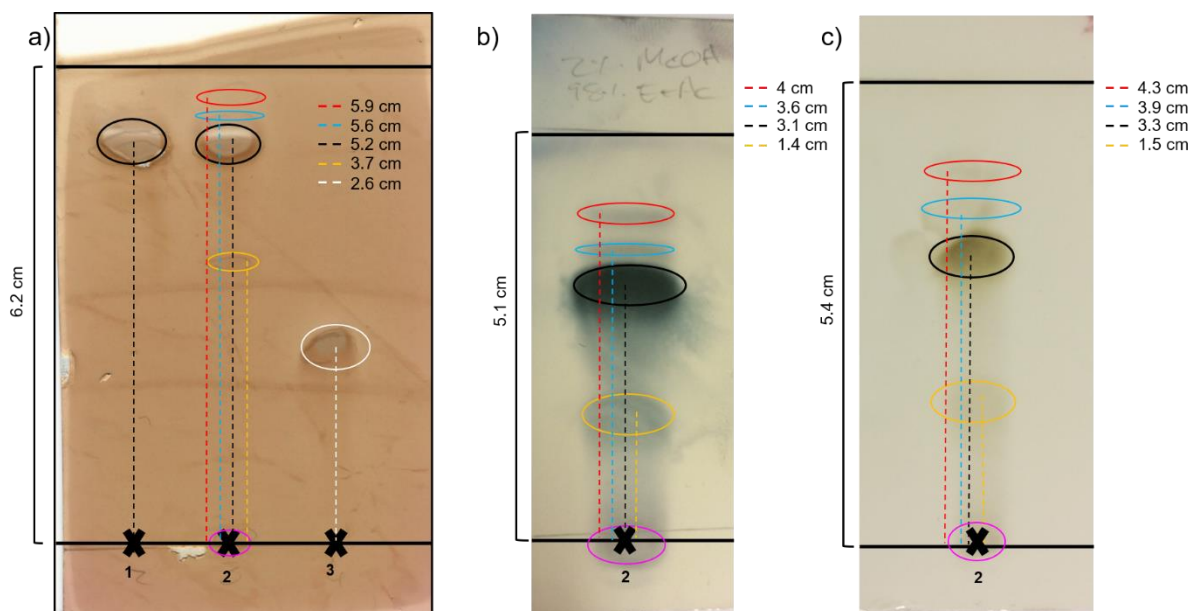
Figure 11 Thin layer chromatography plate developed using 90% ethyl acetate and 10% ethanol solution (a) or 98% ethyl acetate and 2% methanol solution (b and c) showing high purity grade 1α,2α-epoxyscillirosidine (1), lower purity grade 1α,2α-epoxyscillirosidine (2) and lanceotoxin B (3). The compounds were spotted on the origin (x). The plates were viewed under UV light (350 μm), followed by developing the plates in potassium permanganate solution (a), vanillin (b) or 95% ethanol and 5% sulphuric acid solution (c).

4.2 The *in vitro* cytotoxicity of different cardiac glycosides on H9c2 and Neuro-2a cell lines

4.2.1 The *in vitro* cytotoxicity of three different cardiac glycosides on H9c2 cells

The viability of H9c2 cells after exposure to different cardiac glycosides was examined using the MTT assay. The cells were exposed to the cardenolide digoxin, the non-cumulative bufadienolide 1α,2α-epoxyscillirosidine and the cumulative bufadienolide lanceotoxin B, for 24, 48 and 72 h. The EC$_{50}$s of the different cardiac glycosides are depicted in **Table 1**.

Due to solubility issues the cells were only exposed to a maximum of 100 μM digoxin and no non-linear regression curves were constructed as the toxin was unable to kill the cells at that concentration. The EC$_{50}$s of digoxin exposure to H9c2 cells for 24, 48

and 72 h were greater than 100 µM (**Figure 12a**), with 50% cell survival not falling within the 95% confidence interval when the survival was calculated as a percentage of the solvent control. The cell survival after being exposed to 100 µM digoxin (with a 95% CI) for 24 h (n=4) fell between 61% and 98%; for 48 h (n=4) cell survival was between 59% and 81% and between 57% and 75% for 72 h (n=4). There was no significant ($p > 0.05$) time-dependent effect on the H9c2 cells exposed to 100 µM digoxin.

The effect of 1α,2α-epoxyscillirosidine on the H9c2 cells were much more apparent. The EC_{50}s were well below 100 µM and non-linear regression curves were constructed for all incubation times (**Figure 12b**). The EC_{50}s of 1α,2α-epoxyscillirosidine was 41.39 ± 4.37 µM after 24 h exposure, 25.42 ± 6.47 µM after 48 h exposure and 12.65 ± 2.75 µM after 72 h exposure. 1α,2α-Epoxyscillirosidine showed a concentration-dependent effect on H9c2 cells. Cell survival was increased above that of the solvent control at concentrations below the EC_{50} after 24 h exposure and concentrations below 5 µM after 48 h and 72 h exposure. Higher 1α,2α-epoxyscillirosidine concentrations decreased cell survival, showing the expected inverse correlation between cell survival and concentration. A significant time-dependent effect ($p < 0.05$) was seen between 24 h and 48 h and between 24 h and 72 h for concentrations higher than 5 µM. A significant time-dependent effect was seen between 48 h and 72 h only for 1α,2α-epoxyscillirosidine concentrations above 50 µM and below 200 µM.

The maximum lanceotoxin B concentration to which the cells were exposed was 200 µM and no non-linear regression curves could be constructed (**Figure 12c**). After 24 h (n=4), the EC_{50} of lanceotoxin B was greater than 200 µM with a 95% CI of between 64% and 92% cell survival. However, after being exposed to 200 µM lanceotoxin B for 48 h (n=4) the percentage cell survival was around 50% falling between 49% and 68% with a 95% CI. At 72 h (n=4) the EC_{50} was below 200 µM with a 95% CI of between 36% and 48% cell survival. At 200 µM lanceotoxin B, a significant time-dependent effect between 24 h and 48 h, and between 24 h and 72 h was seen. There was no significant difference between 48 h and 72 h. A significant concentration-dependent effect could be seen at 48 h and 72 h, the percentage cell survival decreasing with higher lanceotoxin B concentrations.

4.2.2 The *in vitro* cytotoxicity of three different cardiac glycosides on Neuro-2a cells

Neuro-2a cells were exposed to digoxin, 1α,2α-epoxyscillirosidine and lanceotoxin B for 24, 48 and 72 h. The viability of the cells was measured with the MTT assay. All the EC_{50}s of the different cardiac glycosides are shown in **Table 1**.

Non-linear regression curves could not be constructed to analyse the effect of digoxin exposure on Neuro-2a cells, as the viability of the cells did not decrease below 50% cell survival for the concentrations tested (**Figure 13a**). The EC_{50}s of digoxin was greater than 100 µM (n = 10) for 24, 48 and 72 h with a 95% CI of between 77% and 98%, between 67% and 89% and finally between 58% and 81 % cell survival, respectively.

The exposure of Neuro-2a cells to 1α,2α-epoxyscillirosidine showed a concentration-dependent cytotoxic response (**Figure 13b**), with the percentage cell survival decreasing with higher concentrations of 1α,2α-epoxyscillirosidine. As with exposure to H9c2 cells, 1α,2α-epoxyscillirosidine caused an increase in cell survival at lower concentrations. The EC_{50}s of 1α,2α-epoxyscillirosidine at different exposure times were less than 100 µM. After 24 h exposure the EC_{50} was equal to 35.73 ± 10.59 µM (n=3); after 48 h the EC_{50} was 37.56 ± 3.18 µM (n=3) and after 72 h exposure the EC_{50} equalled 37.35 ± 2.30 µM (n=3). No significant difference (*p > 0.*05) between 24, 48 and 72 h exposure were observed when comparing the EC_{50}s of 1α,2α-epoxyscillirosidine.

Lanceotoxin B had the most potent effect of the three different cardiac glycosides on Neuro-2a cells, with EC_{50}s below 10 µM (**Figure 13c**). When Neuro-2a cells were exposed to the cumulative bufadienolide a concentration-dependent cytotoxic response was observed. A significant difference (*p > 0.05*) between the different exposure times and different concentrations was seen, except at concentrations below 6 µM between 24 h and 48 h exposure. The EC_{50}s for lanceotoxin B after exposing Neuro-2a cells for 24 h was 5.46 ± 0.37 µM (n=4), for 48 h was 5.27 ± 0.59 µM (n=4) and for 72 h was 4.43 ± 0.67 µM (n=4).

Table 1 The EC50 (μM) of different cardiac glycosides on H9c2 cells and Neuro-2a cells after 24, 48 and 72 h exposure.

Cell line	Cardiac glycoside	Exposure Time		
		24 h	48 h	72 h
H9c2 cells	Digoxin	>100 μM (95% CI: 61-98) * n = 4	>100 μM (95% CI: 59-81) * n = 4	>100 μM (95% CI: 57-75) * n = 4
	1α,2α-Epoxyscillirosidine	41.39 ± 4.37 μM n = 3	25.42 ± 3.73 μM n = 3	12.65 ± 2.75 μM n = 3
	Lanceotoxin B	>200 μM (95% CI: 64-92) * n = 4	~200 μM (95% CI: 49-68) * n = 4	<200 μM (95% CI: 36-48) * n = 4
Neuro-2a cells	Digoxin	>100 μM (95% CI: 77-98) * n =10	>100 μM (95% CI: 67-89) * n =10	>100 μM (95% CI: 58-81) * n =10
	1α,2α-Epoxyscillirosidine	35.73 ± 10.59 μM n = 3	37.56 ± 3.18 μM n = 3	37.35 ± 2.30 μM n = 3
	Lanceotoxin B	5.46 ± 0.37 μM n = 4	5.27 ± 0.59 μM n = 4	4.43 ± 0.67 μM n = 4

EC_{50} (μM) ± Standard error of the mean for at least three biological repeats (n).

* The 95% confidence interval (95% CI) of cell survival for concentration cardiac glycosides showed
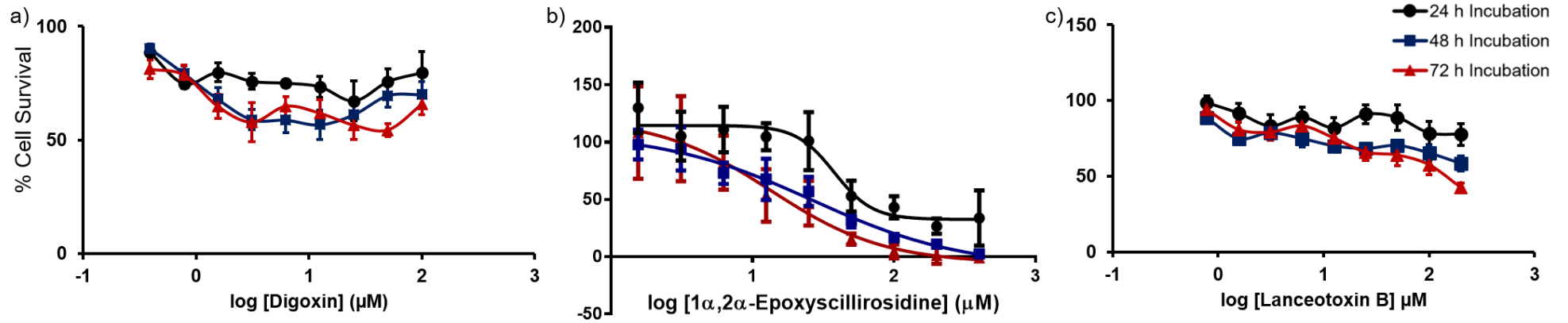
Figure 12 The semi-log concentration-response curves of digoxin, 1α,2α-epoxyscillirosidine and lanceotoxin B on H9c2 cells for 24, 48 and 72 h incubation.
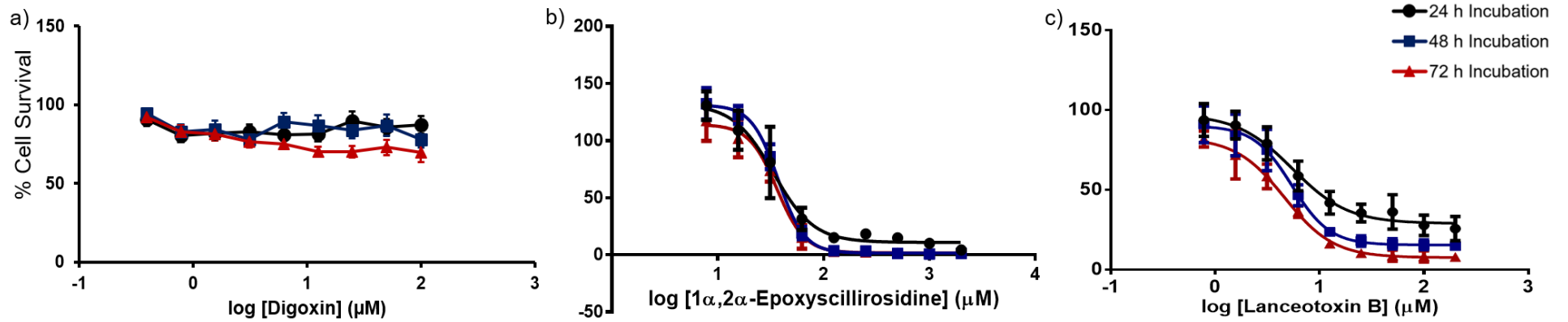
Figure 13 The semi-log concentration-response curves of digoxin, 1α,2α-epoxyscillirosidine and lanceotoxin B on Neuro-2a cells for 24, 48 and 72 h incubation.

4.3 The ultrastructural changes of H9c2 cells after exposure to three different cardiac glycosides

The H9c2 cells were exposed to 5, 25 and 100 µM of digoxin, 1α,2α-epoxyscillirosidine and lanceotoxin B respectively, for 24, 48 and 72 h. The exposed cells were examined using TEM and compared to the untreated control to identify the subcellular changes that occurred as a result of cardiac glycoside exposure. The changes are summarised in **Table 2**, according to exposure time. In addition, the results are summarised according to toxin concentration in **Table 4**. The surface of the cells exposed to 100 µM of the different cardiac glycosides for 24 h and 48 h were studied using SEM.

The H9c2 control cells were thin, long and tapered at one or both ends (**Figure 14**), with rough endoplasmic reticulum (RER) distributed throughout the cytoplasm. The RER were either vesiculated (**Figure 14c**) or in long, continuous stretches (**Figure 14b, d**) and some were dilated (with homogeneous content), but not swollen (diluted content). Some electron-lucent vacuoles and autophagic vesicles could occasionally be seen throughout the cytoplasm. The Golgi complexes were distinct and usually located near the periphery of the nucleus (**Figure 14a, c**). On the cytoplasmic side of the cell the cytoskeleton (microfilaments/actin cytoskeleton) was associated with the plasma membrane (pink arrows and pink box). The mitochondria were electron-dense with lamellar cristae (**Figure 14a, c**). The majority of nuclei were oval, with one or two nucleoli per nucleus (**Figure 14a, b, d**).

The surface of the control H9c2 cells were examined using SEM (**Figure 15**). The cells were large, growing close to each other and had a mat-like appearance. During the dehydration step, cracks formed around what is presumed to be the nuclei of the cells (blue arrows). These dehydration cracks were visible in untreated and treated H9c2 cells but will only be indicated in Figure 15. The surface of the untreated cells was relatively smooth. Multiple long, thin protrusions (pink arrows) formed cell-to-cell attachments. The control cells were used as a reference to compare the ultrastructural changes that occurred in H9c2 cells after the cells were exposed with different cardiac glycosides.
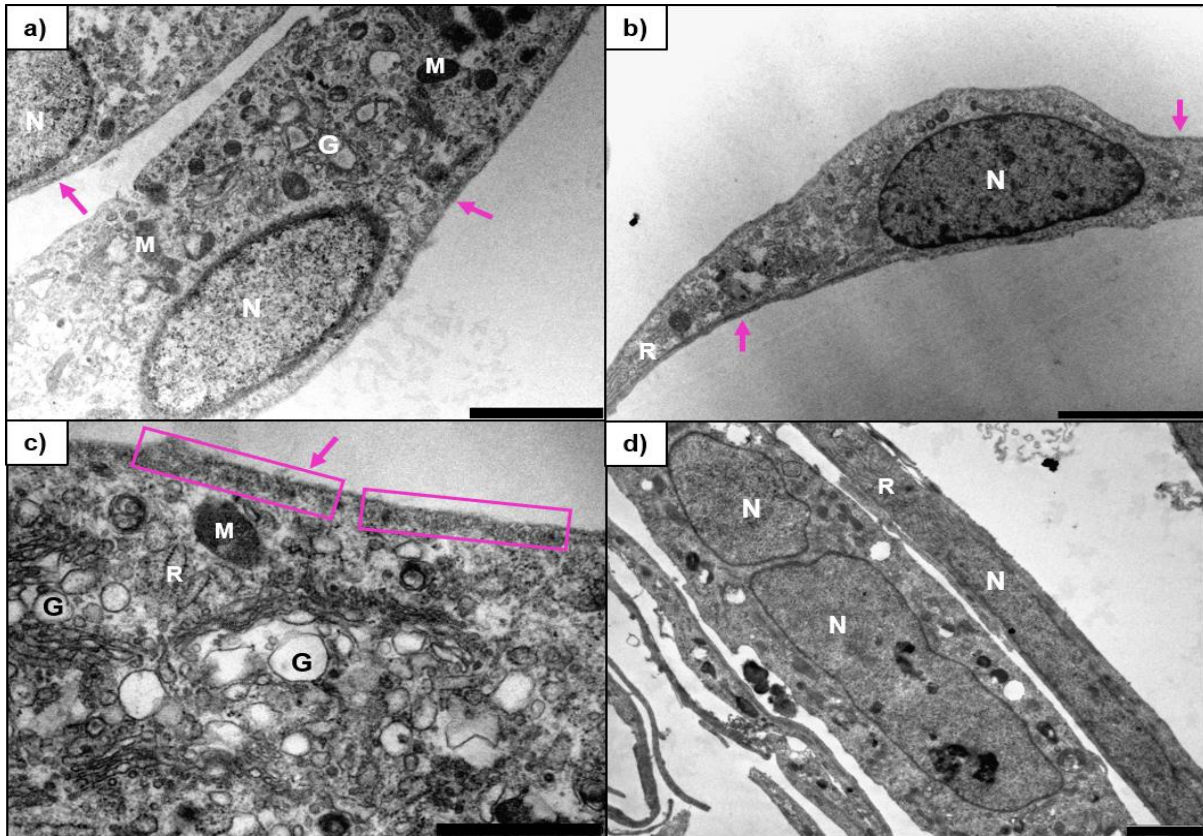
Figure 14 Transmission electron micrographs showing untreated H9c2 cells after 24 h (a, b), 48 h (c) and 72 h (d). The cells were long, thin and with tapered ends. Part of the cytoskeleton can be seen at the edge of the cells associated with the plasma membrane (pink arrows and pink box). The Golgi complexes were distinct and located close to the nucleus. The RER were either vesiculated or long and thin. N - nucleus; G - Golgi complex; R - RER; M - mitochondria. The scale bar at the bottom right corner represents 5 µm (b), 2 µm (a, d) and 1 µm (c).
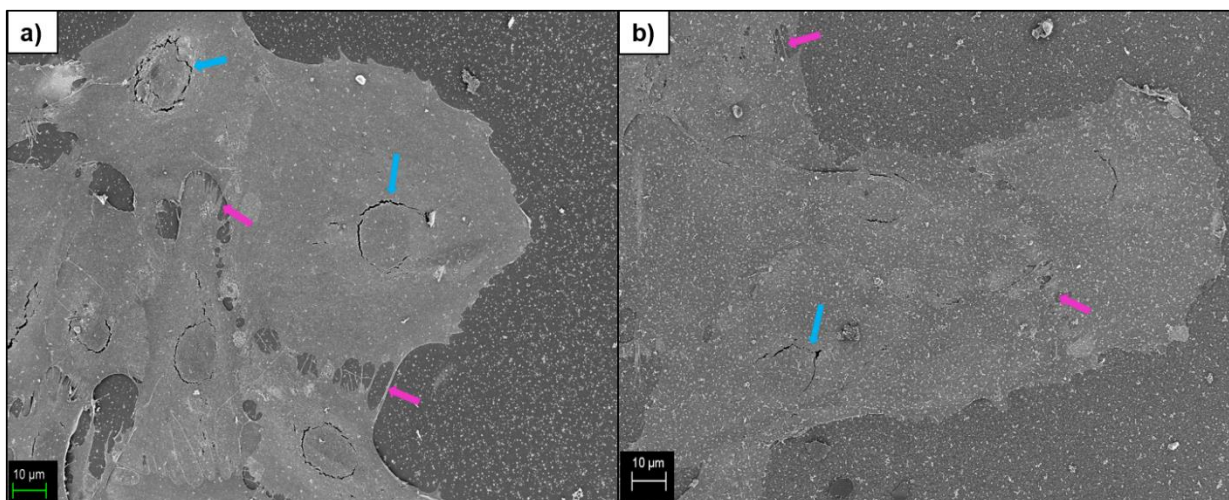
Figure 15 Scanning electron micrograph showing the surface of H9c2 cells after 24 (a) and 48 h (b). The cells had a relatively smooth surface and long protrusions (pink arrows) that facilitated cell-to-cell adhesion. The cells grew close to each, having a mat-like appearance. During SEM preparation dehydration cracks (blue arrows) appeared around the nucleus. Scale bars indicated at bottom left corner.

4.3.1 Ultrastructural changes in H9c2 cells induced by the cardenolide, digoxin

The H9c2 cells were exposed to 5, 25 and 100 µM digoxin for 24, 48 and 72 h. Subsequently, the effect of digoxin on the cell ultrastructure was investigated by TEM and SEM imaging and the changes were grouped and analysed according to incubation time.

After being exposed to digoxin for 24 h, the mitochondria were damaged and swollen (**Figure 16**). In this case "*damaged*" refers to electron lucent spots in the mitochondria (orange arrow heads), while more affected mitochondria are referred to as "*swollen*" and are bloated with diluted content and with cristae moving away from the centre (**Figure 16d**). The number of the autophagic vesicles (red arrows) was increased compared to the control and myelin figures were distributed throughout the cytoplasm. The cytoplasm was sparse and disrupted at certain areas of some cells (red stars). Digoxin appeared to affect the cell membrane (pink arrows). Golgi complexes and RER of the H9c2 cells showed no change compared to the control cells and there was no apparent effect on the nucleus.
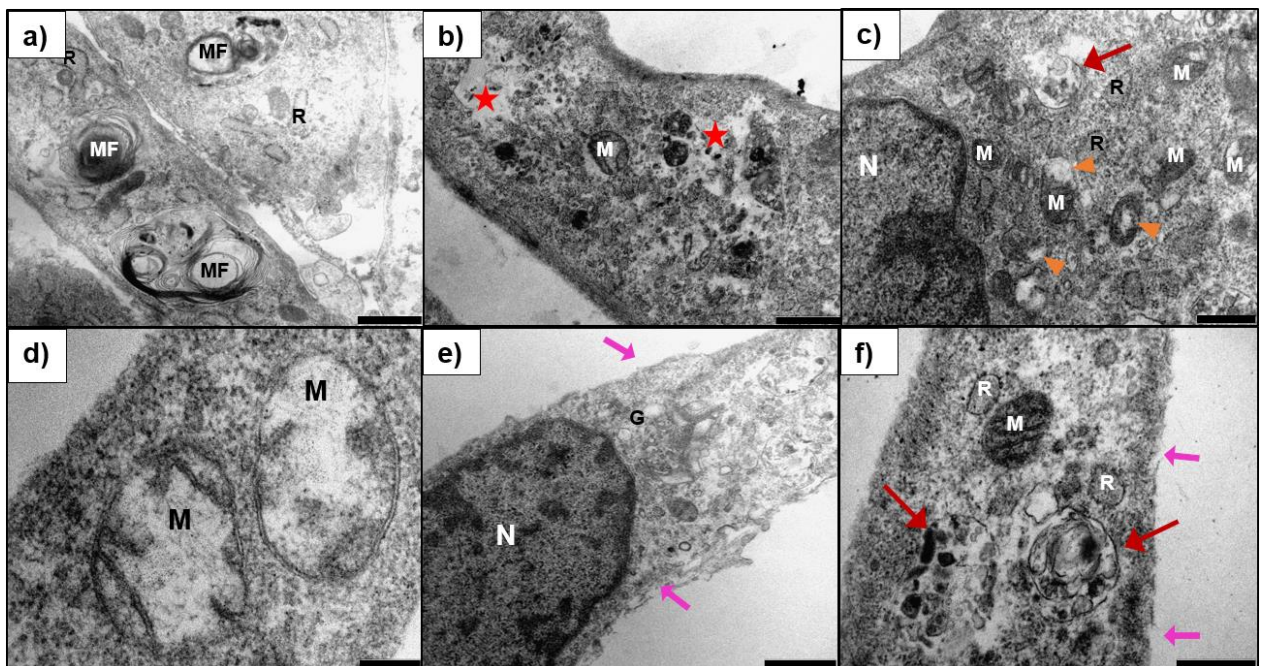
Figure 16 Transmission electron micrograph of H9c2 cells exposed to 5 µM (a), 25 µM (b-d) and 100 µM (e, f) digoxin for 24 h. The number of autophagic vesicles (red arrows) and myelin figures increased, and the cytoplasm was disrupted (red stars). The mitochondria were damaged (orange arrow heads) and swollen (see d). The plasma membrane was slightly damaged (pink arrows). N - nucleus; MF - myelin figures; R - RER; G - Golgi complex; M - mitochondria. The scale bar at the bottom right corner represents 1 µm (a, b, e), 0.5 µm (c, f) and 0.2 µm (d).

After 48 h, the mitochondria were damaged (orange arrow heads) and swollen (**Figure 17c**). Some of the cells were completely destroyed, leaving only cell debris (**Figure 17 h**). After exposure to 5 and 25 µM digoxin, the Golgi complexes of the H9c2 cells were not affected; however, cells exposed to 100 µM digoxin had slightly swollen Golgi. As with 24 h exposure, large parts of the cytoplasm were disrupted or sequestered in autophagic vesicles (red arrows), especially at higher concentrations of digoxin exposure (**Figure 17**). The plasma membrane was clearly damaged, and the associated cytoskeleton (pink arrows) appeared to be affected. The nuclei remained unaffected.
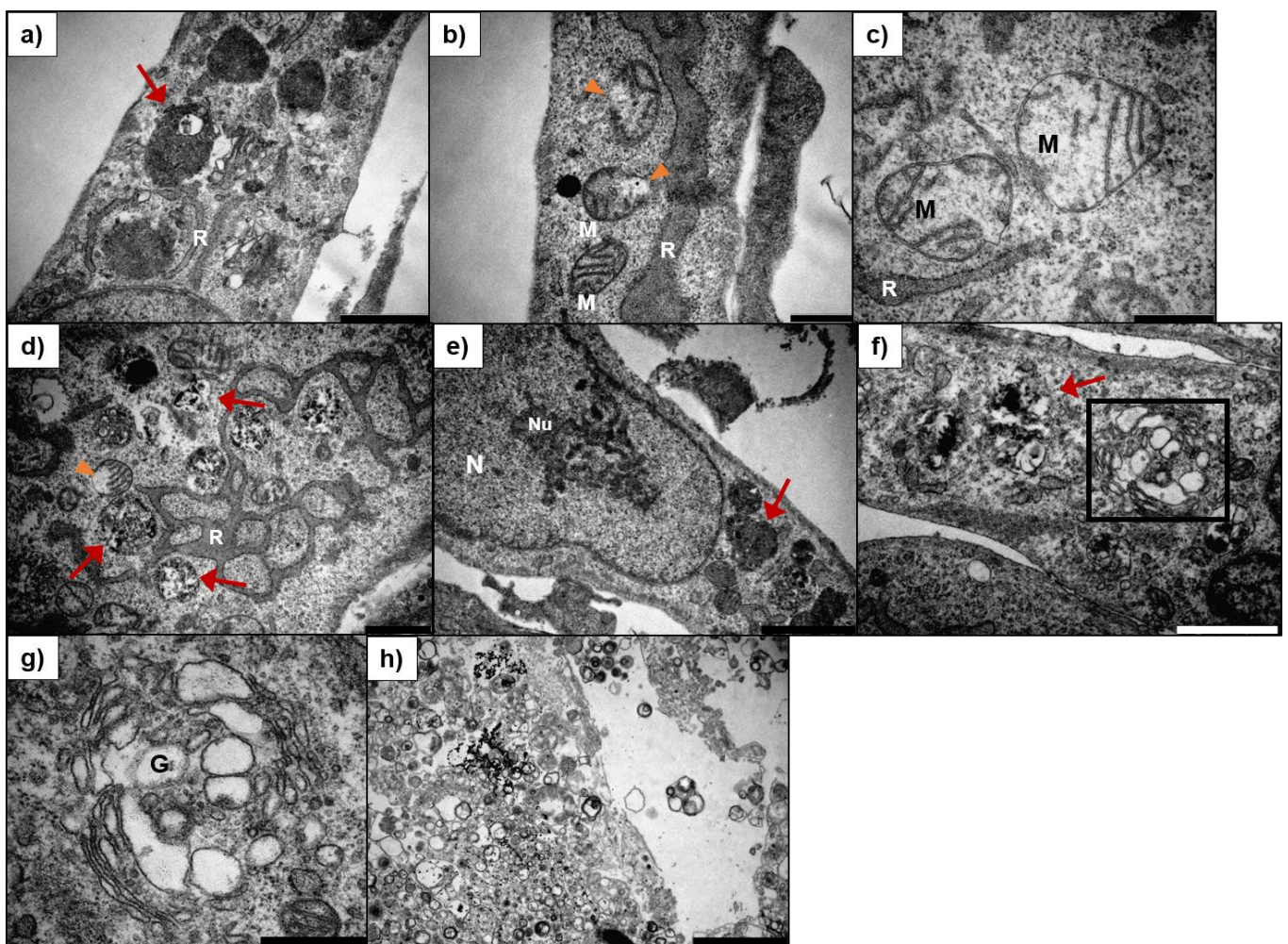
Figure 17 Transmission electron micrograph of H9c2 cells exposed to 5 µM (a, b), 25 µM (c-e) and 100 µM (f-h) digoxin for 48 h. The nuclei and RER remained unaffected, but the Golgi complex (black frame enlarged in g) became swollen at high digoxin concentrations. The number of autophagic vesicles (red arrows) increased and the mitochondria were damaged (orange arrow heads) or swollen (c). The cytoplasm was disrupted, and some cells were completely destroyed (h). N - nucleus; Nu - nucleolus; R - RER; G - Golgi complex; M - mitochondria. The scale bar at the bottom right corner represents 2 µm (e, h), 1 µm (a, d, f) and 0.5 µm (b, c, g).
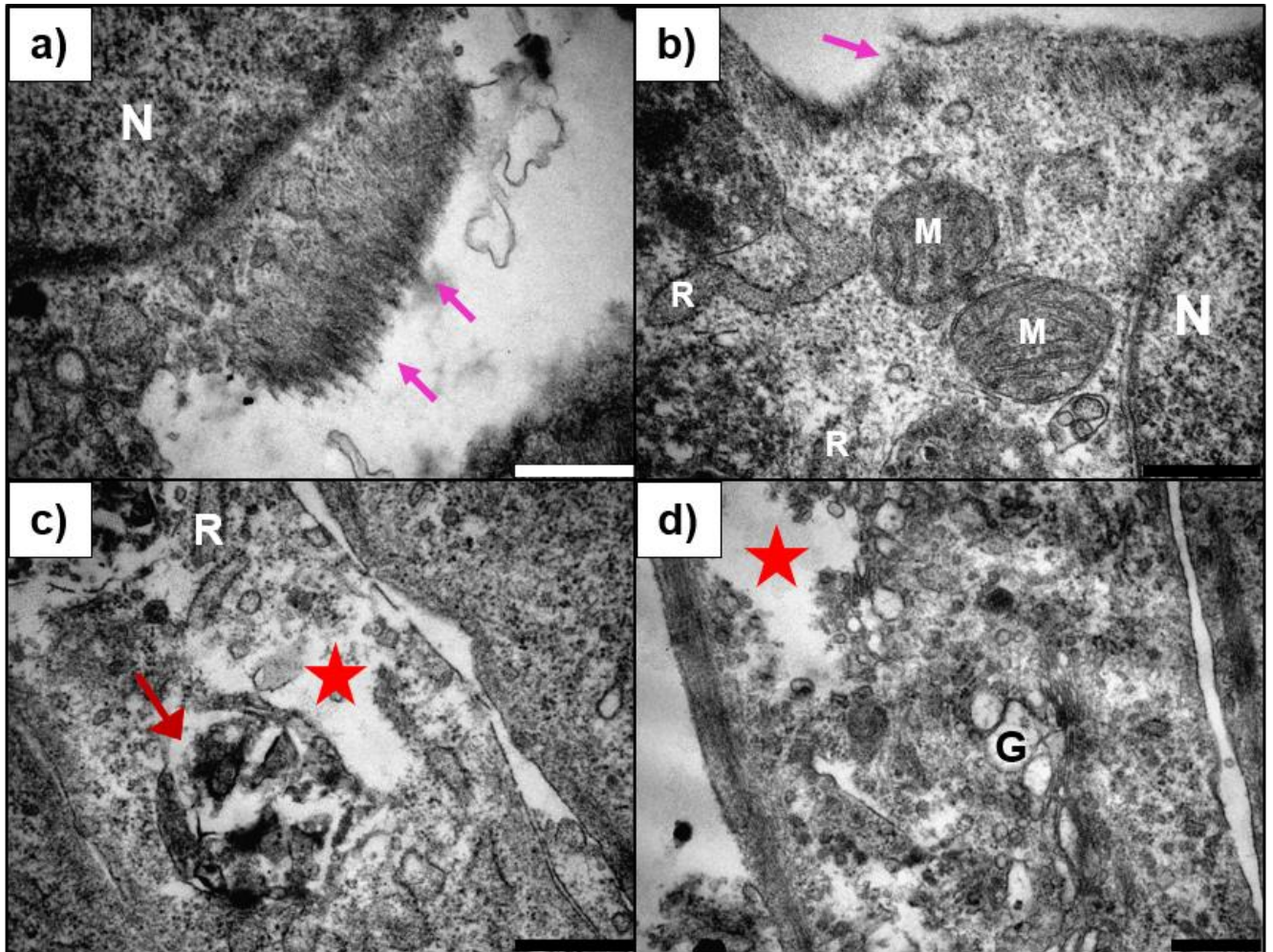
Figure 18 Transmission electron micrograph of the effect of digoxin on the plasma membrane and cytoplasm of H9c2 after 48 h exposure to 25 μM (a, b) and 100 μM (c, d) digoxin. At high digoxin concentrations, gaps occurred in the cytoplasm (red stars). The plasma membrane and associated cytoskeleton (pink arrows) were also affected. Autophagic vesicles (red arrows) were visible within the cytoplasm. N - nucleus; G - Golgi complex; R - RER; M - mitochondria. The scale bar at the bottom right corner represents 0.5 μm (a-d).

At 72 h the mitochondria were damaged (orange arrow heads) and swollen (**Figure 19a**). Much of the cytoplasm was sequestered in autophagic vesicles (red arrows) and the cytoplasm was disrupted, forming gaps (red stars) (**Figure 19**). As with the cells exposed to digoxin for 24 h and 48 h, the plasma membrane was damaged and the associated cytoskeleton (pink arrows) was affected. The cellular debris of destroyed cells were present. The Golgi complexes of the H9c2 cells were slightly swollen and that the RER was unchanged. The nuclei remained unaffected.
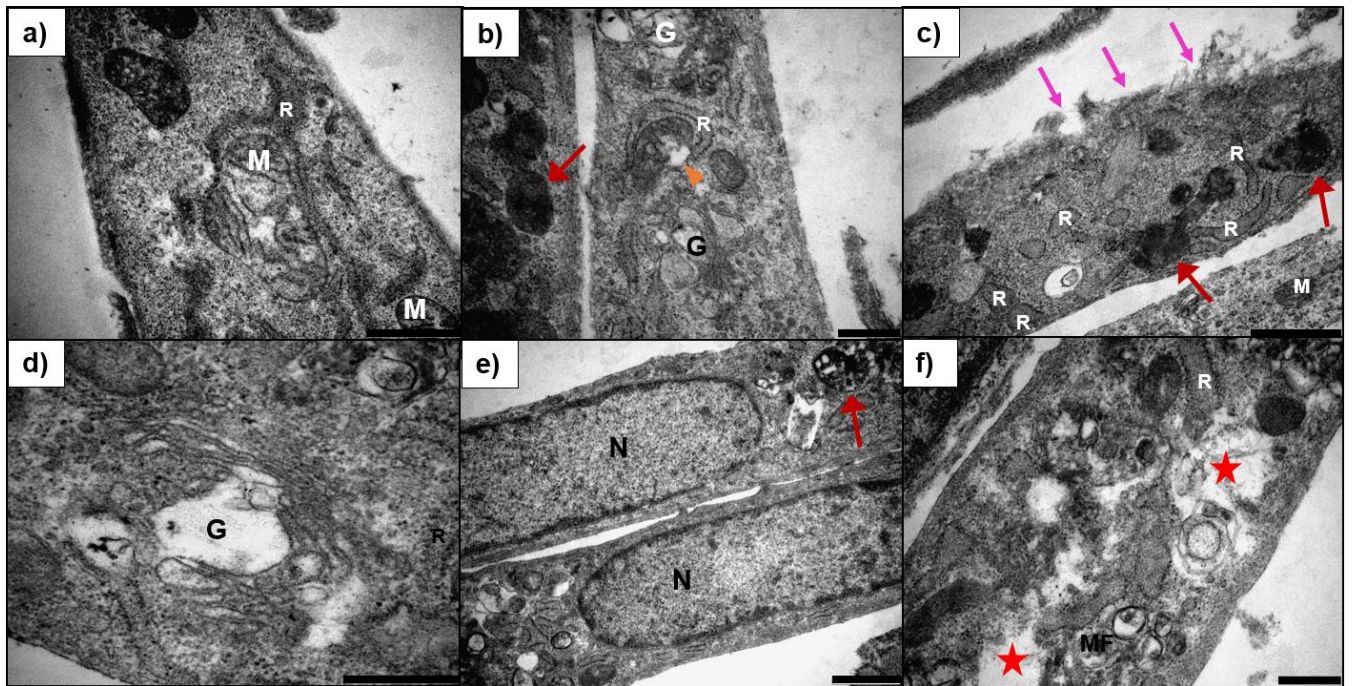
Figure 19 Transmission electron micrograph of H9c2 cells exposed to 5 µM (a, b), 25 µM (c, d) and 100 µM (e, f) digoxin for 72 h. The mitochondria of the H9c2 cells exposed to digoxin was swollen (a) and damaged (orange arrow head). The cytoplasm was sequestered in autophagic vesicles (red arrows), creating gaps (red stars) within the cell. The plasma membrane and associated cytoskeleton appeared to be affected by digoxin exposure (pink arrows). The Golgi complexes were slightly swollen, whilst the RER and nucleus remained mostly unaffected. N - nucleus; G – Golgi complex; MF - myelin figures; R - RER; M - mitochondria. The scale bar at the bottom right corner represents 1 µm (a, c, e) and 0.5 µm (b, d, f).

The surface changes that occurred cells after exposure of the H9c2 cells to 100 μM digoxin for 24 h and 48 h were investigated using SEM (**Figure 20**). After being exposed to digoxin, fewer cells were visible on the coverslip compared to the control. A number of cells had shrunk and had a roundish shape (black circle). The cell surface was relatively smooth, with minor plasma membrane damage (black arrows). The number of protrusions that form cell-to-cell adhesion (pink arrows) seemed to be less compared to the control cells.
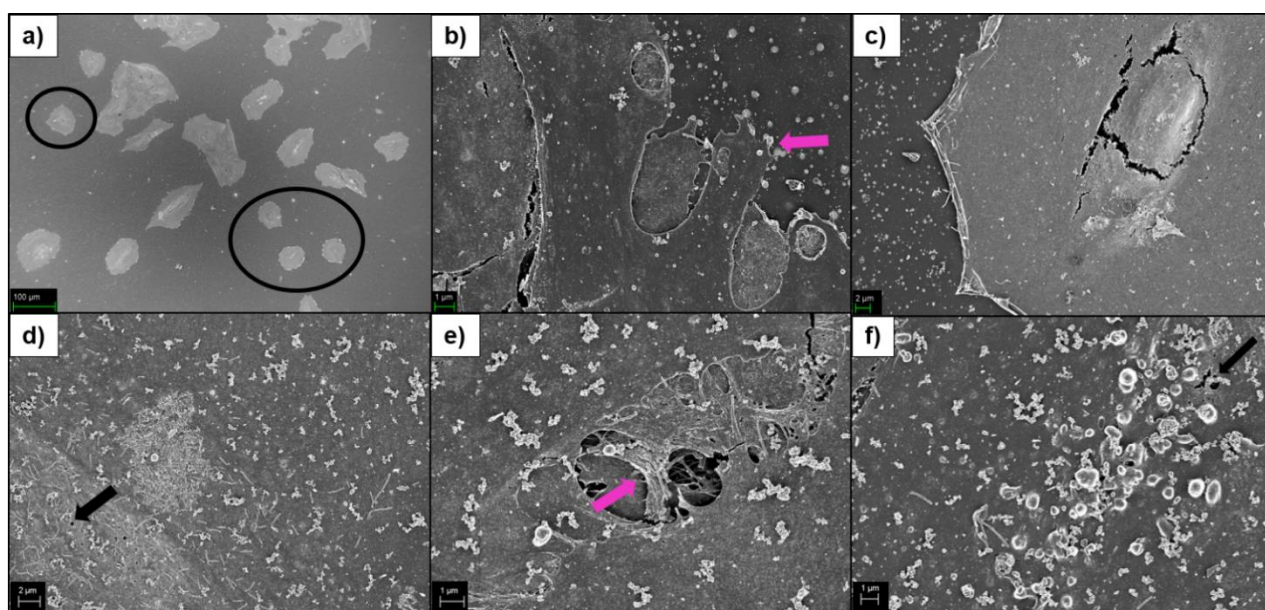
Figure 20 Scanning electron micrograph of H9c2 cells exposed to 100 μM digoxin for 24 h (a-c) and 48 h (d-f). After exposure to digoxin, some of the cells shrunk and became rounder (black box in image a). Minor membrane damage could be seen (black arrows). Cell-to-cell attachments and cell-to-surface attachments were visible (pink arrows). Scale bars indicated at bottom left corner.

4.3.2 Ultrastructural changes in H9c2 cells induced by the non-cumulative bufadienolide 1α,2α-epoxyscillirosidine

The subcellular and surface changes of H9c2 cells exposed to 5, 25 and 100 μM 1α,2α-epoxyscillirosidine for 24, 48 and 72 h were investigated using TEM and SEM. The overall effect of 1α,2α-epoxyscillirosidine, was much more apparent than that of digoxin.

At 24 h exposure, both the Golgi complexes and RER of the H9c2 cells exposed to 1α,2α-epoxyscillirosidine (**Figure 21**) were swollen. Cells exposed to higher concentrations of the toxin showed RER with diluted content and some cells had large, swollen vesicle-like RERs (**Figure 21d**). The Golgi became more swollen at higher

concentrations of 1α,2α-epoxyscillirosidine and the mitochondria were damaged (orange arrow heads). The perinuclear space was clearly swollen (blue arrows) in several cells, but no other visible effect on the nucleus could be seen. The cytoplasm became sparse, with large vacuoles forming within the cell. The number of vacuoles, autophagic vesicles and myelin figures in the cells increased. However, the number of autophagic vesicles were less compared to H9c2 cells exposed to digoxin, while the number of vacuoles were greater. Most of the H9c2 cells exposed to 100 µM 1α,2α-epoxyscillirosidine had severe plasma membrane damage (black arrows) and cell content completely disappearing, while a few cells formed apoptotic bodies (white arrows).
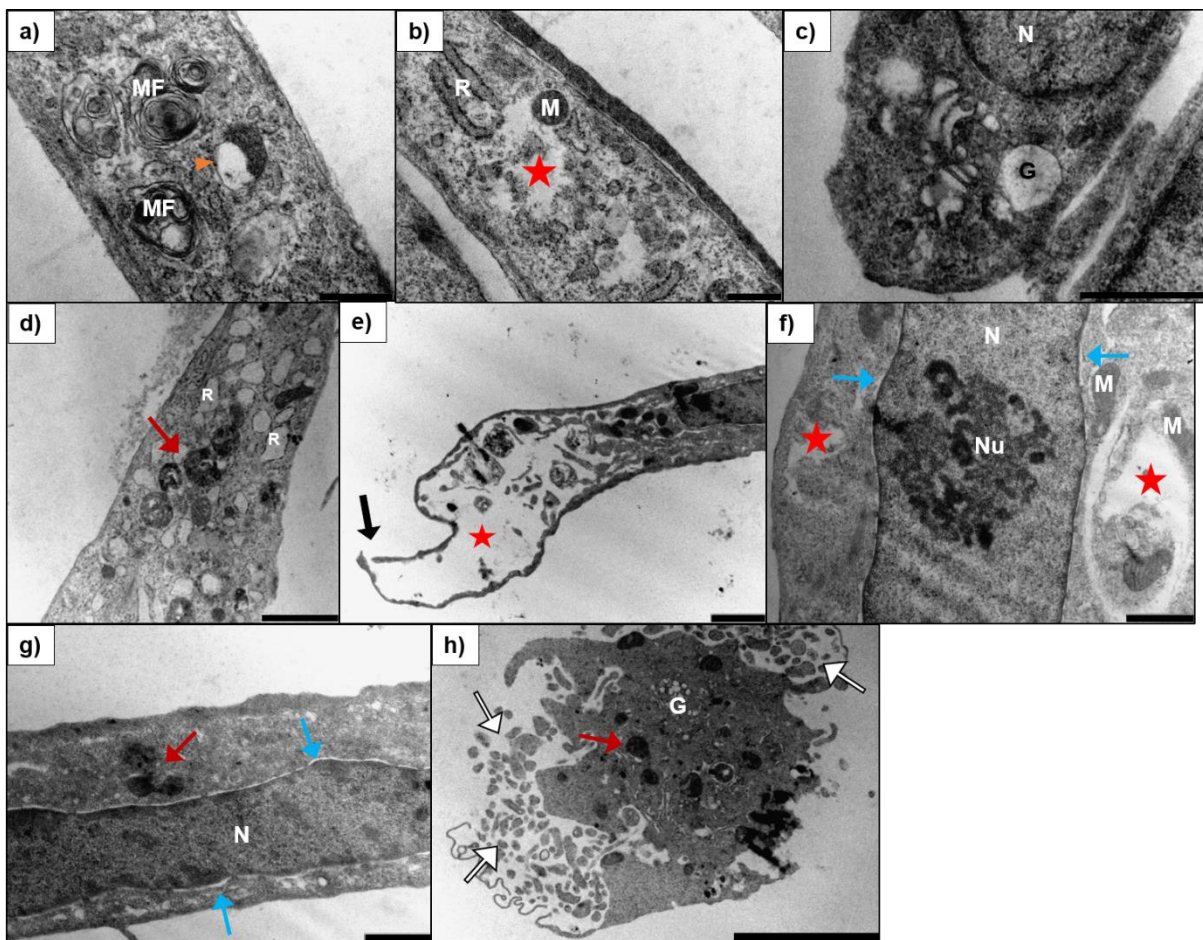
Figure 21 Transmission electron micrograph of H9c2 cells exposed to 5 µM (a, b), 25 µM (c, d) and 100 µM (e-h) 1α,2α-epoxyscillirosidine for 24 h. The Golgi complex, RER and the perinuclear space (blue arrow) of the cells were swollen. Some mitochondria were slightly damaged (orange arrow head). The cytoplasm was disrupted (red stars). Autophagic vesicles (red arrows) and myelin figures were present within the cytoplasm. The plasma membrane in most cells was damaged (black arrows) and some cells formed apoptotic bodies (white arrows). N - nucleus; Nu - nucleolus; G – Golgi complex; MF - myelin figures; R - RER; M - mitochondria. The scale bar at the bottom right corner represents 5 µm (h), 2 µm (d, e), 1 µm (c, f, g) and 0.5 µm (a, b).

After 48 h exposure to 1α,2α-epoxyscillirosidine, the H9c2 cells (**Figure 22**) had swollen Golgi complexes. The RER was also swollen and vesicle-like. Damaged mitochondria (orange arrow heads) were dispersed throughout the cytoplasm. The perinuclear space (blue arrows) of some nuclei were swollen. Nucleolar margination and condensation of nuclear material (X) was observed in cells exposed to high 1α,2α-epoxyscillirosidine concentrations. As with 24 h exposure, the cytoplasm of the cells became sparse in some places and the number of autophagic vesicles (red arrows) and myelin figures within the cells increased. The increase in vacuoles within the cytoplasm was especially pronounced. Many of the cells shrunk and had a rounder form. Plasma membrane damage was seen in cells (black arrows).
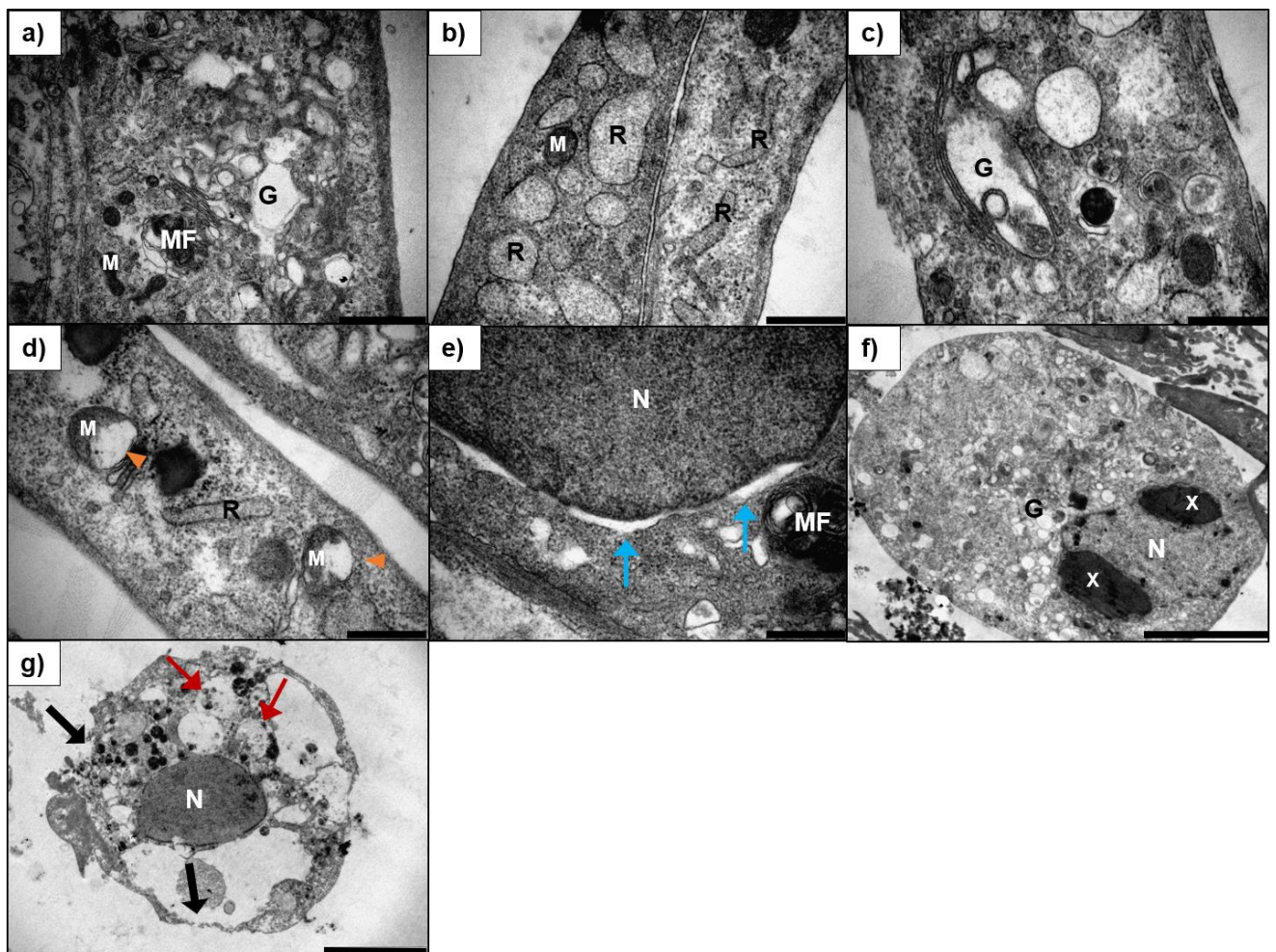
Figure 22 Transmission electron micrograph of H9c2 cells exposed to 5 µM (a), 25 µM (b-d) and 100 µM (e, f) 1α,2α-epoxyscillirosidine for 48 h. The RER and Golgi complexes were swollen. The mitochondria were damaged (orange arrow heads). The nuclei were affected, with clear swelling of the perinuclear space (blue arrows) and chromatin condensation (X) in some cells. Autophagic vesicles and many vacuoles were distributed throughout the cytoplasm. The cells were rounder and plasma membrane damage (black arrows) could be seen. N - nucleus; G – Golgi complex; MF - myelin figures; R - RER; M - mitochondria. The scale bar at the bottom right corner represents 5 µm (f, g), 1 µm (a) and 0.5 µm (b-e).

The H9c2 cells exposed to 1α,2α-epoxyscillirosidine for 72 h (**Figure 23**) had swollen Golgi complexes and RER, with damaged mitochondria (orange arrow heads). At 100 μM some of the mitochondria had ballooned cristae (not indicated). The ribosomes dissociated from the swollen RER (**Figure 23f**). In cells exposed to 100 μM 1α,2α-epoxyscillirosidine nucleolar margination, condensation of the nuclear material (X) and slight swelling of the perinuclear space (blue arrows) was observed. The large number of vacuoles and autophagic vesicles (red arrows) were dispersed throughout the cytoplasm. The cells exposed to 100 μM 1α,2α-epoxyscillirosidine were shrunken and rounded (**Figure 23g**). Cellular debris indicating destroyed cells were also seen.
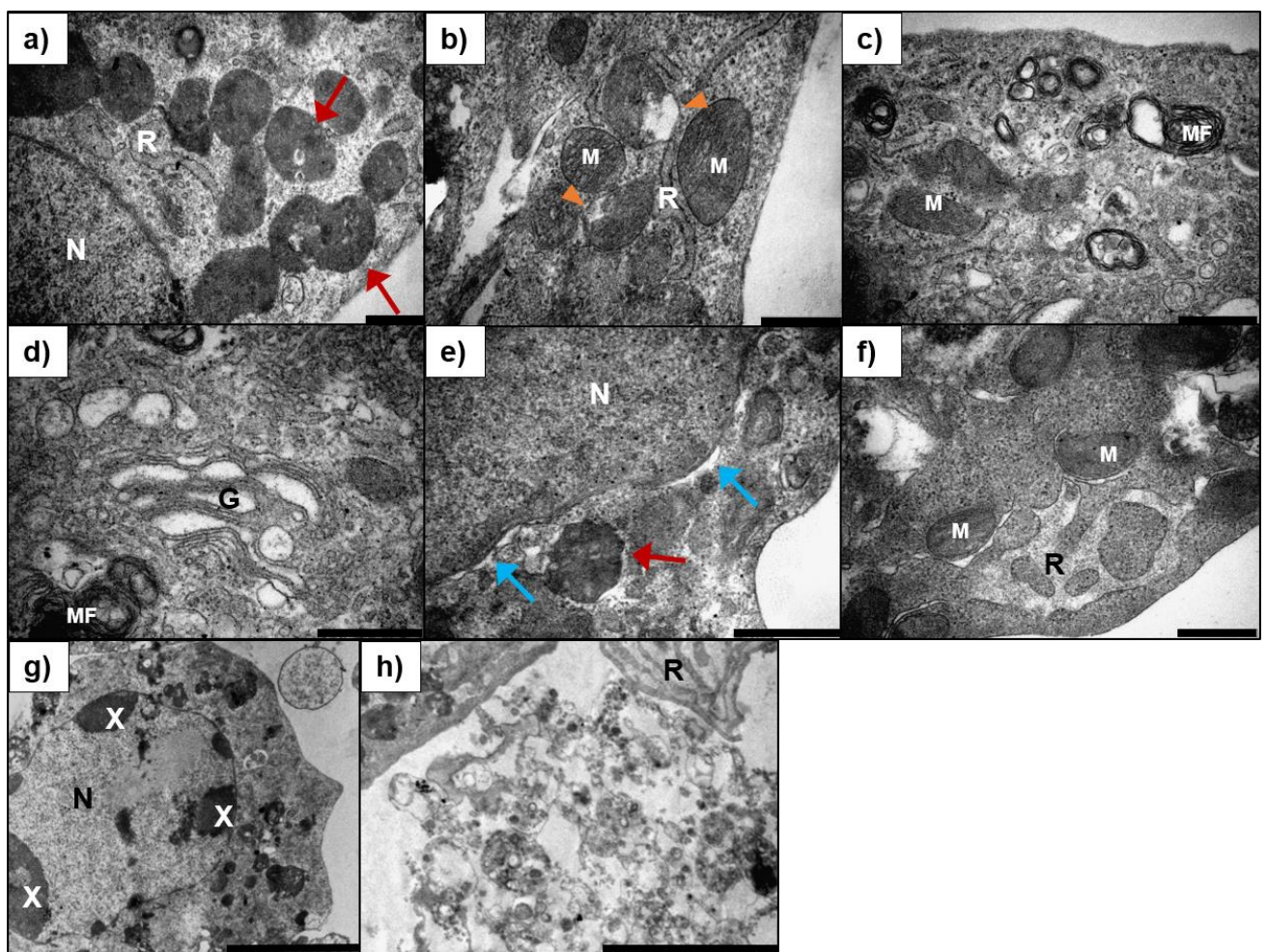
Figure 23 Transmission electron micrographs of H9c2 cells exposed to 5 μM (a, b), 25 μM (c, d) and 100 μM (e-g) 1α,2α-epoxyscillirosidine for 72 h. The Golgi complexes and RER were swollen, with the ribosomes dissociating from some of the RER (f). The mitochondria were damaged (orange arrow heads) and the number of autophagic vesicles (red arrows), vacuoles and myelin figures within the cytoplasm of affected cells increased. The nuclei of the cells were altered, with a swollen perinuclear space (blue arrows) and nucleolar margination and condensed nuclear material (X) observed in some cells. N - nucleus; G – Golgi complex; MF - myelin figures; R - RER, M - mitochondria. The scale bar at the bottom right corner represents 5 μm (g, h) and 0.5 μm (a-f).

The surface of the H9c2 cells exposed to 100 µM 1α,2α-epoxyscillirosidine for 24 and 48 h were studied using SEM (**Figure 24**). Due to the difference in purity of the batch of 1α,2α-epoxyscillirosidine used for SEM compared to the batch used for TEM, the effects of 1α,2α-epoxyscillirosidine exposure were less apparent. The surface of the H9c2 cells appeared to be relatively smooth, with a few, small protrusions. Some cells shrunk, becoming rounder (black circles). Large gaps, indicative of membrane damage (black arrows), was seen on the plasma membrane of H9c2 cells at both 24 h and 48 h exposure. The number of protrusions (pink arrows) that facilitated cell-to-cell attachment was reduced compared to the control cells and some of the protrusions seemed to detach from the coverslip.
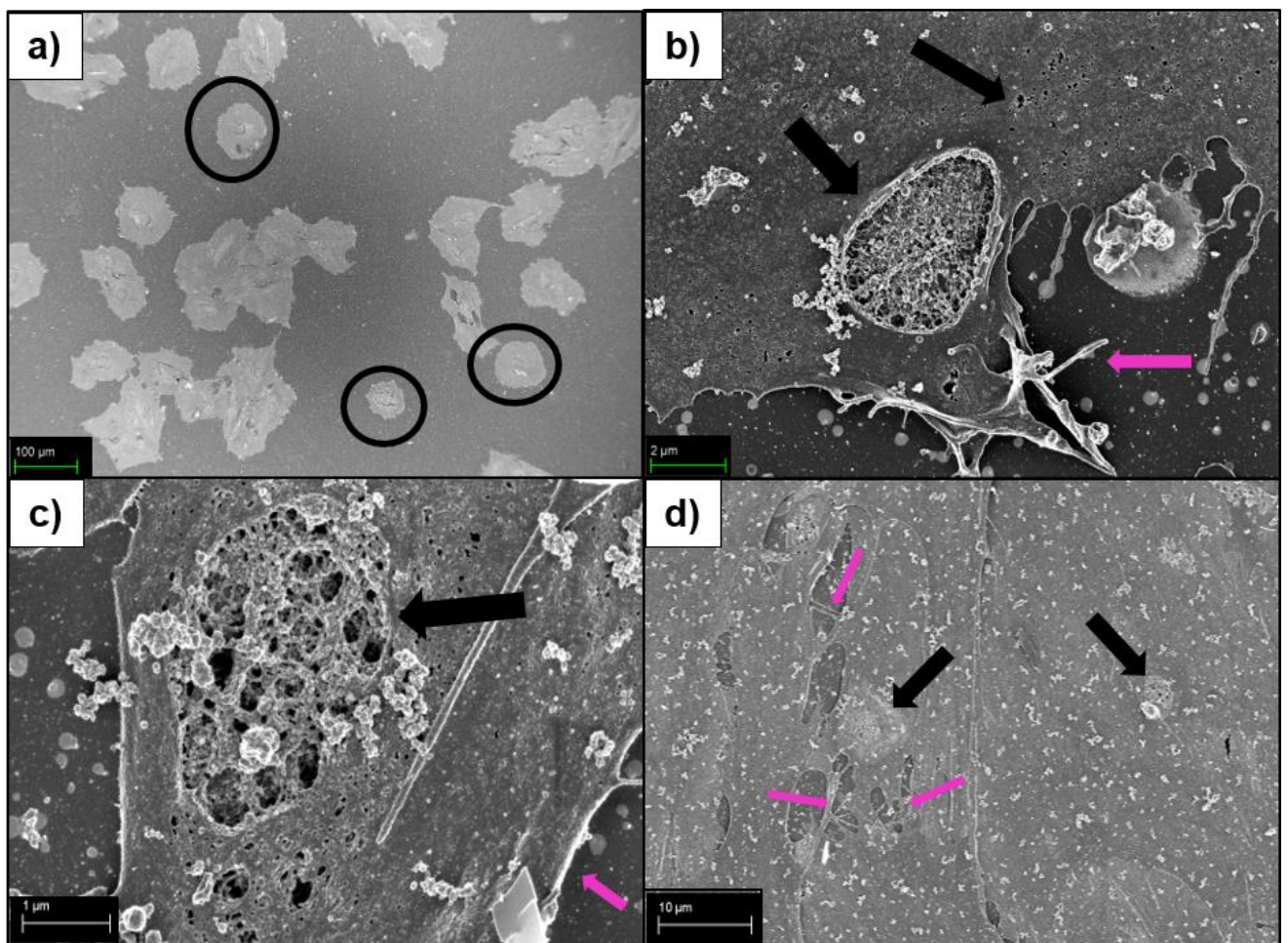
Figure 24 Scanning electron micrograph of the surface of H9c2 cells exposed to 100 µM 1α,2α-epoxyscillirosidine for 24 h (a, b) and 48 h (d, e). Many of the cells were shrunken and exhibited a rounder shape (black circles) when compared to the untreated cells. Clear damage to the plasma membrane (black arrows) could be seen. The number of protrusions (pink arrows) that facilitate cell-to-cell attachment were reduced. Scale bars indicated at bottom left corner.

### 4.3.3 Ultrastructural changes in H9c2 cells induced by the cumulative bufadienolide, lanceotoxin B

The ultrastructural changes of the H9c2 cells after exposure to lanceotoxin B for 24, 48 and 72 h were investigated.

After exposure of the H9c2 cells to lanceotoxin B for 24 h (**Figure 25**), the mitochondria were damaged (orange arrow heads) and somewhat swollen. A large number of autophagic vesicles (red arrows) were observed in the cells and increased in cells exposed to higher concentrations of lanceotoxin B. The nuclei of the cells remained mostly unchanged compared to the control cells, however electron-dense granular deposits (red circles) were present in the nucleoplasm of some cells. Clear blebbing (white arrows) of the plasma membrane could be seen in many of the cells exposed to lanceotoxin B (**Figure 25c**). The Golgi complexes and RER remained unaffected.
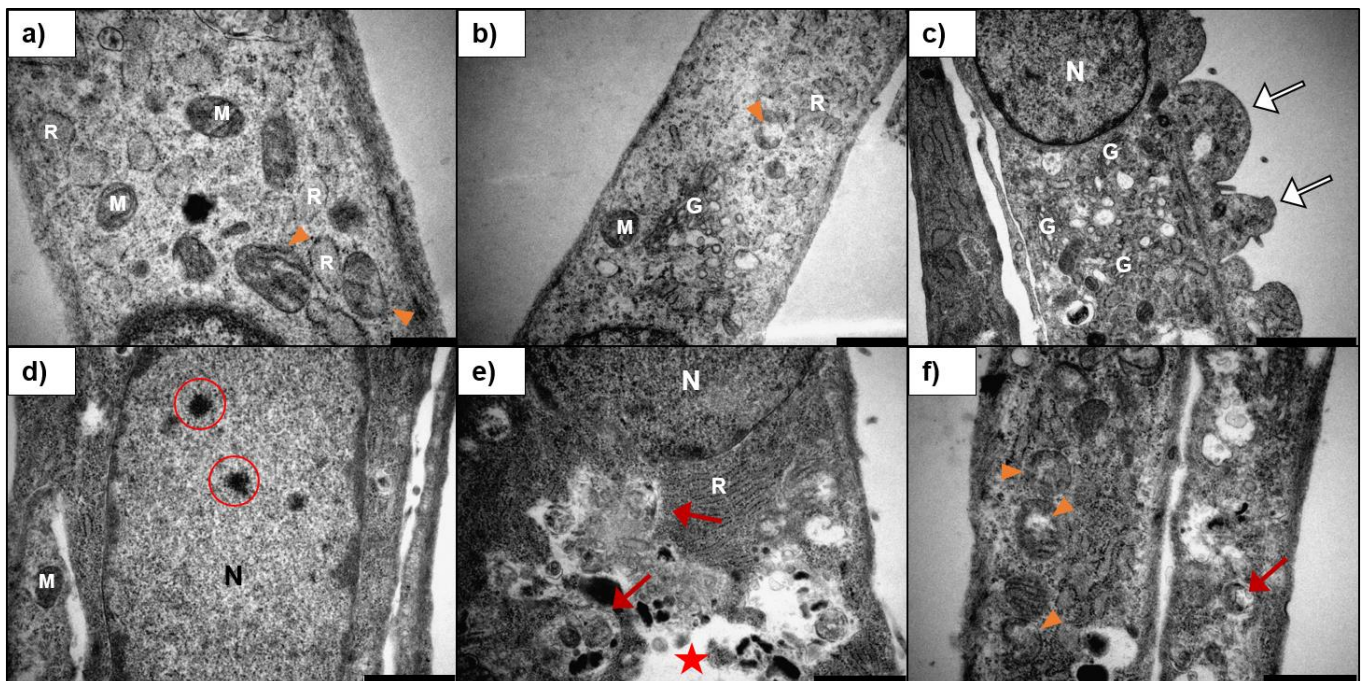
Figure 25 Transmission electron micrograph of H9c2 cells exposed to 5 µM (a, b), 25 µM (c) and 100 µM (d-f) lanceotoxin B for 24 h. The Golgi complexes and RER remained unaffected. The mitochondria were damaged (orange arrow heads). The nuclei of the cells were unaffected, however some electron-dense, granular aggregates (red circles) could be seen in the nuclei of some cells. Many autophagic vesicles (red arrows) could be seen, with gaps (red stars) created within the cytoplasm. Some plasma membrane blebs were formed by some cells (white arrows). N - nucleus; G – Golgi complex; R - RER; M – mitochondria. The scale bar at the bottom right corner represents 2 µm (c), 1 µm (b, d-f) and 0.5 µm (a).

At 48 h exposure (**Figure 26**), damage to the mitochondria (orange arrow heads) was apparent and they became increasingly swollen at higher lanceotoxin B concentrations (**Figure 26e**). The cytoplasm had a large number of autophagic vesicles (red arrows), vacuoles and myelin figures. The nuclei of the cells were unaffected, but with some aggregates in the nucleoplasm. The plasma membrane was slightly damaged, and the associated cytoskeleton was clearly affected (pink arrows). Some cells formed blebs (white arrows) and some cellular debris of broken cells were visible. The RER remained unchanged and the Golgi complexes of the cells were slightly swollen.
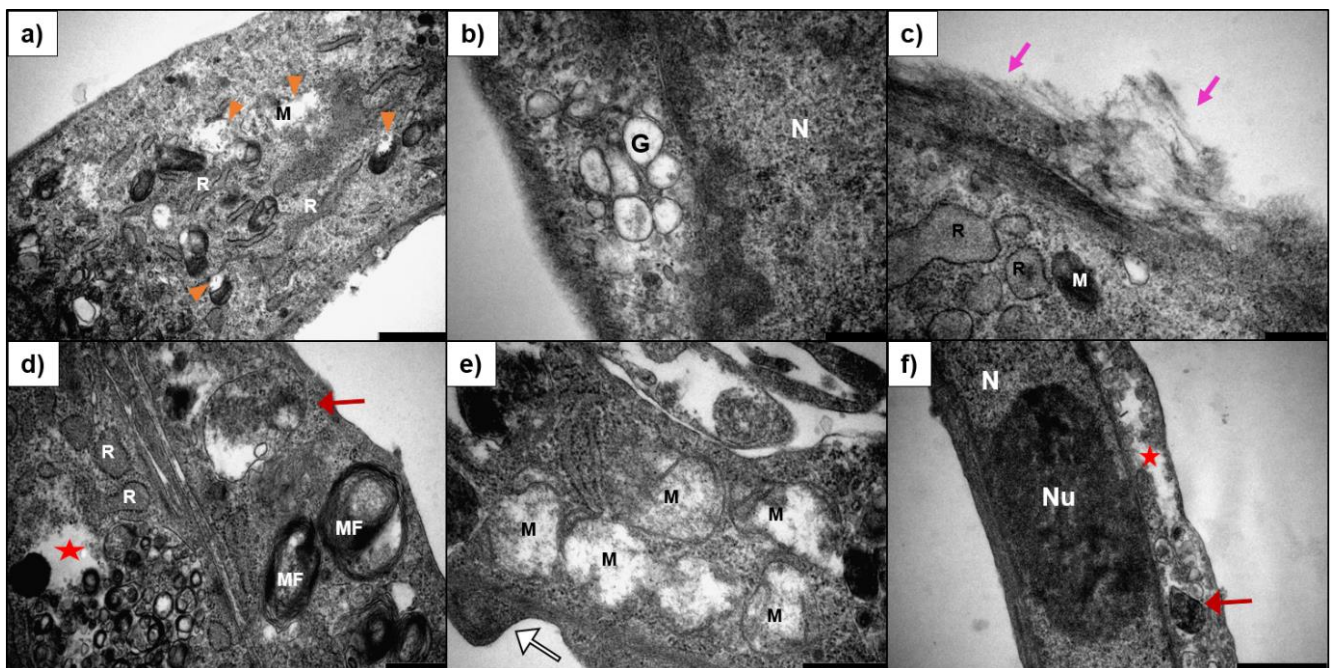
Figure 26 Transmission electron micrograph of H9c2 cells exposed to 5 µM (a, b, c), 25 µM (d) and 100 µM (e, f) lanceotoxin B for 48 h. The RER remained unaffected, but the Golgi complexes were swollen. The mitochondria were swollen (as in e) and damaged (orange arrow heads). The nuclei remained visibly unaffected. The number of autophagic vesicles (red arrows), myelin figures and gaps (red star) within the cytoplasm increased. The cytoskeleton surrounding the cells also seemed to be affected (pink arrows) and the cells formed plasma membrane blebs (white arrows). N - nucleus; Nu - nucleolus; G - Golgi complex; R - RER; MF - myelin figure; M - mitochondria. The scale bar at the bottom right corner represents 1 µm (a, f) and 0.5 µm (b-e).

After 72 h exposure of H9c2 cells to lanceotoxin B (**Figure 27**), the mitochondria were clearly swollen and damaged (orange arrow heads). The cytoplasm of the cells contained vacuoles, autophagic vesicles (red arrows) and myelin figures. The cytoplasm was disrupted in certain areas of the cell, with large gaps forming (red stars). Granular deposits were observed in the nucleoplasm of some nuclei. The RER were largely unchanged, and the Golgi complexes were slightly swollen.
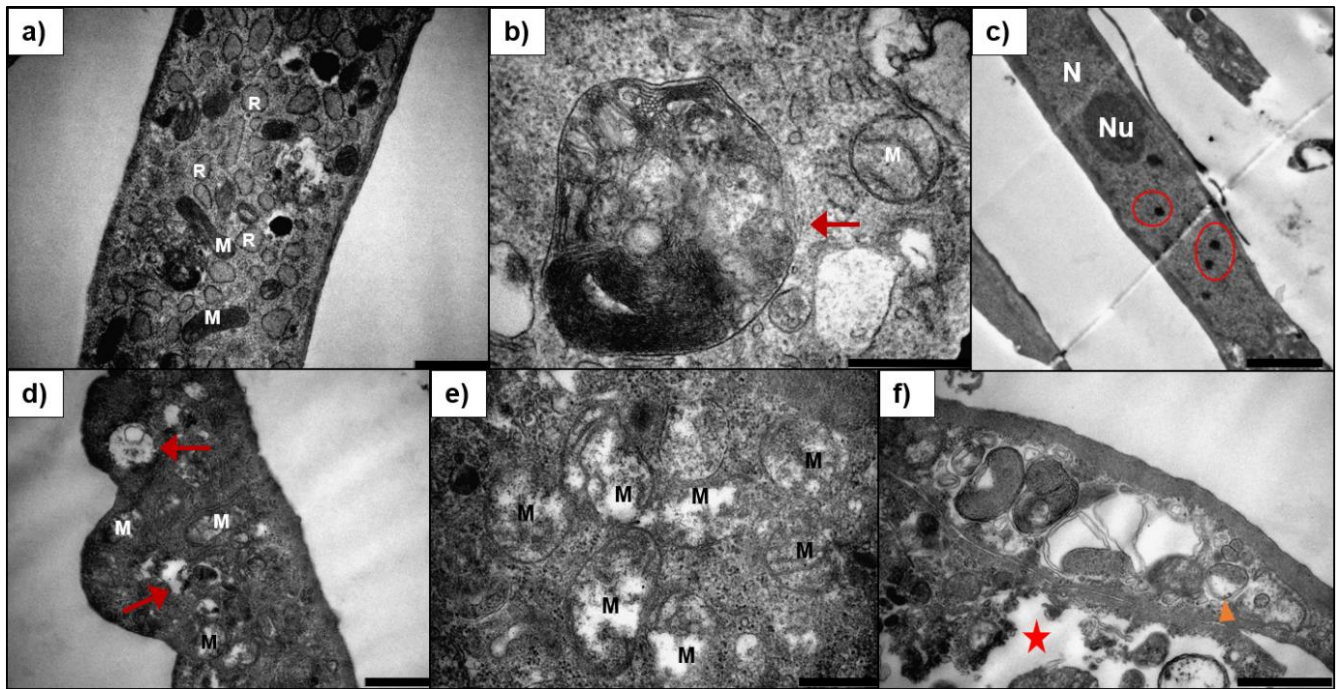
Figure 27 Transmission electron micrograph of H9c2 cells exposed to 5 µM (a, b) and 100 µM (c-f) lanceotoxin B for 72 h. The Golgi complexes were swollen, whilst the RER remained unaffected. Most of the mitochondria were clearly damaged (orange arrow heads) and swollen. The nuclei remained largely unaffected, but some contained electron-dense, granular aggregates (red circles). Vesicles, myelin figures and autophagic vesicles (red arrows) were formed throughout the cytoplasm. Clear gaps could be seen in the cytoplasm of some cells (red stars). N - nucleus; Nu - nucleolus; R - RER; M – mitochondria. The scale bar at the bottom right corner represents 2 µm (c), 1 µm (a, d, f) and 0.5 µm (b, e).

Scanning electron microscopy was used to visualise the cells exposed to 100 μM lanceotoxin B for 24 and 48 h (**Figure 28**). The exposed cells were shrunken, and rounder compared to the control cells (black circles). Plasma membrane blebs were visible on the surface of some cells (white arrows). The protrusions (pink arrows) that allowed cell-to-cell adherence decreased and the cells seemed to be detaching from the coverslip.
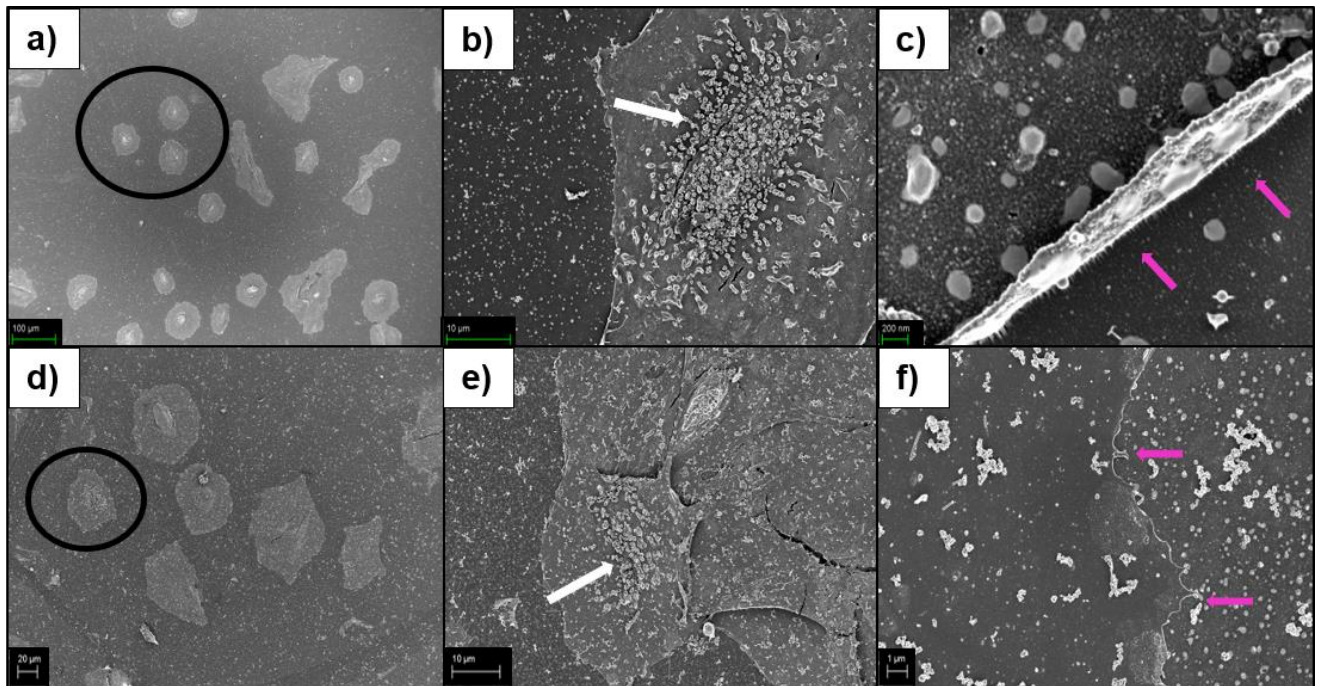
Figure 28 Scanning electron micrograph of the surface of H9c2 cells exposed to 100 μM of lanceotoxin B for 24 h (a-c) and 48 h (d-f). Some of the cells were shrunken and rounded (black circles). Some cells had membrane blebs (white arrows) visible on the surface. The protrusions extending from the cells were reduced and the cells were detaching from the coverslip and from each other (pink arrows). Scale bars indicated at bottom left corner.

4.4 The ultrastructural changes of Neuro-2a cells after exposure to three different cardiac glycosides

Transmission electron microscopy was used to study the subcellular changes that occurred in Neuro-2a cells after being exposed to 5, 25 and 100 μM of digoxin, 1α,2α-epoxyscillirosidine or lanceotoxin B for 24, 48 and 72 h. The ultrastructural changes were identified by comparing the cells to the untreated Neuro-2a cells. All changes are summarised according to incubation time in **Table 3** and additionally, according to toxin concentrations in **Table 5**.

Untreated cells had clearly defined Golgi complexes and electron dense mitochondria with lamellar cristae surrounded by RER (**Figure 29**). A few autophagic vesicles (red arrows) were found scattered within the cytoplasm. The nuclei were somewhat oval,

with few having a more irregular shape. One or more nucleoli were present within the nuclei of each cell. The cells had small, thin and bubble-like protrusions forming around the edge of the cell (orange arrows).
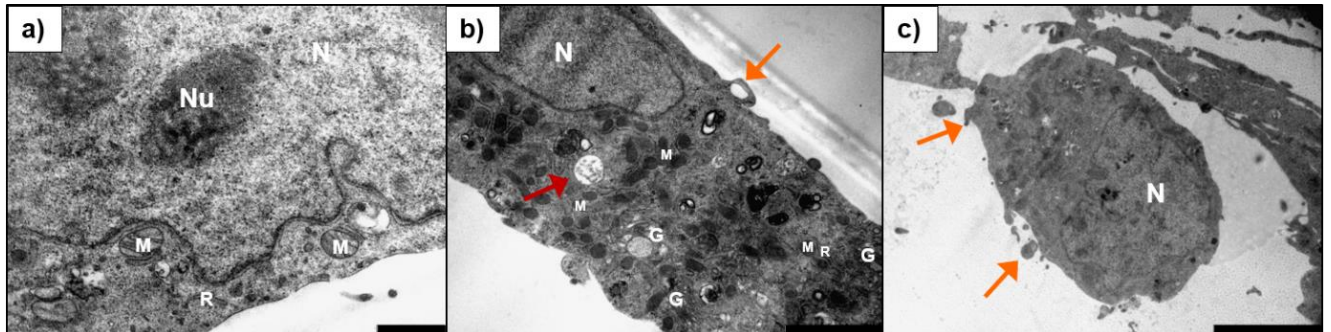
Figure 29 Transmission electron micrograph showing untreated Neuro-2a cells after 24 h (a), 48 h (b) and 72 h (c). The control cells were grown in DMEM supplemented with 10% FBS and 1 U/ml penicillin-streptomycin. The cells had well defined Golgi complexes and a few autophagic vesicles (red arrows). The cells had small, thin and bubble-like protrusions (orange arrows). N - nucleus; Nu - nucleolus; G - Golgi complex; R - RER; M - mitochondria. The scale bar at the bottom right corner represents 5 μm (c), 2 μm (b) and 1 μm (a).

The surface of the cells exposed to 100 μM of the different cardiac glycosides for 24 and 48 h were studied using SEM (**Figure 30**). The cells had numerous protrusions (pink arrows) that allows the cells to attach to each other and to the coverslip. Unlike the H9c2 cell, the surface of the Neuro-2a cells were less smooth and covered with many bubble-like protrusions (orange arrows). Some dehydration cracks (blue arrows) were formed during sample preparation.
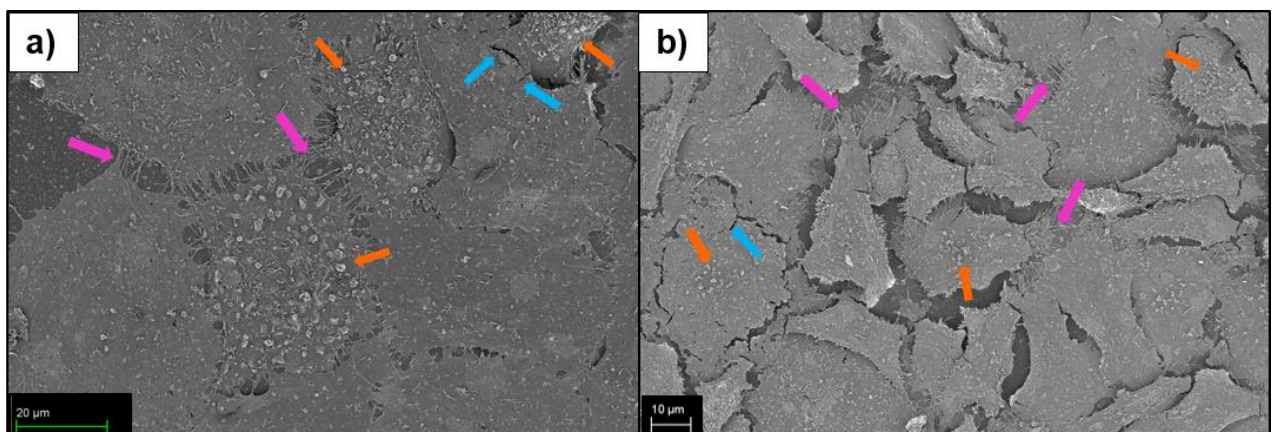
Figure 30 Scanning electron micrograph showing the surface of Neuro-2a cells after 24 h (a) and 48 h (b) exposure. The cells had long protrusions facilitating cell-to-cell attachment (pink arrows) and some bubble-like protrusions (orange arrows) on the surface of the cell. Some dehydration cracks (blue arrows) were formed during sample preparation. Scale bars indicated at bottom left corner.

4.4.1 Ultrastructural changes in Neuro-2a cells induced by the cardenolide digoxin

The subcellular changes that occur in Neuro-2a cells after exposure to 5, 25 and 100 µM digoxin for 24, 48 and 72 h were determined using TEM. Scanning electron microscopy was used to investigate the effect of 100 µM digoxin on the surface of Neuro-2a cells after 24 and 48 h exposure.

After the Neuro-2a cells were exposed to digoxin for 24 h (**Figure 31**) the Golgi complexes were swollen, especially at higher digoxin concentrations. In addition, the mitochondria were also swollen. The number of autophagic vesicles (red arrows) and myelin figures increased, compared to the control cells. Some gaps appeared in the cytoplasm of certain cells (red stars). The plasma membrane was mostly intact, and several cells formed small, thin membrane blebs not different from the control cells. The RER and nuclei remained visibly unaffected.
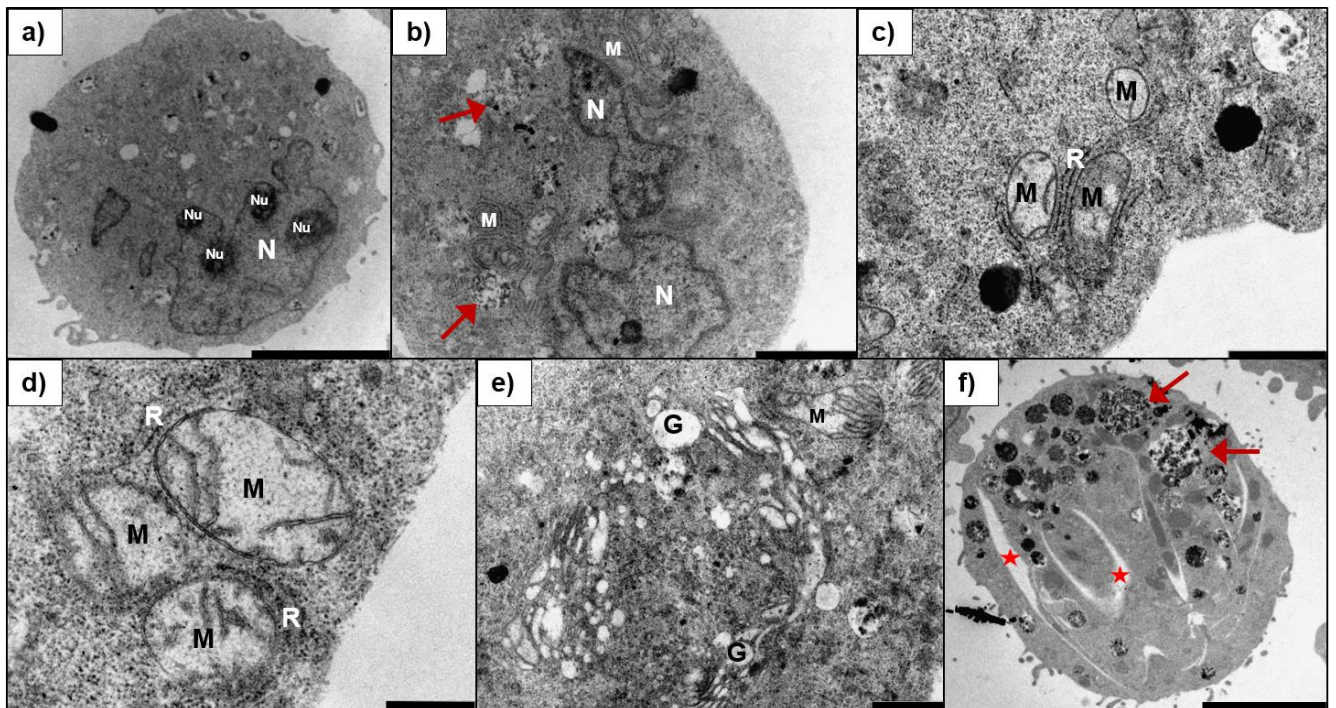
Figure 31 Transmission electron micrograph of Neuro-2a cells exposed to 5 µM (a, b), 25 µM (c, d) and 100 µM (e, f) digoxin for 24 h. The RER remained unaffected after exposure. The Golgi complexes only became swollen at higher digoxin concentrations, whilst the mitochondria were swollen, even at low digoxin concentrations. Many electron-lucent autophagic vesicles (red arrows) and large gaps (red stars) were distributed throughout the cytoplasm. N - nucleus; Nu - nucleolus; G - Golgi complex; R - RER; M – mitochondria. The scale bar at the bottom right corner represents 5 µm (a, f), 2 µm (b), 1 µm (c, e) and 0.5 µm (d).

The Golgi complex of the Neuro-2a cells exposed to digoxin for 48 h (**Figure 32**) were swollen. The mitochondria were damaged (orange arrow heads) and swollen. A large number of autophagic vesicles and vacuoles increased in affected cells. The nuclei remained unaffected. The plasma membrane of the cells remained mostly intact with only a small amount of damage and some plasma membrane blebs (white arrows). The RER remained unaffected.
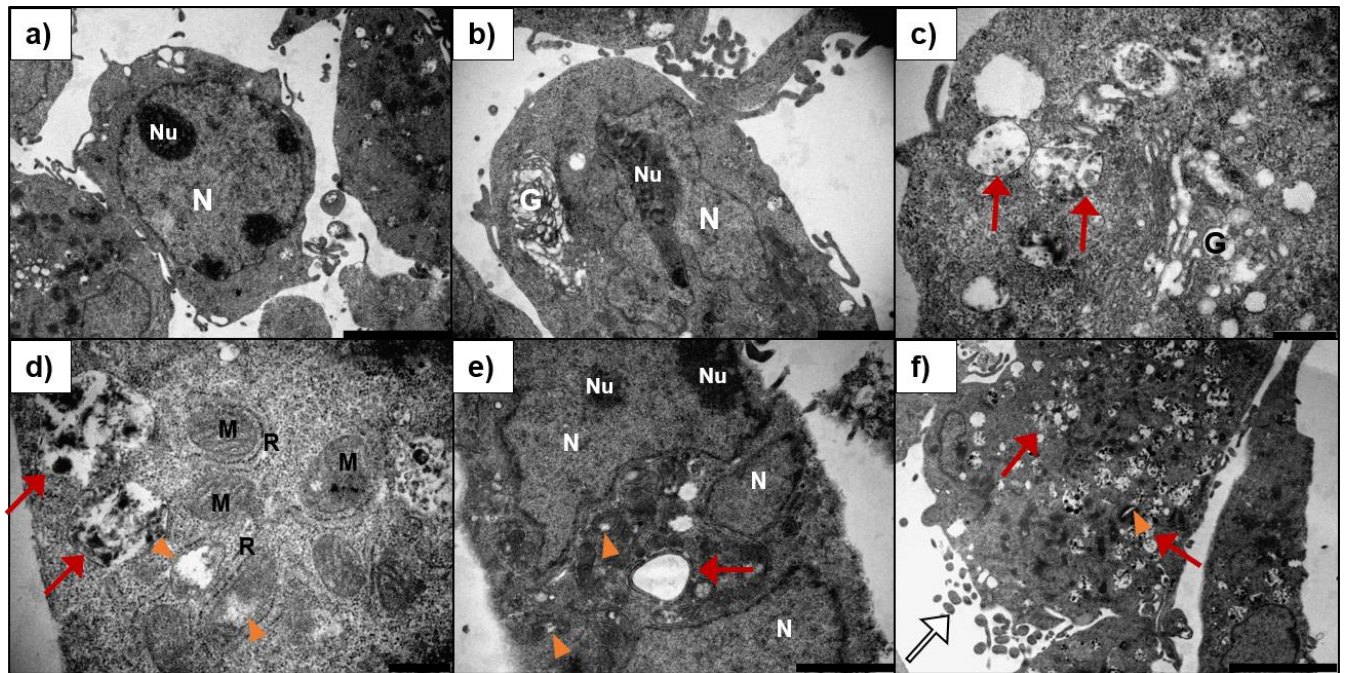
Figure 32 Transmission electron micrograph of Neuro-2a cells exposed to (a, b) 5 µM, (c, d) 25 µM and (e, f) 100 µM digoxin for 48 h. The RER was unaffected, and the Golgi complexes were clearly swollen. The mitochondria were swollen and damaged (orange arrow heads). Electron-lucent autophagic vesicles (red arrows) were distributed throughout the cytoplasm. A few plasma membrane blebs were visible (white arrows). N - nucleus; Nu - nucleolus; G - Golgi complex; R- RER; M - mitochondria. The scale bar at the bottom right corner represents 5 µm (a, f), 2 µm (b, e) and 0.5 µm (c, d).

As with the cells exposed to digoxin for 24 and 48 h, the cells exposed for 72 h (**Figure 33**) had swollen Golgi complexes, but the RER remained unaffected. The mitochondria were no longer swollen, but some were slightly damaged (orange arrow heads). The autophagic vesicles (red arrows), vacuoles and myelin figures were distributed throughout the cytoplasm of affected cells. The nuclei of the cells were unaffected, and the plasma membrane remained mostly intact. The number of cellular protrusions seemed to have increased compared to the control cells.
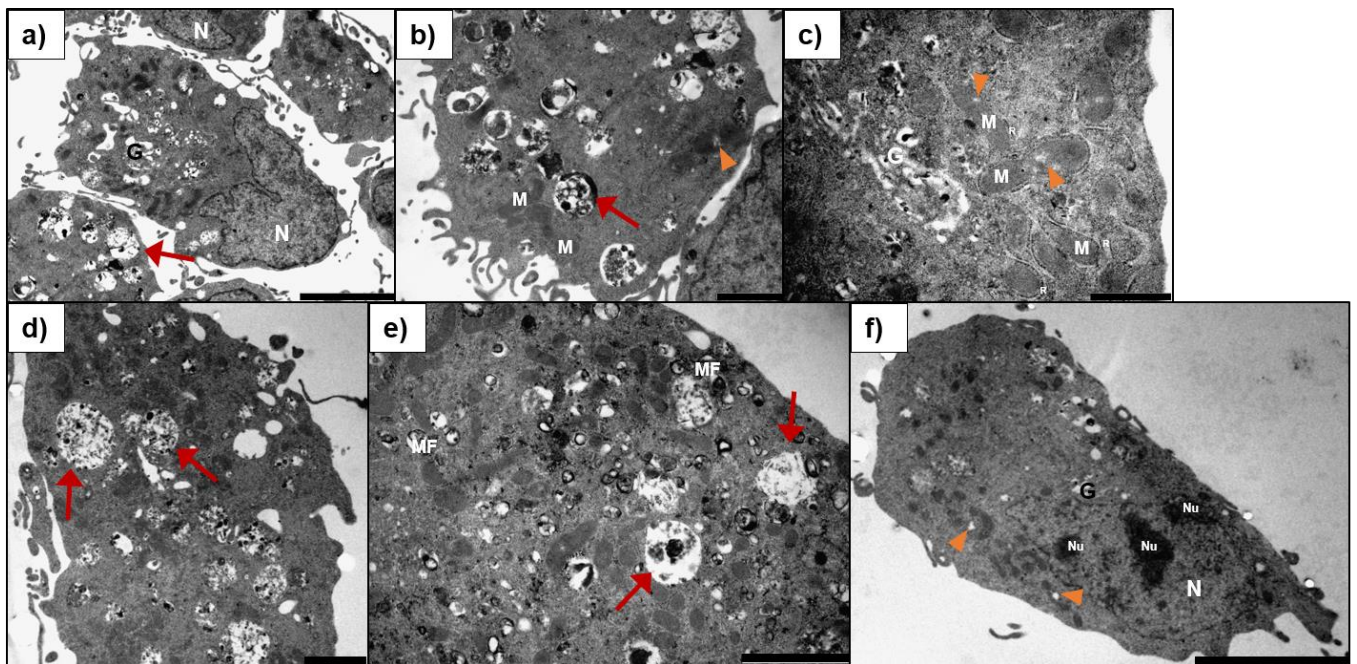
Figure 33 Transmission electron micrograph of Neuro-2a cells exposed to 5 µM (a, b), 25 µM (c) and 100 µM (d-f) digoxin for 72 h. The RER were unaffected. The Golgi complexes were clearly swollen and the mitochondria, though not swollen, were damaged (orange arrow heads). The number of electron-lucent autophagic vesicles (red arrows), vacuoles and myelin figures distributed throughout the cytoplasm increased. The nuclei were unaffected. N - nucleus; Nu - nucleolus; G - Golgi complex; R - RER; M - Mitochondria. The scale bar at the bottom right corner represents 5 µm (a, g), 2 µm (b, d, e) and 1 µm (c).

The Neuro-2a cells exposed to 100 µM digoxin for 24 and 48 h were examined using SEM (**Figure 34**). The cells, especially at 48 h, had numerous blebs on the surface (white arrows). The cells seem to have partially detached from the coverslip and many of the protrusions that link the cells to the surface and each other were broken. Damage to the plasma membrane was observed.
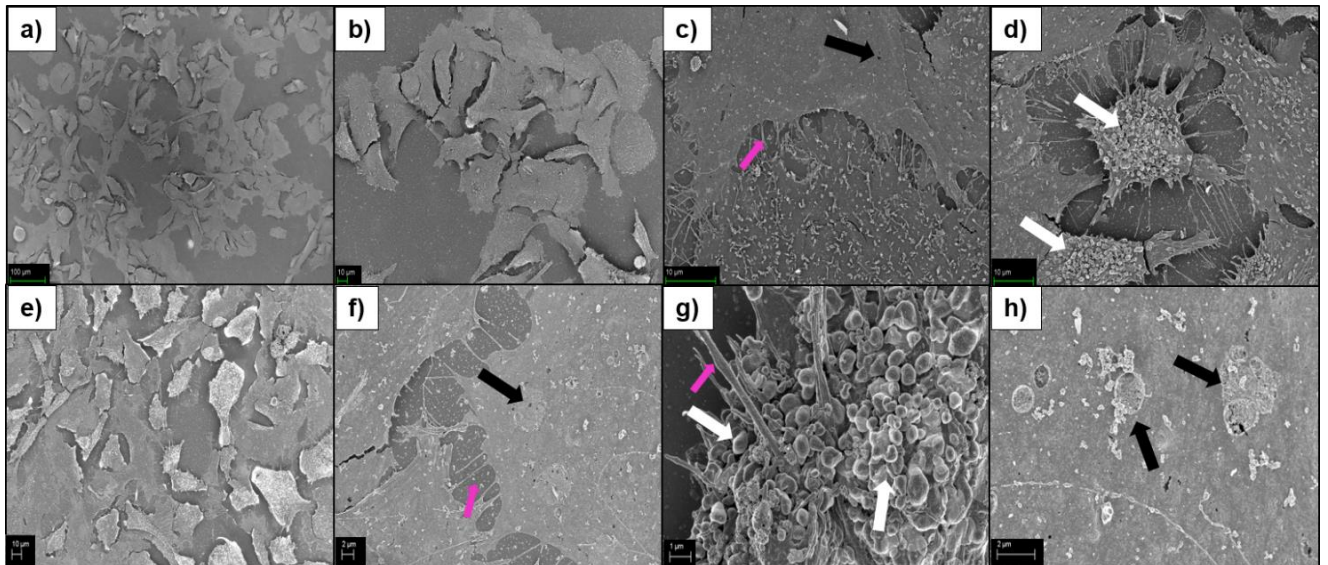
Figure 34 Scanning electron micrograph of the surface of Neuro-2a cells exposed to 100 µM digoxin for 24 h (a-d) and 48 h (e-h). Some cells seem to partially detach from the coverslip. Clear plasma membrane damage (black arrows) could be seen on the surface of the cells. The number of protrusions that formed between cells (pink arrows) were reduced and seemed broken in some cases. Many cells had membrane blebs (white arrows) forming. Scale bars indicated at bottom left corner.

### 4.4.2 Ultrastructural changes in Neuro-2a cells induced by the non-cumulative bufadienolide 1α,2α-epoxyscillirosidine

Neuro-2a cells were exposed to 5, 25 and 100 µM 1α,2α-epoxyscillirosidine for 24, 48 and 72 h and the ultrastructural changes within and on the surface of the cell were subsequently examined using TEM and SEM.

After 24 h exposure to 1α,2α-epoxyscillirosidine (**Figure 35**), the Golgi complexes and RER of the cells were swollen. The mitochondria were damaged (orange arrow heads) and swollen. Some of the mitochondria exposed to 100 µM 1α,2α-epoxyscillirosidine had ballooned cristae (green arrows). A large number of vacuoles were formed within the cytoplasm, as well as a number of autophagic vesicles (red arrows). The nuclei of affected cells were either radially segmented (**Figure 35e**) or irregularly shaped. In this case radially segmented refers to the nucleus forming lobes distributed radially

resembling a cross or clover. In addition, swelling of the perinuclear space (blue arrows) was observed in some cells. Some vacuolisation of the nucleoplasm could also be seen in the most severely affected cells (red stars). The plasma membrane of the cells remained mostly intact with only slight damage. Some cells formed apoptotic bodies (white arrows).
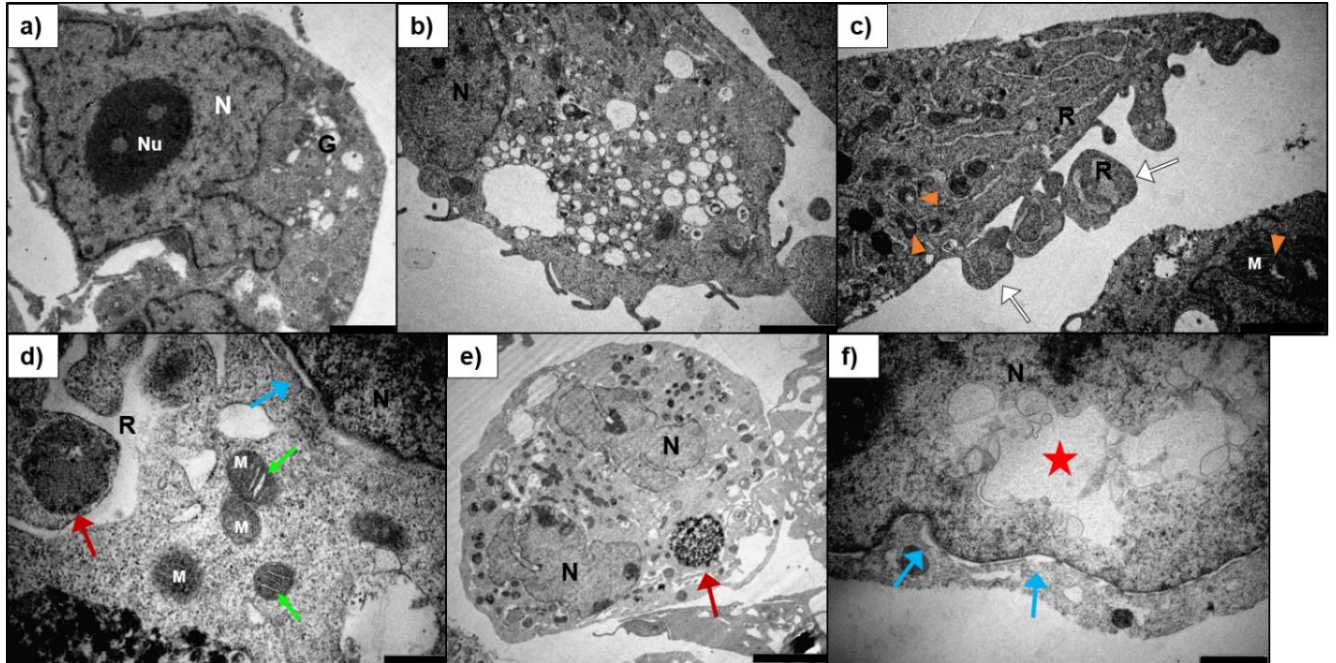
Figure 35 Transmission electron micrograph of Neuro-2a cells exposed to 5 µM (a), 25 µM (b, c) and 100 µM (d-f) 1α,2α-epoxyscillirosidine for 24 h. Both the Golgi complexes and the RER of the cells were swollen. The mitochondria were swollen, damaged (orange arrow heads) and some had ballooned cristae (green arrows). The number of autophagic vesicles (red arrows) and vacuoles within the cytoplasm increased. The perinuclear space of some cells was swollen (blue arrows), and the nuclei themselves were irregularly or radially shaped (see e). Some nuclei had vacuoles (red stars) in the nucleoplasm. Some cells formed apoptotic bodies (white arrows). N - nucleus; Nu - nucleolus; G - Golgi complex; R - RER; M - mitochondria. The scale bar at the bottom right corner represents 5 µm (e), 2 µm (a-c), 1 µm (f) and 0.5 µm (d).

The Neuro-2a cells exposed to 1α,2α-epoxyscillirosidine for 48 h had swollen Golgi and RER, the degree of swelling being greater at higher concentrations of the toxin (**Figure 36**). The ribosomes dissociated from the RER and could be seen clumped within the cytoplasm (red circles). The mitochondria were slightly damaged (orange arrow heads) and swollen, with some of the mitochondria in the cells exposed to 100 μM 1α,2α-epoxyscillirosidine having ballooned cristae (green arrows). The number of vesicles, vacuoles and autophagosomes in the cytoplasm increased considerably compared to the control cells. Clear swelling of the perinuclear space (blue arrows) could be seen. The plasma membrane of the cells remained mostly intact and the number of protrusions were reduced compared to control cells.
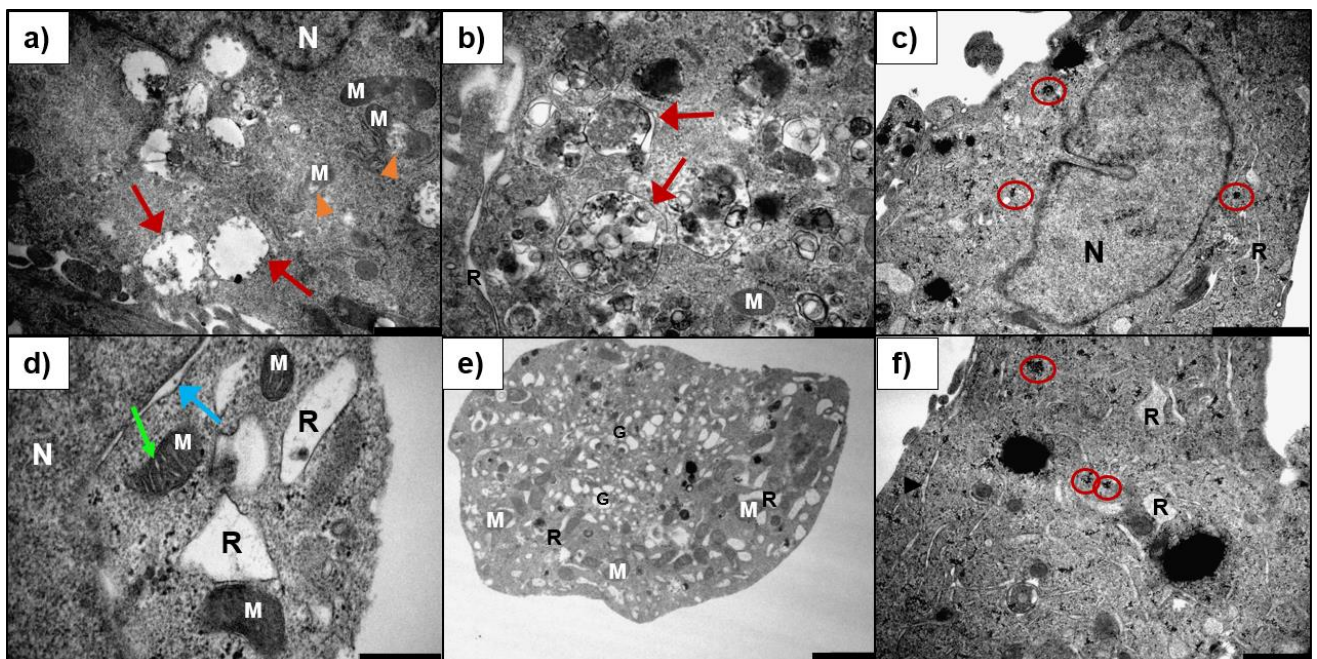
Figure 36 Transmission electron micrograph of Neuro-2a cells exposed to 5 μM (a, b) and 100 μM (c-f) 1α,2α-epoxyscillirosidine for 48 h. Both the Golgi complexes and RER were swollen. Ribosomes dissociated from the RER and could be seen clumped in the cytoplasm (red circles). The number of vacuoles and autophagic vesicles (red arrows) within the cytoplasm increased. The mitochondria were damaged (orange arrow heads) and some had ballooned cristae (green arrows). The perinuclear space of the nuclei was swollen (blue arrows). N -nucleus; G - Golgi complex; R - RER; M - mitochondria. The scale bar at the bottom right corner represents 2 μm (c, e), 1 μm (a, f) and 0.5 μm (b, d).

After 72 h exposure to 1α,2α-epoxyscillirosidine (**Figure 37**), the Golgi complex and RER were slightly swollen, with ribosomes dissociated from the RER. The mitochondria of affected cells were slightly damaged (orange arrow heads) and swollen. The cytoplasm was riddled with vacuoles, autophagic vesicles and some myelin figures. The more severely affected cells have large gaps within the cytoplasm,

stretching throughout the cell (red stars). The nuclei were irregularly shaped. The plasma membrane remained mostly intact, with minor damage and some membrane blebs. The number of cell protrusions were less compared to the untreated control cells.
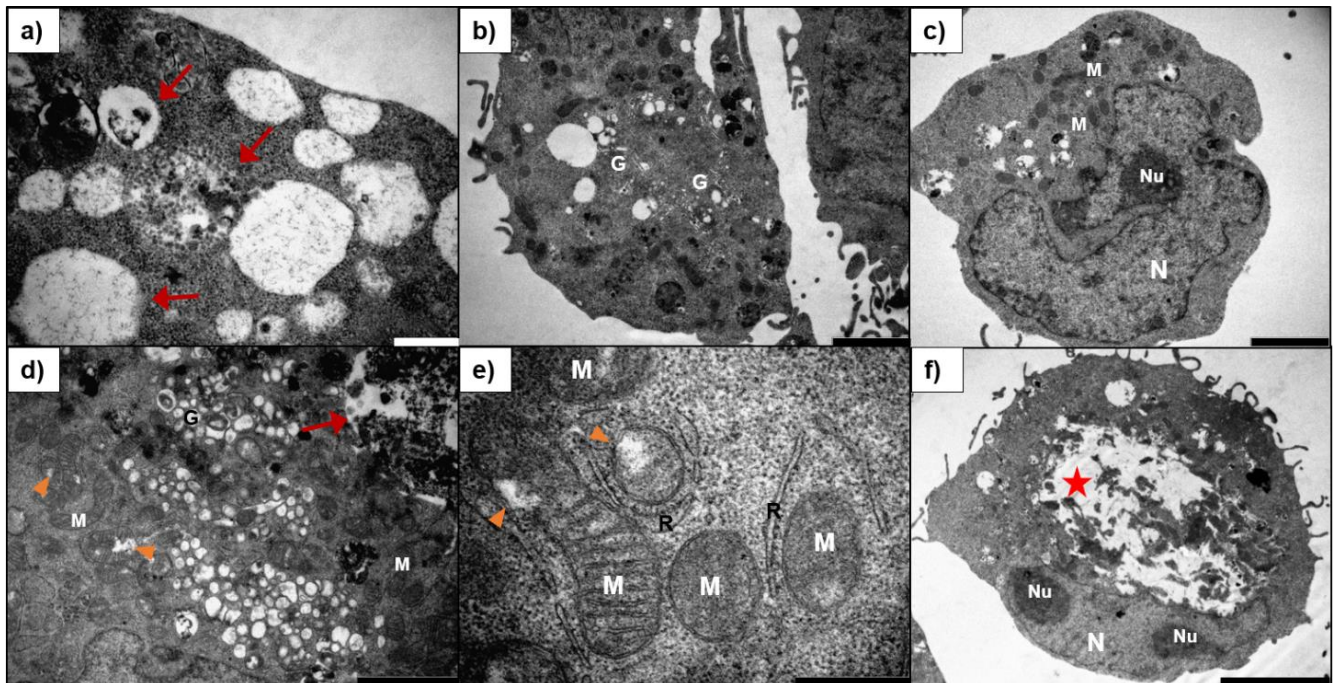
Figure 37 Transmission electron micrograph of Neuro-2a cells exposed to 5 µM (a), 25 µM (b, c) and 100 µM (d-f) 1α,2α-epoxyscillirosidine for 72 h. The RER was not swollen, however some ribosomes still dissociated. The Golgi complexes were swollen, and the mitochondria were damaged (orange arrow heads). The number of electron-lucent autophagic vesicles (red arrows) and vacuoles within the cytoplasm increased. Some parts of the cytoplasm were disrupted (red stars). N - nucleus; Nu - nucleolus; G - Golgi complex; R - RER; M - mitochondria. The scale bar at the bottom right corner represents 5 µm (f), 2 µm (b-d) and 0.5 µm (a, e).

The surface of Neuro-2a cells exposed to 100 µM 1α,2α-epoxyscillirosidine for 24 and 48 h were studied using SEM (**Figure 38**). As with the H9c2 cells, the difference in purity of the batch of 1α,2α-epoxyscillirosidine used for SEM resulted in reduction of the effects of 1α,2α-epoxyscillirosidine exposure to the Neuro-2a cells. The cells were shrunken and rounded (black circles), with many cells seemingly detaching from the coverslip (pink arrows). The cells had fewer protrusions, compared to the control cells. Slight membrane damage was visible on the surface of the cells (black arrows).
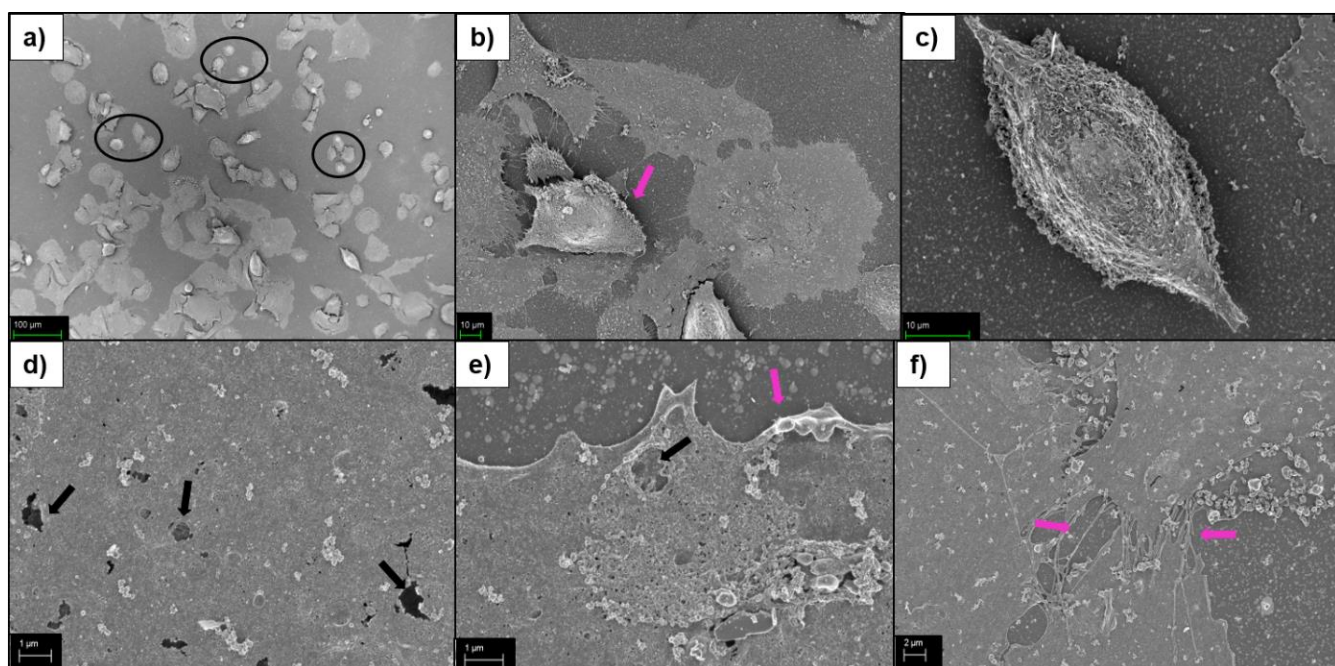
Figure 38 Scanning electron micrograph depicting the surface of Neuro-2a cells exposed to 100 µM 1α,2α-epoxyscillirosidine for 24 h (a-c) and 48 h (d-f). The number of cells on the coverslip was less compared to the untreated, control cells. Some of the cells were shrunken and round (black circles). The cells seemed to detach from coverslip and the cell protrusions that facilitate cell-to-cell attachment and cell-to-surface attachment were reduced (pink arrows). Plasma membrane damage (black arrows) was visible on the surface of the cells. Scale bars indicated at bottom left corner.

4.4.3 Ultrastructural changes in Neuro-2a cells induced by the cumulative bufadienolide, lanceotoxin B

The ultrastructural changes of the Neuro-2a cells exposed to 5, 25 and 100 µM lanceotoxin B for 24, 48 and 72 h, were investigated using TEM and SEM and compared to the control cells.

After 24 h exposure to lanceotoxin B (**Figure 39**), the Golgi complexes and mitochondria of the Neuro-2a cells were clearly swollen. The RER remained

unaffected, except for cells exposed to 5 µM lanceotoxin B that had clearly swollen RER. Likewise, the nuclei were unaffected, except for those exposed to 5 µM that had swollen perinuclear spaces (blue arrows). The number of vacuoles and autophagic vesicles (red arrows) in the cytoplasm increased drastically. Large parts of some cells were sequestered in the autophagic vesicles and gaps formed in the cytoplasm (red stars). Some of the sequestered content seem to be extruded to the outside of the cell (orange arrows). The cells were rounder and blebs formed from the plasma membrane (white arrows).
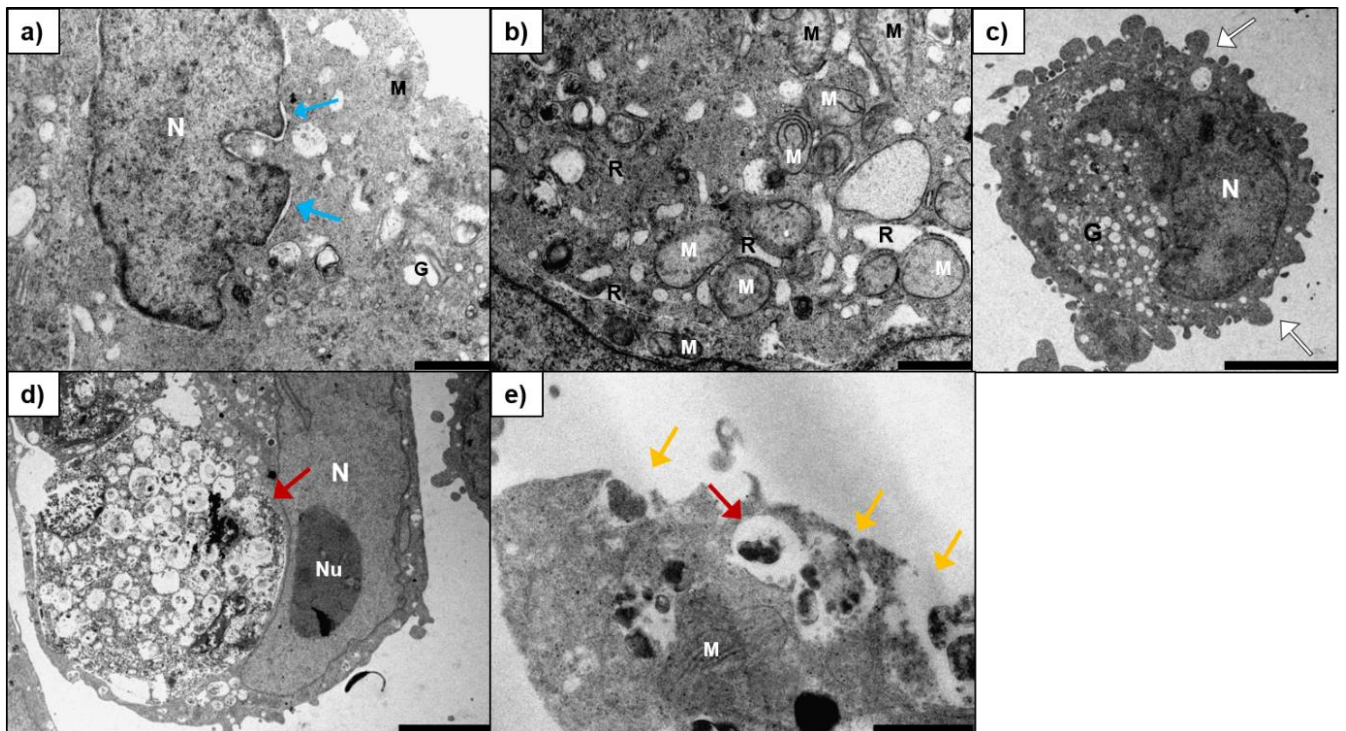
Figure 39 Transmission electron micrograph of Neuro-2a cells exposed to 5 µM (a, b), 25 µM (c, d) and 100 µM (e) of lanceotoxin B for 24 h. The RER and perinuclear space (blue arrows) of cells exposed to 5 µM lanceotoxin B were swollen. In contrast, the Golgi and mitochondria were clearly swollen at all concentrations. Many vacuoles and autophagic vesicles (red arrows) formed within the cytoplasm. Some of the sequestered content was extruded to the outside of the cell (orange arrows). Some cells were rounded with blebbing of the plasma membrane (white arrows). N - nucleus; Nu - nucleolus; G - Golgi complex; R - RER; M - mitochondria. The scale bar at the bottom right corner represents 5 µm (c, d) and 1 µm (a, b, f).

The cells exposed to lanceotoxin B for 48 h had swollen Golgi complexes and mitochondria (**Figure 40**). Large autophagic vesicles (red arrows) and vacuoles were distributed throughout the cytoplasm. The cells extruded the sequestered content (orange arrows). The nuclei were unaffected. The plasma membrane of the cells was mostly intact, with some membrane blebs visible. The cellular protrusions were reduced compared to the untreated, control cells. The RER was not swollen.
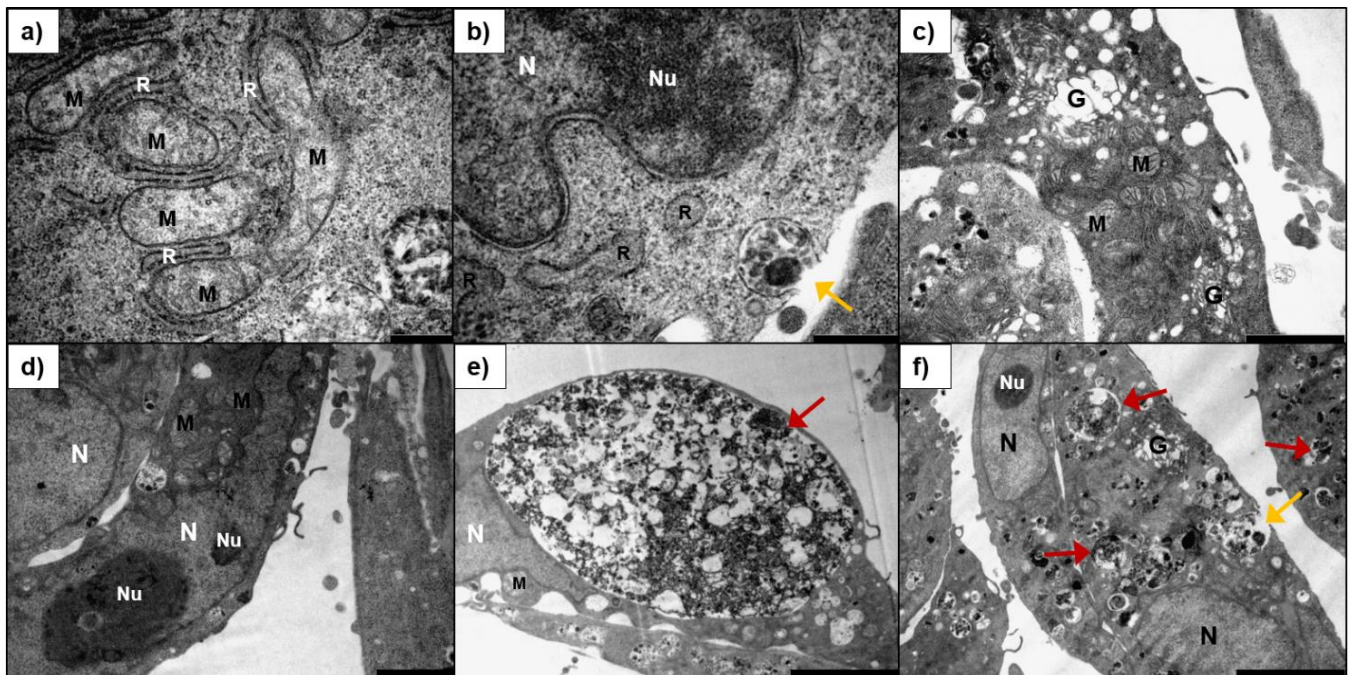
Figure 40 Transmission electron micrograph of Neuro-2a cells exposed to 5 µM (a, b), 25 µM (c-e) and 100 µM (f) lanceotoxin B for 48 h. The RER remained unaffected. The Golgi complexes and mitochondria were swollen. Autophagic vesicles (red arrows) and vacuoles were distributed throughout the cytoplasm. Some of the sequestered content was extruded to the outside of the cell (orange arrows). N - nucleus; Nu - nucleolus; G - Golgi complex; R - RER; M - mitochondria. The scale bar at the bottom right corner represents 5 µm (e, f), 2 µm (c, d) and 0.5 µm (a, b).

As with the 24 and 48 h exposures, Neuro-2a cells exposed to lanceotoxin B for 72 h had swollen Golgi, while the RER remained unaffected (**Figure 41**). The mitochondria were grossly swollen. The autophagic vesicles (red arrows) and vacuoles were distributed throughout the cytoplasm. The cells seemed to extrude their sequestered content to the outside (orange arrows). The plasma membrane was mostly intact, and some cells were shrunken, rounder and formed plasma membrane blebs (not shown). The nuclei were unaffected.
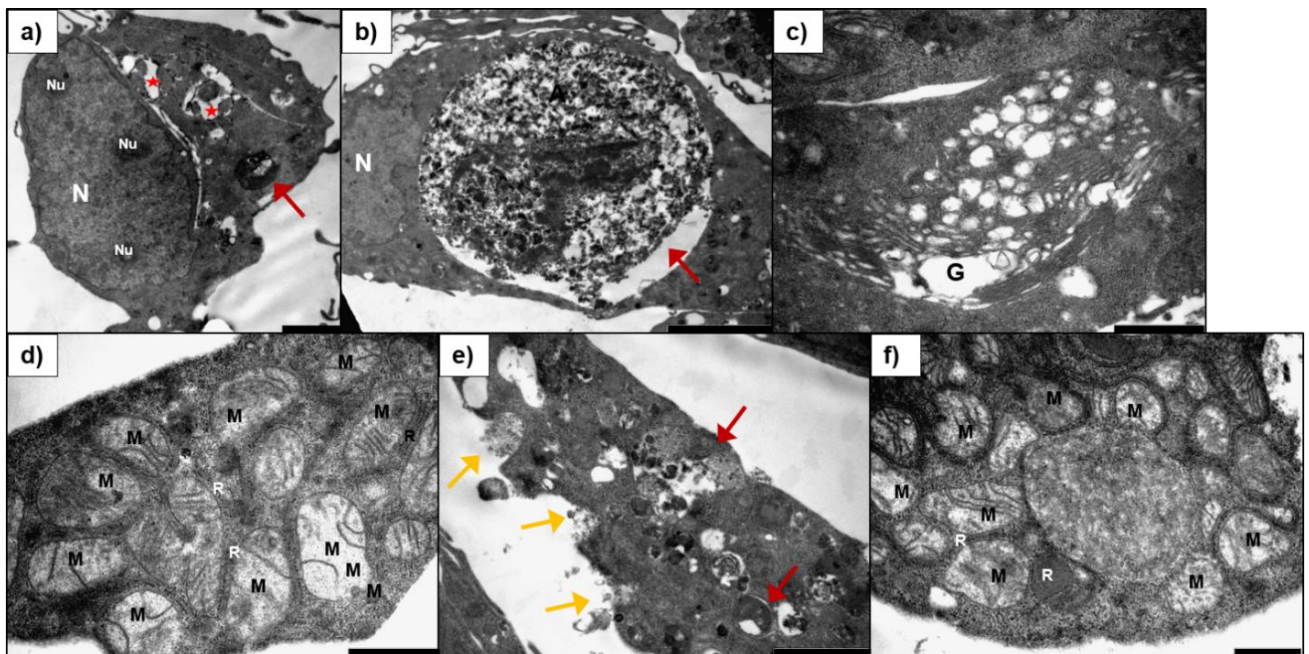
Figure 41 Transmission electron micrograph of Neuro-2a cells exposed to 5 µM (a), 25 µM (b-d) and 100 µM (e, f) lanceotoxin B for 72 h. The RER were unaffected, whilst the Golgi complexes and mitochondria were swollen. Many vacuoles and autophagic vesicles (red arrows) were distributed throughout the cytoplasm and gaps (red stars) formed. Some of the sequestered content was extruded to the outside of the cell (orange arrows). N - nucleus; Nu - nucleolus; G - Golgi complex; R - RER; M - mitochondria. The scale bar at the bottom right corner represents 5 µm (b), 2 µm (a, e) and 1 µm (c, d, f).

The Neuro-2a cells were exposed to 100 µM lanceotoxin B for 24 and 48 h and observed using SEM (**Figure 42**). The number of cells were drastically reduced compared to the control cells. There were fewer cell-to-cell attachments and the cells seemed to be detaching from the coverslip (pink arrows). Many cells were rounded, and membrane damage could be seen (black arrows). Some cells had protrusions (white arrows) on their surface.
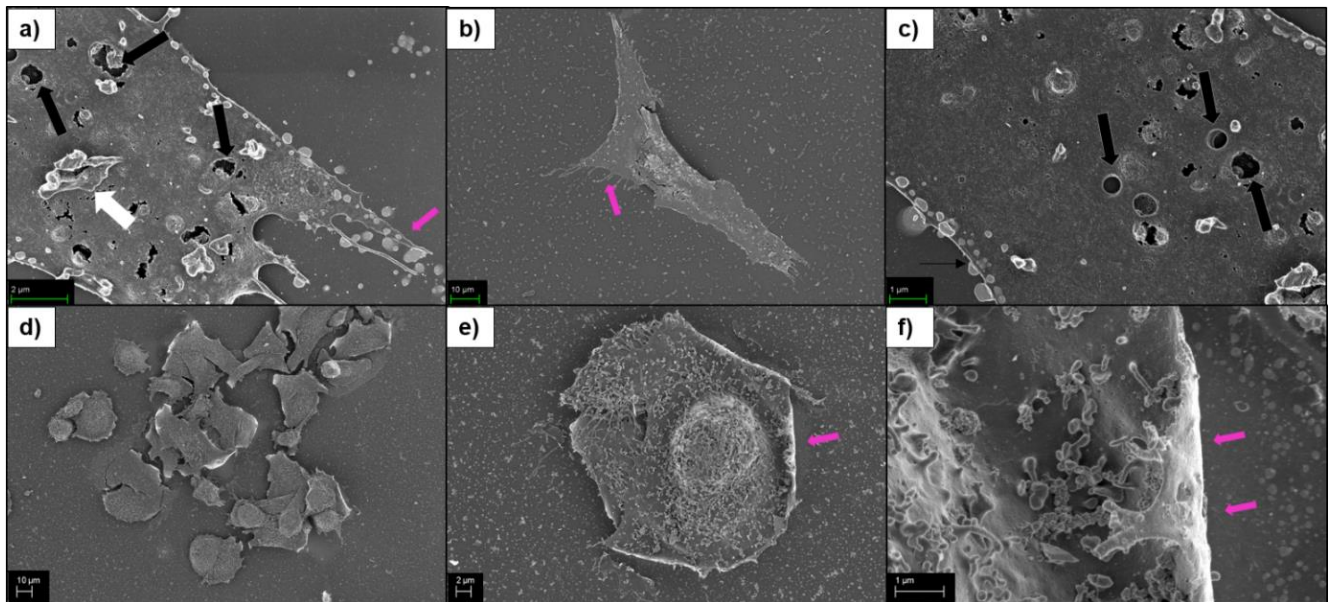

Figure 42 Scanning electron micrograph showing the surface of Neuro-2a cells exposed to 100 µM lanceotoxin B for 24 h (a-c) and 48 h (d-f). The number of cells were drastically reduced compared to the untreated, control cells. The cells were detaching from the coverslip as the cell-to-cell and cell-to-surface attachments were reduced (pink arrows). Damage to the plasma membrane (black arrows) and surface protrusions (white arrows) was also observed. Many of the cells were rounded. Scale bars indicated at bottom left corner.

4.5 Summary of results, additional tables and graphs
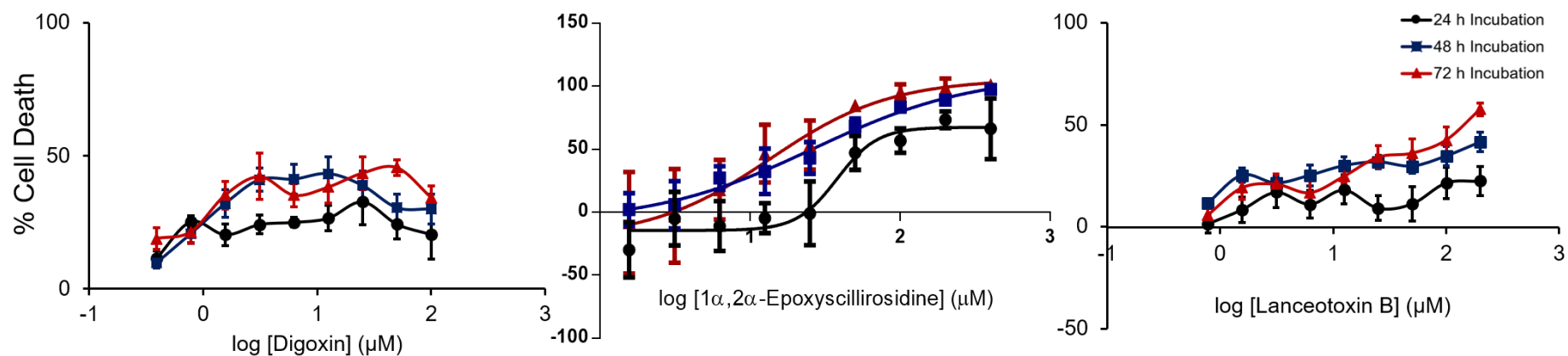
Figure 43 The semi-log concentration-response (expressed as percentage cell death) curves of digoxin, 1α,2α-epoxyscillirosidine and lanceotoxin B on H9c2 cells for 24, 48 and 72 h incubation.
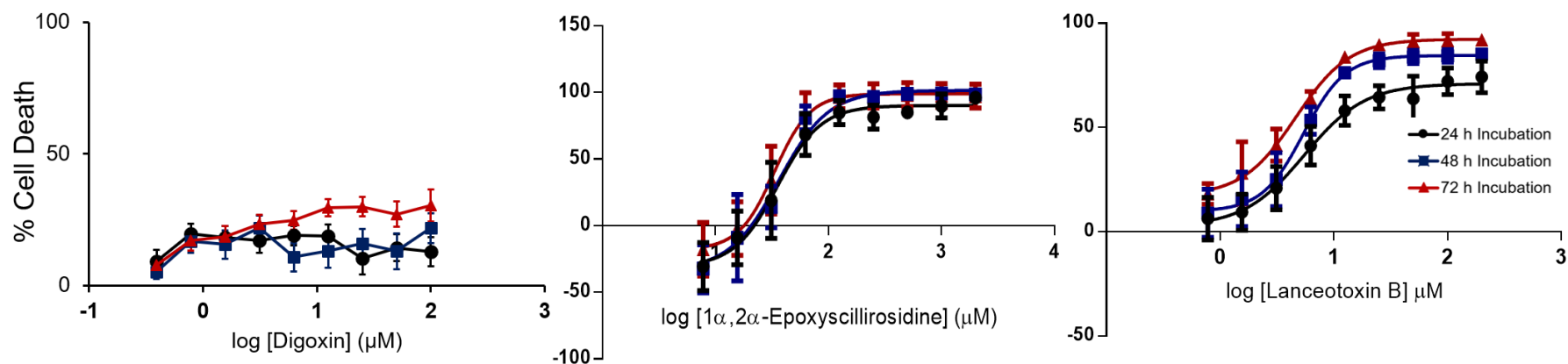
Figure 44 The semi-log concentration-response (expressed as percentage cell death) curves of digoxin, 1α,2α-epoxyscillirosidine and lanceotoxin B on Neuro-2a cells for 24, 48 and 72 h incubation.

Table 2 Summary of the subcellular changes that occurred in H9c2 cells after being exposed to different cardiac glycosides.

Toxin	Time	Golgi Complex	RER	Mitochondria	Nuclei	Vesicles, vacuoles and other	Plasma membrane and cell form
Digoxin	24 h	Unaffected	Unaffected	Damaged and swollen	Nuclei remained unaffected.	Autophagic vesicles and myelin figures in cytoplasm. Gaps in cytoplasm.	Slight plasma membrane damage.
	48 h	Swollen at higher concentrations	Unaffected	Damaged and swollen	Nuclei remained unaffected.	Autophagic vesicles and myelin figures in cytoplasm. Gaps in cytoplasm.	The plasma membrane and associated cytoskeleton was damaged. Cellular debris of broken cells visible.
	72 h	Slightly swollen	Unaffected	Damaged and swollen	Nuclei remained unaffected.	Many autophagic vesicles and myelin figures in cytoplasm. Gaps in cytoplasm	The plasma membrane and associated cytoskeleton was damaged. Cellular debris of broken cells visible.
1α,2α-Epoxyscillirosidine	24 h	Slightly swollen	Swollen	Damaged	Perinuclear space was swollen.	Some autophagic vesicles in cytoplasm. Extensive vacuolation of cytoplasm. Gaps in cytoplasm	Severe plasma membrane damage in many cells. Some cells formed apoptotic bodies.
	48 h	Swollen	Swollen	Damaged	Perinuclear space was swollen. Condensed nuclear material at higher concentrations.	Autophagic vesicles and myelin figures in cytoplasm. Extensive vacuolation of cytoplasm Gaps in cytoplasm.	Severe plasma membrane damage. Cells are shrunken, rounded and formed apoptotic bodies. Cellular debris of broken cells visible.
	72 h	Slightly swollen	Swollen. Ribosomes dissociated	Damaged. Mitochondria have ballooned cristae	Perinuclear space was slightly swollen. Condensed nuclear material at higher concentrations.	Autophagic vesicles and myelin figures visible in cytoplasm. Extensive vacuolation of cytoplasm.	Severe plasma membrane damage. Cells are shrunken, rounded and formed apoptotic bodies. Cellular debris of broken cells visible.
Lanceotoxin B	24 h	Slightly swollen	Unaffected	Damaged and slightly swollen	Granular electron dense aggregates in nucleoplasm.	Many autophagic vesicles (electron lucent) present in the cytoplasm. The cytoplasm is disrupted in certain areas.	Plasma membrane damage and membrane blebs.
	48 h	Slightly swollen	Unaffected	Damaged and swollen	Nuclei remained unaffected.	Many autophagic vesicles (electron lucent) and myelin figures present in the cytoplasm.	The plasma membrane and associated cytoskeleton was damaged. Plasma membrane blebs visible Some cells are shrunken and rounded. Cellular debris of broken cells visible.
	72 h	Swollen	Unaffected	Swollen	Granular electron dense aggregates in nucleoplasm.	Many autophagic vesicles (electron lucent), myelin figures and vacuoles present in the cytoplasm. The cytoplasm is disrupted in certain areas.	The plasma membrane and associated cytoskeleton was damaged. Plasma membrane blebs visible. Cellular debris of broken cells visible.

Table 3 Summary of the subcellular changes that occurred in Neuro-2a cells after being exposed to different cardiac glycosides grouped by exposure time.

Toxin	Time	Golgi Complex	RER	Mitochondria	Nuclei	Vesicles, vacuoles and other	Plasma membrane and cell form
Digoxin	24 h	Swollen at higher concentrations	Not swollen	Swollen	Nuclei remain unaffected	Autophagic vesicles and myelin figures visible in the cytoplasm. Disruption of the cytoplasm.	A few plasma membrane blebs and slight membrane damage
	48 h	Swollen	Not swollen	Damaged and swollen	Nuclei remain unaffected	Autophagic vesicles and vacuoles visible in the cytoplasm. Disruption of the cytoplasm.	Some plasma membrane damage. Cells formed plasma membrane blebs.
	72 h	Swollen	Not swollen	Damaged	Nuclei remain unaffected	Autophagic vesicles, myelin figures and vacuoles visible in cytoplasm.	Increased number of cellular protrusions.
1α,2α-Epoxyscillirosidine	24 h	Swollen	Swollen. Ribosomes dissociated	Damaged and swollen Mitochondria had ballooned cristae	Radially segmented and irregularly shaped nuclei. Vacuoles in nucleoplasm. The perinuclear space was swollen.	Many autophagic vesicles and vacuoles visible in cytoplasm. Extensive vacuolation of cytoplasm.	Cells were rounded and formed membrane blebs and apoptotic bodies. Some plasma membrane damage. Fewer cellular protrusions.
	48 h	Slightly swollen	Swollen. Ribosomes dissociated	Damaged. Mitochondria had ballooned cristae	The perinuclear space was swollen	Many autophagic vesicles, vacuoles and myelin figures visible in cytoplasm. Extensive vacuolation of cytoplasm. Ribosome aggregates in cytoplasm.	Cells were rounded and formed membrane blebs. Fewer cellular protrusions.
	72 h	Slightly swollen	Slightly swollen. Ribosomes dissociated	Damaged	Nuclei remain unaffected	Many autophagic vesicles, vacuoles and myelin figures visible in cytoplasm. Extensive vacuolation of cytoplasm. Cytoplasm is disrupted.	Cells were rounded and formed membrane blebs. Some plasma membrane damage. Fewer cellular protrusions.
Lanceotoxin B	24 h	Swollen	Swollen after exposure to 5 µM lanceotoxin B.	Swollen	The perinuclear space was swollen after exposure to 5 µM lanceotoxin B.	Many autophagic vesicles visible in cytoplasm. Large portions of the cell are sequestered in autophagic vesicles. Vacuolation of cytoplasm.	Cells were rounded and formed membrane blebs. Some plasma membrane damage. Autophagic vesicles extrude content to the outside.
	48 h	Swollen	Not swollen. Slightly dilated	Swollen	Nuclei remained unaffected.	Many autophagic vesicles visible in cytoplasm. Large portions of the cell are sequestered in autophagic vesicles. Vacuolation of cytoplasm. Electron dense granular aggregates in cytoplasm.	Cells were rounded and formed membrane blebs. Some plasma membrane damage. Autophagic vesicles extrude content to the outside.
	72 h	Swollen	Not swollen	Swollen	Nuclei remain unaffected	Many autophagic vesicles seen in cytoplasm. Large portions of the cell are sequestered in autophagic vesicles. Vacuolation of cytoplasm.	Cells were rounded and formed membrane blebs and apoptotic bodies. Some plasma membrane damage. Autophagic vesicles extrude content to the outside. Cellular debris of broken cells.

Table 4 Summary of the subcellular changes that occurred in H9c2 cells after being exposed to different cardiac glycosides grouped by toxin concentration.

Toxin	Conc.	Golgi Complex	RER	Mitochondria	Nuclei	Vesicles, vacuoles and other	Plasma membrane and cell form
Digoxin	5	Swelling increased with incubation time	Unaffected.	Damaged and swollen	Nuclei remained unaffected.	Autophagic vesicles and myelin figures visible in cytoplasm. Gaps in cytoplasm.	The plasma membrane and associated cytoskeleton was damaged.
	25	Swelling increased with incubation time	Unaffected	Damaged and swollen	Nuclei remained unaffected.	Autophagic vesicles visible in cytoplasm. Gaps in cytoplasm.	The plasma membrane and associated cytoskeleton was damaged. Cellular debris of destroyed cells visible.
	100	Swelling increased with incubation time. Not swollen at 72 h	Unaffected	Damaged and swollen	Nuclei remained unaffected.	Autophagic vesicles visible in cytoplasm. Gaps in cytoplasm.	The plasma membrane and associated cytoskeleton was damaged. Cellular debris of destroyed cells visible.
1α,2α-Epoxyscillirosidine	5	Not swollen	Unaffected	Damaged	Nuclei remained mostly unaffected. Aggregates were present in the nucleoplasm.	Some autophagic vesicles visible in cytoplasm. Gaps in cytoplasm. Aggregates present in cytoplasm.	The plasma membrane and associated cytoskeleton was damaged at 72 h.
	25	Slightly swollen	Swollen	Slightly damaged.	The perinuclear space was swollen.	Autophagic vesicles, myelin figures and vacuoles visible in cytoplasm. Gaps in cytoplasm.	Some damage to plasma membrane. Cells form membrane blebs.
	100	Swollen	Swollen	Slightly damaged. Mitochondria had ballooned cristae.	The perinuclear space was swollen. Some nuclei had condensed nuclear material.	Autophagic vesicles and vacuoles visible in cytoplasm.	Severe plasma membrane damage. Cells were rounded, formed blebs and apoptotic bodies. Cellular debris of destroyed cells visible.
Lanceotoxin B	5	Swollen at 48 h.	Unaffected	Damaged and swollen.	Nuclei remained unaffected.	Autophagic vesicles visible in cytoplasm. Gaps in cytoplasm.	The plasma membrane and associated cytoskeleton was slightly damaged. Cells formed membrane blebs.
	25	Swollen at 48 h.	Unaffected	Damaged and swollen.	Some nuclei had condensed nuclear material. Aggregates were present in the nucleoplasm.	Autophagic vesicles and myelin figures visible in cytoplasm. Gaps in cytoplasm.	The plasma membrane and associated cytoskeleton was slightly damaged. Cells formed membrane blebs and apoptotic bodies.
	100	Swollen	Unaffected	Damaged and swollen.	Aggregates were present in the nucleoplasm.	Autophagic vesicles and vacuoles visible in cytoplasm. Gaps in cytoplasm.	The plasma membrane and associated cytoskeleton was slightly damaged. Cells were rounded, formed blebs and apoptotic bodies. Cellular debris of destroyed cells visible.

Table 5 Summary of the subcellular changes that occurred in Neuro-2a cells after being exposed to different cardiac glycosides grouped by toxin concentration.

Toxin	Conc.	Golgi Complex	RER	Mitochondria	Nuclei	Vesicles, vacuoles and other	Plasma membrane and cell form
Digoxin	5	Swollen at 48 and 72 h	Unaffected	Damaged and swollen.	Unaffected	Few autophagic vesicles visible in cytoplasm.	Some damage to plasma membrane.
	25	Slightly swollen	Unaffected	Damaged and swollen.	Unaffected	Autophagic vesicles visible in cytoplasm.	Some damage to plasma membrane.
	100	Swollen	Unaffected	Damaged and swollen.	Unaffected	Autophagic vesicles visible in cytoplasm. Clumped ribosomes in cytoplasm.	Damage to plasma membrane. Some cells formed plasma membrane blebs.
1α,2α-Epoxyscillirosidine	5	Slightly swollen	Unaffected	Damaged	Unaffected	Autophagic vesicles and vacuoles visible in cytoplasm.	Unaffected
	25	Swollen at 24 h	Swollen at 24 h.	Damaged and swollen.	Unaffected	Autophagic vesicles visible in cytoplasm. Gaps in cytoplasm.	Damage to plasma membrane. Some cells formed plasma membrane blebs
	100	Swollen	Swollen. Ribosomes dissociated. Not swollen at 72 h.	Damaged. Mitochondria had ballooned cristae.	Radially segmented at 24 h. The perinuclear space was swollen. Vacuoles in nucleoplasm.	Autophagic vesicles and vacuoles visible in cytoplasm. Clumped ribosomes in cytoplasm. Gaps in cytoplasm.	Damage to plasma membrane. Some cells were rounded, formed blebs and apoptotic bodies. Fewer protrusions
Lanceotoxin B	5	Slightly swollen	Swollen at 24 h.	Swollen	The perinuclear space was swollen at 24 h.	Autophagic vesicles visible in cytoplasm. Electron-dense granular aggregates in cytoplasm.	Cells were rounded, formed blebs and apoptotic bodies.
	25	Swollen	Unaffected	Swollen	Unaffected	Autophagic vesicles and vacuoles visible in cytoplasm.	Cells were rounded, formed blebs and apoptotic bodies. Cellular debris of destroyed cells visible.
	100	Swollen	Unaffected	Swollen	Unaffected	Autophagic vesicles and vacuoles visible in cytoplasm. Gaps in cytoplasm.	Some plasma membrane damage Cells formed apoptotic bodies. Cellular debris of destroyed cells visible. Autophagic vesicles were extruding content to outside.

Table 6 Summary of the ultrastructural changes that occurred on the surface of H9c2 and Neuro-2a cells after being exposed to different cardiac glycosides as seen with scanning electron microscopy.

Cell lines	Toxin	Cell shape	Cell-to-cell and cell-to-surface adhesion	Plasma membrane and cell surface
H9c2 cells	Digoxin	Some cells are shrunken and rounded.	Fewer attachments	Some plasma membrane damage.
	1α,2α-Epoxyscillirosidine	Few cells are rounder.	Fewer attachments. Cells seem to detach from coverslip.	Clear plasma membrane damage in the form of large holes in the membrane.
	Lanceotoxin B	Cells are shrunken and rounder.	Fewer attachments. Cells seem to detach from coverslip.	Cells formed what appears to be apoptotic bodies.
Neuro-2a cells	Digoxin	Similar to control cells.	Broken attachments. Some cells appear apoptotic and seem to detach from the coverslip.	Many cells formed what appears to be apoptotic bodies. Some plasma membrane damage visible. Increased number of membrane protrusions.
	1α,2α-Epoxyscillirosidine	Some cells are shrunken and rounded.	Fewer attachments. Cells seem to detach from coverslip.	Plasma membrane damage. Some cells formed what appears to be apoptotic bodies.
	Lanceotoxin B	Cells are shrunken and rounder.	Fewer attachments. Cells seem to detach from coverslip.	Plasma membrane damage.

Table 7 Ultrastructural features that belong to type I, type II or type III cell death pathways induced when H9c2 and Neuro-2a cells was exposed to different cardiac glycosides.

Cell lines	Toxin	Apoptosis (Type I)	Autophagy (Type II)	Necrosis (Type III)
H9c2 cells	Digoxin	-	Autophagic vesicles are distributed through the cytoplasm.	Gaps in cytoplasm. Damaged plasma membrane and associated cytoskeleton. Swollen Golgi.
	1α,2α-Epoxyscillirosidine	Some cells form apoptotic bodies. Pyknotic nuclear material. Shrunken cells.	Autophagic vesicles are distributed through the cytoplasm.	Caps in cytoplasm. Damaged plasma membrane and associated cytoskeleton. Swollen Golgi complex and RER. Pyknotic nuclear material. Cellular debris.
	Lanceotoxin B	Apoptotic bodies. Shrunken and rounded cells. Membrane blebbing.	Autophagic vesicles are distributed through the cytoplasm.	Cellular debris. Slightly swollen Golgi.
Neuro-2a cells	Digoxin	Membrane blebs. Apoptotic cells	Autophagic vesicles are distributed through the cytoplasm.	
	1α,2α-Epoxyscillirosidine	Some apoptosis.	Autophagic vesicles are distributed through the cytoplasm.	Swollen RER. Damaged plasma membrane.
	Lanceotoxin B	Some apoptosis.	Large parts of the cell are sequestered into autophagic vesicles and some autophagic vesicles seem to extrude their content to the outside of the cell.	Membrane damage.

Table 8 Unique ultrastructural changes that occurred in H9c2 and Neuro-2a cells as a result of exposure to the different cardiac glycosides.

	Digoxin	1α,2α-Epoxyscillirosidine	Lanceotoxin B
H9c2 cells	Digoxin affected the plasma membrane and associated cytoskeleton. The mitochondria were swollen.	Swollen RER and perinuclear space. Ribosomes dissociated from RER. Vacuolation of cytoplasm. Mitochondria are damaged, but not swollen. Some mitochondria have ballooned cristae.	Cells undergo apoptosis. The mitochondria were distinctly swollen. Granular aggregates in nucleoplasm. Many autophagic vesicles.
Neuro-2a cells	Increased number of cellular protrusions. Disruption of cytoplasm.	Cytoplasm was largely vacuolised. Swollen RER and perinuclear space. Ribosomes dissociated. Mitochondria had ballooned cristae	Large parts of the cells were sequestered in autophagic vesicles. Autophagic vesicles extruded content to the outside. RER and perinuclear space swollen at 24 h for 5 µM.

Chapter 5 Discussion

Cardiac glycosides affect the cardiovascular and nervous system of poisoned animals. To this end, we used the H9c2 and Neuro-2a cell lines to determine the effect of a cardenolide, a non-cumulative bufadienolide and a cumulative bufadienolide on heart muscle and nerve cells.

The purity of the bufadienolides isolated by Dr Anderson was evaluated using TLC. Digoxin was acquired form Sigma-Aldrich and had a purity of 97.1% according to the package insert, thus was not tested using TLC. In contrast to digoxin, both 1α,2α-epoxyscillirosidine and lanceotoxin B were previously isolated from *M. pallida* and *K. lanceolata*, respectively, by Dr Anderson and their purity not confirmed. Two batches of 1α,2α-epoxyscillirosidine were used during the course of the project. Silica gel was used as the stationary phase and is highly polar; thus, the more polar compounds would tend to stick to the silica instead of moving with the solvent front of the mobile phase. In both batches, 1α,2α-epoxyscillirosidine had a Rf value of 0.84 while being developed with 90% ethyl acetate to 10% ethanol. Within this solvent mixture, ethyl acetate is non-polar while ethanol is the more polar solvent. As seen on the TLC plate, the first batch of 1α,2α-epoxyscillirosidine had only one spot and therefore quite pure. The second batch of 1α,2α-epoxyscillirosidine was less pure with four other compounds in low concentrations in addition to 1α,2α-epoxyscillirosidine. Two of the unknown compounds were more polar compared to 1α,2α-epoxyscillirosidine, with one of the compounds being extremely polar and remaining on the origin. The other two compounds were slightly less polar than 1α,2α-epoxyscillirosidine, being nearer to the solvent front. To confirm that the second batch 1α,2α-epoxyscillirosidine had five compounds in total, the batch was separated using a 98% ethyl acetate to 2% methanol solution. The plates were visualised, in addition to placing the plates under UV light, with vanillin and an ethanol/sulphuric acid solution. On both these plates five spots were seen, with 1α,2α-epoxyscillirosidine being the largest spot. The R_f values of the compounds were similar on both plates, as expected since the different spots represent the same compounds developed using the same solvent system. The second batch of 1α,2α-epoxyscillirosidine was less pure than the first batch. This also explains why the observed effect of 1α,2α-epoxyscillirosidine on H9c2 and Neuro-2a cells as visualised with scanning electron micrographs was less noticeable when

compared with the results of the MTT assay and the transmission electron micrographs. Finally, lanceotoxin B also only showed one spot and was therefore considered pure. Compared to 1α,2α-epoxyscillirosidine, lanceotoxin was more polar with a lower retention factor.

Digoxin, 1α,2α-epoxyscillirosidine and lanceotoxin B were incubated with H9c2 and Neuro-2a cells respectively for 24, 48 and 72 h. The *in vitro* cytotoxic effects of these cardiac glycosides were determined using the MTT vitality assay to assess cell viability. All cardiac glycosides tested had EC_{50}s starting in the micromolar range (**Table 1**). This was not unexpected as previous studies have indicated that rodents are less susceptible to cardiac glycosides compared to other animals, due to the Na^+/K^+-ATPase α-isoform expressed on the surface of the cells (Price and Lingrel, 1988; Weinhouse et al., 1983). Compared to the bufadienolides tested, both cell lines remained rather insensitive towards digoxin; the cardenolide had EC_{50}s exceeding 100 μM (highest test concentration) for all incubation times and for both cell lines (**Figure 12 and Figure 13**). The H9c2 cells were the most susceptible to 1α,2α-epoxyscillirosidine of the cardiac glycosides tested with EC_{50}s below 100 μM and decreasing at longer exposure times. The Neuro-2a cells were also relatively susceptible to 1α,2α-epoxyscillirosdine with EC_{50}s below 100 μM but showing no significant difference between the EC_{50}s of different exposure times. A hormetic effect was observed for 1α,2α-epoxyscillirosidine in both cell lines, with low 1α,2α-epoxyscillirosidine concentrations resulting in enhanced cell survival above that of the solvent control. Lanceotoxin B was neurotoxic with EC_{50} values below 10 μM when exposed to Neuro-2a cells. In contrast, when exposed to H9c2 cells lanceotoxin B exhibited EC_{50}s more than 10 times greater than those for Neuro-2a cells. This provides credence to the notion of referring to the cumulative bufadienolides as neurotoxic (Botha, 2016). No hormetic effect was seen at the lanceotoxin B concentrations tested. However, this does not exclude the possibility that lower lanceotoxin B concentrations might enhance cell proliferation. Additionally, lower digoxin concentrations could also potentially enhance cell survival. The cytotoxicity of cardiac glycosides is mainly as a result of the direct inhibition of the Na^+/K^+-ATPase disrupting the ionic gradient; as well as the various signalling pathways triggered upon binding of the cardiac glycosides. The biphasic response of the H9c2 cells and Neuro-2a cells to 1α,2α-epoxyscillirosidine, has been demonstrated before by cells exposed

to ouabain. It has been reported that low concentrations of ouabain, that were unable to cause any changes to the intracellular ionic concentration, increased the proliferation of various cell types including rat cardiomyocytes, canine vascular smooth muscle cells and rat renal proximal tubule cells (Aydemir-Koksoy et al., 2001; Li et al., 2006; Peng et al., 1996). The cardiac glycoside binds to the Na^+/K^+-ATPase and transactivates Src kinase, which then phosphorylates EGFR (Aydemir-Koksoy et al., 2001). EGFR, in turn, causes a cascade of phosphorylation events and activates the Ras/Raf/MAPK signal transduction pathway. This leads to the expression of genes involved in cell growth (Xie and Cai, 2003). Thus 1α,2α-epoxyscillirosidine may be capable of inducing cell proliferation by a similar pathway. In addition to the proliferative effects, cardiac glycosides have also been shown to have anti-apoptotic effects (Li et al., 2006).

The *in vitro* effect of a cardiac glycoside on a cell ultimately depends on the type of cardiac glycoside, the type of cell and the environment. Factors such as the cardiac glycoside structure, the species and organ of origin of the cell, the subcellular location of the Na^+/K^+-ATPase, the pH of the media and the presence or absence of potassium in the culture medium, all influence the end response of a cell to the cardiac glycoside (Riganti et al., 2011). All these factors thus contribute to the different EC_{50}s obtained for digoxin, 1α,2α-epoxyscillirosidine and lanceotoxin B. The results obtained during *in vitro* studies, often differ from *in vivo* studies. The subcutaneous LD_{50} of digoxin is 0.60 mg/kg (768 nmol/kg) for guinea-pigs and 30 mg/kg (38.4 µmol/kg) for rats (Weinhouse et al., 1983). For 1α,2α-epoxyscillirosidine the subcutaneous LD_{50} is 0.194 mg/kg (411 nmol/kg) for guinea-pigs and 3.6 mg/kg (7.62 µmol/kg) for mice (Naude and Potgieter, 1990). Lastly, the acute subcutaneous LD_{50} of lanceotoxin B for guinea-pigs is 0.10 mg/kg (165 nmol/kg) and unknown for mice or rats (Anderson et al., 1983b). In contrast the cardiac glycosides had EC_{50}s within the micromolar range when exposed to rat myocardial and mouse neuroblastoma cells *in vitro*. Despite the difference in the potency of cardiac glycosides between *in vivo* and *in* vitro studies, a similar trend was seen in the order of toxicity (**Table 9**). Digoxin had the highest LD_{50} *in vivo*, followed by 1α,2α-epoxyscillirosidine and finally lanceotoxin B respectively. This was similar to that of the cardiac glycosides exposed to Neuro-2a cells *in vitro* but differed slightly in the order of toxicity when exposed to the H9c2 cells.

Table 9 Comparison between LD_{50} obtained during *in vivo* studies on guinea-pigs and EC_{50}s on Neuro-2a cells obtained *in vitro*.

Cardiac glycoside	*In vivo* studies in guinea-pigs	*In vitro* studies using Neuro-2a cells
Digoxin	0.60 mg/kg (768 nmol/kg)	> 100 µM
1α,2α-Epoxyscillirosidine	0.194 mg/kg (411 nmol/kg)	35.73 ± 10.59 µM 37.56 ± 3.18 µM 37.35 ± 2.30 µM
Lanceotoxin B	0.10 mg/kg (165 nmol/kg)	5.46 ± 0.37 µM 5.27 ± 0.59 µM 4.43 ± 0.67 µM

The consequences of cardiac glycoside cytotoxicity are reflected in the ultrastructural changes that occur in the exposed cells. We thus examined H9c2 and Neuro-2a cells exposed to digoxin, 1α,2α-epoxyscillirosidine and lanceotoxin B with transmission- and scanning electron microscopy. Some of the ultrastructural changes that occurred in exposed cells were universal, and others limited to specific cardiac glycosides or specific cell lines.

Mitochondrial alteration is one of the first signs of cellular damage, and correspondingly, all exposures had some form of mitochondrial change. Mitochondria damage presented as vacuolization of the mitochondrial matrix and paucity of inner membrane cristae, later progressing to distinct swelling of the organelle. Mitochondria contain two chambers capable of swelling, the intermembrane space and the mitochondrial matrix. Due to the differences in permeability the chambers swell independently or sequentially. In some of the cells exposed to 1α,2α-epoxyscillirosidine the intermembrane space was swollen, resulting in ballooned cristae (**Figure 35 and Figure 36**). Cardiac glycosides indirectly cause an increase in the intracellular calcium concentrations of affected cells which is absorbed into the mitochondrial matrix once the intracellular calcium levels reach a certain concentration. The increase in intra-mitochondrial calcium concentration causes mitochondrial permeability transition that, if sustained, leads to collapse of the mitochondrial membrane potential, reduced ATP production and eventual cell death via apoptosis or necrosis (Dong et al., 2006). Indirectly, cardiac glycosides alter

mitochondrial metabolism by activating the Ras/MAPK signal transduction pathway. This occurs by Ras opening the ATP sensitive K^+-channels, altering the mitochondrial membrane potential and increasing ROS production (Tian et al., 2003). Similar to the mitochondria, the Golgi complexes were almost consistently affected, appearing swollen for all cells exposed to the cardiac glycosides. The swelling of the Golgi is likely a consequence of the disruption of the osmotic balance and the accompanying influx of water.

In contrast, swelling of the RER was seen only in cells exposed to 1α,2α-epoxyscillirosidine and, in Neuro-2a cells exposed to 5 µM lanceotoxin B for 24 h. The RER was either continuous or vesiculated in both treated and untreated H9c2 cells and the vesiculation is not due to the cardiac glycosides. Swelling of the ER was sometimes accompanied by the dissociation of ribosomes. Ribosomes are distributed throughout the cytoplasm and attach to the membrane of ER forming the RER. In some cells the ribosomes aggregated together within the cytoplasm, indicating compromised protein synthesis.

Likely due to insensitivity of H9c2 cells toward digoxin, the nuclei of the cells remained unaffected. Nuclei in control and unaffected H9c2 cells were oval in shape and longitudinally aligned with the cell. In comparison, the nuclei of untreated Neuro-2a cells were much more polymorphous but retained a somewhat rounded shape and had one to six nucleolar bodies. The structural stability of the nucleus is due to lamins, intermediate filament proteins that form a meshwork called the nuclear lamina underlying the inner nuclear membrane. Change in the shape of the nucleus can be a result of either a change in the nuclear lamina or due to forces in the cytoplasm (Webster et al., 2009). Surrounding the nucleus is the nuclear envelope, consisting of an inner and outer nuclear membrane which forms the perinuclear space between the two membranes. The outer nuclear membrane is connected with the endoplasmic reticulum of the cell. Both H9c2 and Neuro-2a cells exposed to 1α,2α-epoxyscillirosidine, as well as Neuro-2a cells exposed to 5 µM lanceotoxin B for 24 h, had a swollen perinuclear space. In addition, cells with a swollen perinuclear space had swollen RER. Mutant reductases and alteration to the reductase activity of lamin B receptor was shown to cause swelling of the perinuclear space and ER (Zwerger et al., 2010). A similar phenomenon was seen during autosis (Liu and Levine, 2015). A

possible explanation for the swelling of the perinuclear space and the RER is the disruption of cholesterol metabolism. The basic structure of cardiac glycosides is similar to sterols. Digoxin and ouabain upregulates the activity and expression of 3-hydroxy-3-methylglutaryl coenzyme A reductase in rat myocardial cells, increasing cholesterol and ubiquinone synthesis (Campia et al., 2012). The swelling of the RER and perinuclear space is minor when compared to that seen during autosis and mutations of reductases and the lamin B receptor. Alternatively, the swelling could be due to alteration in the homeostasis of the RER and perinuclear space due to the disruption in the ionic gradient. The perinuclear space functions, among other things, as a calcium storage site. Both the inner and outer nuclear membrane contain ion channels such as R-type Ca^{2+} channel, Na^+/K^+-ATPase, Na^+/H^+-exchanger, Na^+/Ca^{2+}-exchanger, K^+-channels and Cl^--channels, that regulate ion homeostasis of the perinuclear space and the nucleoplasm (Bkaily et al., 2009). The membrane potential of the inner and outer nuclear membrane and regulation of voltage-dependent ion channels such as Ca^{2+} and Cl^- channels may be controlled by K^+-channels. Swelling was not seen in cells exposed to digoxin or H9c2 cells exposed to lanceotoxin B, possibly due to the lower sensitivity of these cells to the cardiac glycosides tested. However, Neuro-2a cells, that were quite sensitive to lanceotoxin B, only showed swelling of the perinuclear space and ER following exposure to 5 µM for 24 h. At higher concentrations and longer exposure times, both the perinuclear space and the RER regained their normal morphology.

In H9c2 cells, cytoskeleton filaments associated with the plasma membrane was observed, which was visibly disrupted when exposed to digoxin and lanceotoxin B. As seen with the scanning electron micrographs, many of the cells were rounded and had fewer protrusions. The cytoskeleton plays an important role in various cellular processes including cell growth, proliferation, differentiation and motility as well as maintaining cell shape, adhesion and mechanical stability. The cytoskeleton is anchored to the plasma membrane through adhesion molecules as well as ion transporters such as the Na^+/K^+-ATPase (Denker and Barber, 2002). It has been reported that digitoxin supresses α-tubulin formation in non-small cell lung cancer H1975 cells (Zhang et al., 2016) and UNBS1450, a hemi-synthetic cardenolide, caused disorganization of the actin cytoskeleton in human glioblastoma cells (Lefranc et al., 2008). Elevated intracellular Ca^{2+} activate hydrolytic enzymes such as calpains

that degrade and disrupt the cytoskeleton of cells and cause membrane blebbing (Dong et al., 2006). Cell shrinkage on the other hand is possibly due to the reduced intracellular K^+ concentration.

Extensive cytoplasmic vacuolization was observed in some of the cells exposed to cardiac glycosides. Vacuoles can be derived from lysosomes, the ER, the Golgi complex and autophagic vesicles. Dilated autophagic vesicles are not considered true vacuoles, but due to the dilation of their content they appear as electron lucent vacuoles (Aki et al., 2012). 1α,2α-Epoxyscillirosidine caused both H9c2 and Neuro-2a cells to form many vacuoles from the ER, the Golgi complexes and some from autophagic vesicles with diluted content. Digoxin caused the formation of few vacuoles, with the few formed being either from the Golgi or from autophagic vesicles with diluted content. Lanceotoxin B, corresponding to the different susceptibility of the two cell lines, formed few vacuoles in H9c2 cells and many in Neuro-2a. In both cases the vacuoles appeared to be from autophagic vesicles with diluted content and not from the ER, Golgi or lysosomes. Autophagy can either facilitate cell survival or induce cell death depending on the levels of autophagy within the cell. Autophagic vacuolization could be seen in all cells exposed to cardiac glycosides, especially in Neuro-2a cells exposed to lanceotoxin B. Although an excessive amount of autophagy can lead to cell death, a cell can only be classified as dying via autophagic cell death if the process is blocked by knocking down at least two essential autophagic proteins according to the NCCD (Galluzzi et al., 2012). Such studies were not performed; thus, we cannot conclude whether autophagy, as a result of cardiac glycoside exposure causes cell death or plays a role in protecting the cells. Autophagic cell death is connected to an over expression of Ras. Ras-induced cell death in neuronal cells is a programmed cell death related to autophagy (Botella et al., 2003; Gärtner et al., 1999; Kitanaka et al., 2002; Lüth et al., 2000). Cardiac glycosides increase Ras expression in cells via the Src/EGFR pathway. This increase can serve as an alternative explanation for the increase in the number of autophagic vesicles within the cytoplasm of the cells exposed to cardiac glycosides. During the normal autophagic process, cells sequester cellular components into an autophagosome, after which the autophagosome fuse with lysosomes and degrade the content whereby it's delivered to the cytoplasm for recycling. However, the content of the autophagic vesicles were

extruded to the outside of the cell in Neuro-2a cells exposed to lanceotoxin B (**Figure 39, 40, 41**).

Scanning electron micrographs of the cells exposed to cardiac glycosides demonstrated a decrease in cell attachment to the growth surface and other cells when H9c2 cells were exposed to lanceotoxin B and Neuro-2a cells exposed to any of the three cardiac glycosides. The Na^+/K^+-ATPase plays a role in cell attachment (Contreras et al., 2004), corroborating the observed decrease in cell adherence following cardiac glycoside exposure. In contrast, autosis, an autophagy related cell death pathway that is disrupted by the inhibition of the Na^+/K^+-ATPase, cause among other things, enhanced substrate adherence (Liu et al., 2013). Thus, cell detachment from the growth surface can be attributed to either the inhibition of the Na^+/K^+-ATPase or due to cell death. Contreras et al. (2004) noted that exposure to ouabain caused an increase in tyrosine phosphorylation, which in turn causes alteration to the molecules involved in the cell-to-cell and cell-to-substrate adhesion (Contreras et al., 2004). The inhibition of the Na^+/K^+-ATPase causes an indirect increase in the levels of intracellular calcium, which in turn plays a role in tyrosine phosphorylation (Contreras et al., 1999). Ouabain, in addition to increasing tyrosine phosphorylation, activates cell signalling pathways for the activation of MAPK and Rho small G-proteins which retrieved the attaching molecules (ZO-1, cytokeratin, E-cadherin and vinculin) from the cell membrane (Contreras et al., 1999). However, it should be noted that cell type plays a role in the susceptibility towards detachment following the exposure to the same and/or different cardiac glycosides. As seen with SEM, the Neuro-2a cells are more likely to detach from the surface and each other compared to H9c2 cells. If viable cells are detached from the growth surface after exposure to low concentrations of cardiac glycosides the MTT assay results might be affected. The MTT assay measures cell viability; however, if during the washing process the viable, but detached cells are washed away the actual cellular lethality of the cardiac glycosides at those concentration might be overestimated.

After exposure to a toxic substance, such as cardiac glycosides, cells can either recover or die. As mentioned previously, cells die by a variety of pathways including apoptosis, autophagy and necrosis. By analysing the morphological changes that occurred to the cells after exposure we can determine by which pathway the cells die.

The conclusion drawn by morphological classification of cell death can be confirmed via molecular methods. Both H9c2 and Neuro-2a cells exposed to any of the three cardiac glycosides showed some heterogeneity with regards to the exact pathway of cell death. Some individual cells showed signs indicative of both apoptosis and necrosis. Other cell populations had some cells dying via apoptosis and other dying via necrosis. According to the morphological signs, digoxin and 1α,2α-epoxyscillirosidine caused the majority of H9c2 cells to die via necrosis. Digoxin had a relatively high EC_{50} and comparatively fewer cells were fatally affected. Of those cells affected signs of plasma membrane damage, swollen mitochondria, gaps within the cytoplasm and myelin figures were all indicative of necrosis. H9c2 cells exposed to 1α,2α-epoxyscillirosidine, showed the above morphological features with the addition of swollen RER and pyknotic nuclear material as expected of necrotic cells. Additionally, a few H9c2 cells exposed to 1α,2α-epoxyscillirosidine also showed signs of undergoing apoptotic cell death, with cells being shrunken, rounded and many forming clear membrane blebs and apoptotic bodies. In contrast, lanceotoxin B caused apoptosis in the majority of the H9c2 cells, with a few necrotic cells. Neuro-2a cells were more prone to apoptosis with all three cardiac glycosides showing at least some apoptotic cells. Digoxin exposure of Neuro-2a cells induced an apoptotic effect in the majority of the cells, with a few cells either having membrane damage or were clearly destroyed (Necrosis). 1α,2α-Epoxyscillirosidine had more cells showing signs of necrosis compared to those showing signs of apoptosis. Apoptotic cells were also visible in cultures exposed to lanceotoxin B, especially within the first 24 h of exposure. Moreover, in a large number of Neuro-2a cells exposed to lanceotoxin B autophagic vesicles that sequestered large parts of the cell cytoplasm or more, were seen. This might be indicative of autophagic cell death playing a role in lanceotoxin B cytotoxicity in Neuro-2a cells. Evidently, this cannot be confirmed without additional molecular tests. These mixed features of cell death are not limited to the current study. Crosstalk between apoptosis, necrosis and autophagy is commonly seen, as many of the signalling cascades that regulate each pathway overlap (Nikoletopoulou et al., 2013). Stimuli such as the increased intracellular Ca^{2+} concentration and the production of ROS due to Na^+/K^+-ATPase inhibition can cause either apoptosis or necrosis.

Chapter 6 Conclusion

The *in vitro* cytotoxic effects and ultrastructural changes caused by three types of cardiac glycosides i.e. the cardenolide digoxin, the non-cumulative bufadienolide 1α,2α-epoxyscillirosidine and the cumulative bufadienolide lanceotoxin B were evaluated on myocardial (H9c2) and neuroblastoma (Neuro-2a) cells. 1α,2α-Epoxyscillirosidine had the greatest cytotoxic effect on H9c2 cells of all three cardiac glycosides. On the other hand, lanceotoxin B had the greatest effect on Neuro-2a cells and could thus be considered neurotoxic. Future studies should focus on understanding the effect of chronic exposure of cumulative bufadienolides to nerve cells and how it differs from a single, acute exposure. Based on the ultrastructural changes observed in affected cells, the cells died via both apoptosis and necrosis. H9c2 cells exposed to digoxin and 1α,2α-epoxyscillirosidine died mostly due to necrosis, while H9c2 cells exposed to lanceotoxin B died mostly due to apoptosis. The cell population of Neuro-2a cells exposed to any of the three cardiac glycosides had some apoptotic cells, apoptosis being especially evident in Neuro-2a cells exposed to digoxin. 1α,2α-Epoxyscillirosidine showed necrotic signs in the majority of the cells, with some cells also showing signs of apoptosis. It should be noted that the Neuro-2a cells exposed to lanceotoxin B had large portions of the cell sequestered in autophagic vesicles, to a far greater extent than those caused by any other cardiac glycoside. This could indicate that Neuro-2a cells, in addition to the apoptotic pathway, die via autophagy. However, additional biochemical and molecular experiments should be carried out in order to investigate this. Cardiac glycoside-containing plants cause a significant number of stock mortalities annually. Krimpsiekte, caused by cumulative bufadienolides, contributes significantly to losses experienced in small stock. Investigating the cellular effects caused by the cumulative bufadienolides on nervous cells, after inhibition of the Na^+/K^+-ATPase and triggering of the various signalling cascades, might contribute to our understanding of the mechanism of toxicity underlying krimpsiekte.

References

Aki, T., Nara, A., Uemura, K., 2012. Cytoplasmic vacuolization during exposure to drugs and other substances. Cell biology and toxicology 28, 125-131.

Anderson, L., Joubert, J., Kellerman, T., Schultz, R., Procos, J., Olivier, P., 1983a. The experimental production of krimpsiekte in sheep with *Tylecodon grandiflorus* (Burm. f.) Toelken and some of its bufadienolides. The Onderstepoort journal of veterinary research 50, 301-307.

Anderson, L., Schultz, R., Joubert, J., Prozesky, L., Kellerman, T., Erasmus, G., Procos, J., 1983b. Krimpsiekte and acute cardiac glycoside poisoning in sheep caused by bufadienolides from the plant *Kalanchoe lanceolata* Forsk. The Onderstepoort journal of veterinary research 50, 295-300.

Anderson, L.A., Steyn, P.S., van Heerden, F.R., 1984. The characterization of two novel bufadienolides, lanceotoxins A and B from *Kalanchoe lanceolata* [Forssk.] Pers. Journal of the Chemical Society, Perkin Transactions 1, 1573-1575.

Aperia, A., Akkuratov, E.E., Fontana, J.M., Brismar, H., 2016. Na+-K+-ATPase, a new class of plasma membrane receptors. American Journal of Physiology-Cell Physiology 310, 491-495.

Araujo, J., Téran, F., Oliveira, R., Nour, E., Montenegro, M., Campos, J., Vazoller, R., 2003. Comparison of hexamethyldisilazane and critical point drying treatments for SEM analysis of anaerobic biofilms and granular sludge. Journal of electron microscopy 52, 429-433.

Ashkenazi, A., Dixit, V.M., 1998. Death receptors: signaling and modulation. Science, 1305-1308.

Aslani, M., Rezakhani, A., 2000. A case report of oleander (*Nerium oleander*) intoxication in cattle. International Journal of Tropical Agriculture 18, 185-187.

Aslani, M.R., Movassaghi, A., Janati-Pirouz, H., Karazma, M., 2007. Experimental oleander (*Nerium oleander*) poisoning in goats: a clinical and pathological study. Iranian Journal of Veterinary Research 8, 58-63.

Aslani, M.R., Movassaghi, A.R., Mohri, M., Abbasian, A., Zarehpour, M., 2004. Clinical and pathological aspects of experimental oleander (*Nerium oleander*) toxicosis in sheep. Veterinary research communications 28, 609-616.

Aydemir-Koksoy, A., Abramowitz, J., Allen, J.C., 2001. Ouabain-induced signaling and vascular smooth muscle cell proliferation. Journal of Biological Chemistry 276, 46605-46611.

Azuma, H., Sekizaki, S., Akizawa, T., Yasuhara, T., Nakajima, T., 1986. Activities of novel polyhydroxylated cardiotonic steroids purified from nuchal glands of the snake, *Rhabdophis tigrinus*. Journal of pharmacy and pharmacology 38, 388-390.

Bkaily, G., Avedanian, L., Jacques, D., 2009. Nuclear membrane receptors and channels as targets for drug development in cardiovascular diseases. Canadian journal of physiology and pharmacology 87, 108-119.

Botella, J., Kretzschmar, D., Kiermayer, C., Feldmann, P., Hughes, D., Schneuwly, S., 2003. Deregulation of the Egfr/Ras signaling pathway induces age-related brain degeneration in the Drosophila mutant vap. Molecular biology of the cell 14, 241-250.

Botha, C., 2016. Potential health risks posed by plant-derived cumulative neurotoxic bufadienolides in South Africa. Molecules 21, 348.

Botha, C., Coetser, H., Schultz, R., Labuschagne, L., Van der Merwe, D., 2013. Spatial variation of epoxyscillirosidine concentrations in *Moraea pallida* (yellow tulp) in South Africa. Onderstepoort Journal of Veterinary Research 80, 00-00.

Botha, C., Gehring, R., Van Rooyen, J., Venter, D., 2002. The effect of three bufadienolide cardiac glycosides on contraction of isolated rat jejunum. Onderstepoort Journal of Veterinary Research 69, 243-246.

Botha, C., Kellerman, T., Schultz, R., Erasmus, G., Retief, E., 1998. Krimpsiekte in a sheep following a single dose of *Tylecodon ventricosus* (Burm. f.) Toelken and the isolation of tyledoside D from this plant species. Onderstepoort Journal of Veterinary Research 65.

Botha, C., Naudé, T., 2002. Plant poisonings and mycotoxicoses of importance in horses in southern Africa. Journal of the South African Veterinary Association 73, 91-97.

Brain, V., 1994. Case report/Gevalverslag Suspected cardiac glycoside poisoning in elephants (*Loxodonta africana*). Journal of the South African Veterinary Association 65, 173-174.

Button, C., Reyers, F., Meltzer, D.G.A., Mulders, M.S., Killeen, V.M., 1983. Some physiopathological features of experimental *Homeria glauca* (Wood & Evans) NE Br. poisoning in Merino sheep. Onderstepoort Journal of Veterinary Research 50, 191-196.

Calderón-Montaño, J.M., Burgos-Morón, E., Orta, M.L., Maldonado-Navas, D., García-Domínguez, I., López-Lázaro, M., 2014. Evaluating the cancer therapeutic potential of cardiac glycosides. BioMed research international 2014.

Campia, I., Sala, V., Kopecka, J., Leo, C., Mitro, N., Costamagna, C., Caruso, D., Pescarmona, G., Crepaldi, T., Ghigo, D., 2012. Digoxin and ouabain induce the efflux

of cholesterol via liver X receptor signalling and the synthesis of ATP in cardiomyocytes. Biochemical Journal 447, 301-311.

Cheeke, P.R., 1989. Toxicants of plant origin: Glycosides. CRC Press, Boca Raton, Fla.

Contreras, R., Flores-Maldonado, C., Lazaro, A., Shoshani, L., Flores-Benitez, D., Larre, I., Cereijido, M., 2004. Ouabain Binding to Na+, K+-ATPase Relaxes Cell Attachment and Sends a Specific Signal (NACos) to the Nucleus. The Journal of membrane biology 198, 147-158.

Contreras, R., Shoshani, L., Flores-Maldonado, C., Lazaro, A., Cereijido, M., 1999. Relationship between Na (+), K (+)-ATPase and cell attachment. Journal of cell science 112, 4223-4232.

Cook, D., Campbell, G., Meldrum, A., 1990. Suspected *Cryptostegia grandiflora* (rubber vine) poisoning in horses. Australian veterinary journal 67, 344.

Denker, S.P., Barber, D.L., 2002. Ion transport proteins anchor and regulate the cytoskeleton. Current opinion in cell biology 14, 214-220.

Department of health, 2015. Standard treatment guidelines and essential drugs list for South Africa: adults: hospital level.

Dong, Z., Saikumar, P., Weinberg, J.M., Venkatachalam, M.A., 2006. Calcium in cell injury and death. Annual Review of Pathology Mechanisms of Disease 1, 405-434.

Elmore, S., 2007. Apoptosis: a review of programmed cell death. Toxicologic pathology 35, 495-516.

Enslin, P., Naudé, T., Potgieter, D., Van Wyk, A., 1966. 1α, 2α-epoxyscillirosidine, the main toxic principle of *Homeria glauca* (Wood and Evans) NE Br. Tetrahedron 22, 3213-3220.

Festjens, N., Berghe, T.V., Vandenabeele, P., 2006. Necrosis, a well-orchestrated form of cell demise: signalling cascades, important mediators and concomitant immune response. Biochimica et Biophysica Acta (BBA)-Bioenergetics 1757, 1371-1387.

Freshney, I., 2001. Application of cell cultures to toxicology, In: Cell Culture Methods for In Vitro Toxicology. Springer, pp. 9-26.

Galluzzi, L., Vitale, I., Abrams, J., Alnemri, E., Baehrecke, E., Blagosklonny, M., Dawson, T., Dawson, V., El-Deiry, W., Fulda, S., 2012. Molecular definitions of cell death subroutines: recommendations of the Nomenclature Committee on Cell Death 2012. Cell death and differentiation 19, 107.

Gärtner, U., Holzer, M., Arendt, T., 1999. Elevated expression of p21ras is an early event in Alzheimer's disease and precedes neurofibrillary degeneration. Neuroscience 91, 1-5.

Golstein, P., Kroemer, G., 2007. Cell death by necrosis: towards a molecular definition. Trends in biochemical sciences 32, 37-43.

Gunn, J., 1924. Slangkop poisoning. Journal of the Department of Agriculture 9, 141-142.

Henning, M.W., 1932. Animal Diseases In South Africa Vol. 2. Central News: South Africa.

Horvath, S., 1980. Cytotoxicity of drugs and diverse chemical agents to cell cultures. Toxicology 16, 59-66.

Hughes, K., Dart, A., Hodgson, D., 2002. Suspected *Nerium oleander* (Oleander) poisoning in a horse. Australian veterinary journal 80, 412-415.

James, L.F., Nielsen, D.B., Panter, K.E., 1992. Impact of poisonous plants on the livestock industry. Journal of Range Management, 3-8.

Joubert, R.A., 1982a. The treatment of *Moraea polystacha* (Thunb) Ker-Gawl (cardiac glycoside) poisoning in sheep and cattle with activated charcoal and potassium chloride. Journal of the South African Veterinary Association 53, 249-253.

Joubert, R.A., 1982b. The treatment of *Urginea sanguinea* Schinz poisoning in sheep with activated charcoal and potassium chloride. Journal of the South African Veterinary Association 53, 25-28.

Kamboj, A., Rathour, A., Kaur, M., 2013. Bufadienolides and their medicinal utility: a review. International Journal of Pharmacy and Pharmaceutical Sciences 5, 20-27.

Katzung, B.G., Masters, S.B., Trevor, A.J., 2004. Basic & clinical pharmacology.

Kellerman, T., Coetzer, J., Naudé, T., Botha, C., 2005. Plant poisonings and mycotoxicoses of livestock in Southern Africa. Oxford University Press Southern Africa.

Kellerman, T., Naudé, T., Fourie, N., 1996. The distribution, diagnoses and estimated economic impact of plant poisonings and mycotoxicoses in South Africa. Onderstepoort Journal of Veterinary Research 63, 65-90.

Kerr, J.F., Wyllie, A.H., Currie, A.R., 1972. Apoptosis: a basic biological phenomenon with wide-ranging implications in tissue kinetics. British journal of cancer 26, 239.

Kischkel, F., Hellbardt, S., Behrmann, I., Germer, M., Pawlita, M., Krammer, P., Peter, M., 1995. Cytotoxicity-dependent APO-1 (Fas/CD95)-associated proteins form a death-inducing signaling complex (DISC) with the receptor. The EMBO journal 14, 5579-5588.

Kitanaka, C., Kato, K., Ijiri, R., Sakurada, K., Tomiyama, A., Noguchi, K., Nagashima, Y., Nakagawara, A., Momoi, T., Toyoda, Y., 2002. Increased Ras expression and caspase-independent neuroblastoma cell death: possible mechanism of spontaneous neuroblastoma regression. Journal of the National Cancer Institute 94, 358-368.

Kren, V., Martínková, L., 2001. Glycosides in medicine:"The role of glycosidic residue in biological activity". Current medicinal chemistry 8, 1303-1328.

Krishna, A.B., Manikyam, H.K., Sharma, V.K., Sharma, N., 2015. Plant cardenolides in therapeutics. International Journal of Indigenous Medicinal Plants 48, 1871-1896.

Kroemer, G., Galluzzi, L., Vandenabeele, P., Abrams, J., Alnemri, E., Baehrecke, E., Blagosklonny, M., El-Deiry, W., Golstein, P., Green, D., 2009. Classification of cell death: recommendations of the Nomenclature Committee on Cell Death 2009. Cell death and differentiation 16, 3.

Kroemer, G., Levine, B., 2008. Autophagic cell death: the story of a misnomer. Nature reviews Molecular cell biology 9, 1004.

Lefranc, F., Mijatovic, T., Kondo, Y., Sauvage, S., Roland, I., Debeir, O., Krstic, D., Vasic, V., Gailly, P., Kondo, S., 2008. Targeting the α 1 subunit of the sodium pump to combat glioblastoma cells. Neurosurgery 62, 211-222.

Levine, B., Yuan, J., 2005. Autophagy in cell death: an innocent convict? The Journal of clinical investigation 115, 2679-2688.

Li, J., Zelenin, S., Aperia, A., Aizman, O., 2006. Low doses of ouabain protect from serum deprivation–triggered apoptosis and stimulate kidney cell proliferation via activation of NF-κB. Journal of the American Society of Nephrology 17, 1848-1857.

Liu, Y., Levine, B., 2015. Autosis and autophagic cell death: the dark side of autophagy. Cell death and differentiation 22, 367.

Liu, Y., Shoji-Kawata, S., Sumpter, R.M., Wei, Y., Ginet, V., Zhang, L., Posner, B., Tran, K.A., Green, D.R., Xavier, R.J., 2013. Autosis is a Na+, K+-ATPase–regulated form of cell death triggered by autophagy-inducing peptides, starvation, and hypoxia–ischemia. Proceedings of the National Academy of Sciences 110, 20364-20371.

Lodish, H.F., 2012. Molecular cell biology, 7th ed., International ed. / ed. W.H. Freeman; Palgrave [distributor], New York, Basingstoke.

Luft, J., 1961. Improvements in epoxy resin embedding methods. The Journal of Cell Biology 9, 409-414.

Lüth, H., Holzer, M., Gertz, H.-J., Arendt, T., 2000. Aberrant expression of nNOS in pyramidal neurons in Alzheimer's disease is highly co-localized with p21ras and p16INK4a. Brain research 852, 45-55.

Mahin, L., Marzou, A., Huart, A., 1984. A case report of *Nerium oleander* poisoning in cattle. Vet Hum Toxicol 26, 303-304.

Masuda, Y., Kawazoe, N., Nakajo, S., Yoshida, T., Kuroiwa, Y., Nakaya, K., 1995. Bufalin induces apoptosis and influences the expression of apoptosis-related genes in human leukemia cells. Leukemia research 19, 549-556.

McGavin, M., 1969. Rubber-vine (*Cryptostegia grandiflora*) toxicity for ruminants. Queensland Journal of Agricultural and Animal Sciences 26, 9-19.

Milewski, L.M., Khan, S.A., 2006. An overview of potentially life-threatening poisonous plants in dogs and cats. Journal of Veterinary Emergency and Critical Care 16, 25-33.

Mitchell, D., Canham, A., Bayer, A., 1934. *Urginea capitata* Baker-the Berg Slangkop. Its toxic effect on ruminants. Onderstepoort Journal of Veterinary Science and Animal Industry 2, 681-689.

Mosmann, T., 1983. Rapid colorimetric assay for cellular growth and survival: application to proliferation and cytotoxicity assays. Journal of immunological methods 65, 55-63.

Naude, T., Potgieter, D., 1990. Studies on South African cardiac glycosides. I. Isolation of toxic principles of *Homeria glauca* (W. & E.) NE Br. and observations on their chemical and pharmacological properties. The Onderstepoort journal of veterinary research.

Naudé, T.W. 1990. Studies on South African cardiac glycosides. II. The isolation and some chemical and pharmacological properties of toxic principles of *Homeria glauca* (W and E.) N.E. BR, The Onderstepoort journal of veterinary research

Nel, P., Jordaan, P., Anderson, L., Kellerman, T., Reid, C., Schultz, R., 1987. Cardiac glycoside poisoning in sheep caused by *Urginea physodes* (Jacq.) Bak. and the isolated physodine A. Onderstepoort Journal of Veterinary Research 54, 641-644.

Nikoletopoulou, V., Markaki, M., Palikaras, K., Tavernarakis, N., 2013. Crosstalk between apoptosis, necrosis and autophagy. Biochimica et Biophysica Acta (BBA)-Molecular Cell Research 1833, 3448-3459.

Nogawa, T., Kamano, Y., Yamashita, A., Pettit, G.R., 2001. Isolation and structure of five new cancer cell growth inhibitory bufadienolides from the Chinese traditional drug Ch'an Su. Journal of natural products 64, 1148-1152.

Peng, M., Huang, L., Xie, Z., Huang, W.-H., Askari, A., 1996. Partial inhibition of Na/K-ATPase by ouabain induces the Ca-dependent expressions of early-response genes in cardiac myocytes. Journal of Biological Chemistry 271, 10372-10378.

Platz, E.A., Yegnasubramanian, S., Liu, J.O., Chong, C.R., Shim, J.S., Kenfield, S.A., Stampfer, M.J., Willett, W.C., Giovannucci, E., Nelson, W.G., 2011. A novel two-stage, transdisciplinary study identifies digoxin as a possible drug for prostate cancer treatment. Cancer discovery.

Price, E.M., Lingrel, J.B., 1988. Structure-function relationships in the sodium-potassium ATPase. alpha. subunit: site-directed mutagenesis of glutamine-111 to arginine and asparagine-122 to aspartic acid generates a ouabain-resistant enzyme. Biochemistry 27, 8400-8408.

Qu, X., Zou, Z., Sun, Q., Luby-Phelps, K., Cheng, P., Hogan, R.N., Gilpin, C., Levine, B., 2007. Autophagy gene-dependent clearance of apoptotic cells during embryonic development. Cell 128, 931-946.

Radford, D.J., Gillies, A.D., Hinds, J.A., Duffy, P., 1986. Naturally occurring cardiac glycosides. The Medical Journal of Australia 144, 540-544.

Raff, M., 1998. Cell suicide for beginners. Nature 396, 119.

Renehan, A.G., Booth, C., Potten, C.S., 2001. What is apoptosis, and why is it important? BMJ: British Medical Journal 322, 1536.

Renier, A.C., Kass, P.H., Magdesian, K.G., Madigan, J.E., Aleman, M., Pusterla, N., 2013. Oleander toxicosis in equids: 30 cases (1995–2010). Journal of the American Veterinary Medical Association 242, 540-549.

Reynolds, E., 1963. The use of lead citrate at high pH as an electron-opaque stain in electron microscopy. The Journal of cell biology 17, 208.

Rezakhani, A., Maham, M., 1992. Oleander poisoning in cattle of the Fars province, Iran. Vet Hum Toxicol 34, 549.

Riganti, C., Campia, I., Kopecka, J., Gazzano, E., Doublier, S., Aldieri, E., Bosia, A., Ghigo, D., 2011. Pleiotropic effects of cardioactive glycosides. Current medicinal chemistry 18, 872-885.

Saelens, X., Festjens, N., Walle, L.V., Van Gurp, M., van Loo, G., Vandenabeele, P., 2004. Toxic proteins released from mitochondria in cell death. Oncogene 23, 2861.

Seawright, A.A., Australia. Department of Primary, I., Energy. Bureau of Rural, R., 1989. Chemical and plant poisons, 2nd ed. ed. Australian Govt. Pub. Service, Canberra.

Smith, C.A., Farrah, T., Goodwin, R.G., 1994. The TNF receptor superfamily of cellular and viral proteins: activation, costimulation, and death. Cell 76, 959-962.

Smith, P.A., Aldridge, B.M., Kittleson, M.D., 2003. Oleander toxicosis in a donkey. Journal of veterinary internal medicine 17, 111-114.

Smith, S., 1930. LXXII.—Digoxin, a new digitalis glucoside. Journal of the Chemical Society (Resumed), 508-510.

Steyn, D., 1928. Tulp poisoning. Pretoria: Government Printer and Stationery Office.

Steyn, P.S., van Heerden, F.R., 1998. Bufadienolides of plant and animal origin. Natural Product Reports 15, 397-413.

Tailler, M., Senovilla, L., Lainey, E., Thepot, S., Metivier, D., Sebert, M., Baud, V., Billot, K., Fenaux, P., Galluzzi, L., 2012. Antineoplastic activity of ouabain and pyrithione zinc in acute myeloid leukemia. Oncogene 31, 3536.

Tian, J., Liu, J., Garlid, K.D., Shapiro, J.I., Xie, Z., 2003. Involvement of mitogen-activated protein kinases and reactive oxygen species in the inotropic action of ouabain on cardiac myocytes. A potential role for mitochondrial KATP channels, In: Cardiac Cell Biology. Springer, pp. 181-187.

Tustin, C., 1984. An outbreak of *Cotyledon orbiculata* L. poisoning in a flock of angora goat rams. Journal of the South African Veterinary Association 55, 181-184.

Vahrmeijer, J., 1981. Poisonous plants of southern Africa that cause stock losses. Tafelberg Publishers, Limited.

Wallick, E.T., Pitts, B.J., Lane, L.K., Schwartz, A., 1980. A kinetic comparison of cardiac glycoside interactions with Na+, K+-ATPases from skeletal and cardiac muscle and from kidney. Archives of biochemistry and biophysics 202, 442-449.

Webster, M., Witkin, K.L., Cohen-Fix, O., 2009. Sizing up the nucleus: nuclear shape, size and nuclear-envelope assembly. Journal of cell science 122, 1477-1486.

Weinhouse, E., Kaplanski, J., Posner, J., 1983. Comparison of digoxin-induced cardiac toxicity in resistant and sensitive species. Journal of pharmacy and pharmacology 35, 580-583.

Wilson, F.W., 1909. Oleander poisoning of livestock. College of Agriculture, University of Arizona (Tucson, AZ).

World Health Organization, 2017. WHO Model List of Essential Medicines (March 2017).

WT. Parsons, E.C., 2001. Noxious Weeds of Australia, 2nd ed. CSIRO Publishing, Collingwood, Vic.

Xie, Z., Cai, T., 2003. Na+-K+–ATPase-mediated signal transduction: from protein interaction to cellular function. Molecular interventions 3, 157.

Yeh, J.Y., Huang, W.J., Kan, S.F., Wang, P.S., 2003. Effects of bufalin and cinobufagin on the proliferation of androgen dependent and independent prostate cancer cells. The Prostate 54, 112-124.

Yoda, A., 1974. Association and dissociation rate constants of the complexes between various cardiac monoglycosides and Na, K-ATPase. Annals of the New York Academy of Sciences 242, 598-616.

Yoda, A., Hokin, L.E., 1970. On the reversibility of binding of cardiotonic steroids to a partially purified (Na+ K)-activated adenosinetriphosphatase from beef brain. Biochemical and biophysical research communications 40, 880-886.

Yonekawa, T., Thorburn, A., 2013. Autophagy and cell death. Essays in biochemistry 55, 105-117.

Zhang, H., Qian, D.Z., Tan, Y.S., Lee, K., Gao, P., Ren, Y.R., Rey, S., Hammers, H., Chang, D., Pili, R., 2008. Digoxin and other cardiac glycosides inhibit HIF-1α synthesis and block tumor growth. Proceedings of the National Academy of Sciences 105, 19579-19586.

Zhang, Y.-Z., Chen, X., Fan, X.-X., He, J.-X., Huang, J., Xiao, D.-K., Zhou, Y.-L., Zheng, S.-Y., Xu, J.-H., Yao, X.-J., 2016. Compound library screening identified cardiac glycoside digitoxin as an effective growth inhibitor of gefitinib-resistant non-small cell lung cancer via downregulation of α-tubulin and inhibition of microtubule formation. Molecules 21, 374.

Zwerger, M., Kolb, T., Richter, K., Karakesisoglou, I., Herrmann, H., 2010. Induction of a massive endoplasmic reticulum and perinuclear space expansion by expression of lamin B receptor mutants and the related sterol reductases TM7SF2 and DHCR7. Molecular biology of the cell 21, 354-368.